PREPARATION AND MICROWAVE DIELECTRIC PROPERTIES OF CERAMICS IN THE SYSTEM (MgCa) TiO_3-$MgAl_2O_4$

by

RASMI RANJAN DAS

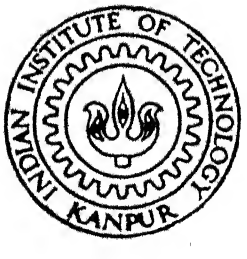

MATERIALS SCIENCE PROGRAMME

INDIAN INSTITUTE OF TECHNOLOGY, KANPUR

NOVEMBER, 1998

PREPARATION AND MICROWAVE DIELECTRIC PROPERTIES OF CERAMICS IN THE SYSTEM $(MgCa)TiO_3$-$MgAl_2O_4$

A Thesis Submitted

in Partial Fulfillment of the Requirements

for the Degree of

Master of Technology

by

RASMI RANJAN DAS

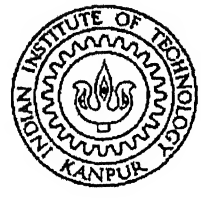

to the

MATERIALS SCIENCE PROGRAMME
INDIAN INSTITUTE OF TECHNOLOGY KANPUR

NOVEMBER 1998

CERTIFICATE

It is certified that the work contained in this thesis entitled " *Preparation and Microwave Dielectric Properties of Ceramics in the System* $(MgCa)TiO_3$-$MgAl_2O_4$", by *Rasmi Ranjan Das*, has been carried out under my supervision and that this work has not been submitted elsewhere for any degree.

Dr. D.C. Agrawal
Professor
Materials Science Programme,
Indian Institute of Technology, Kanpur
November, 1998

Dedicated to

My Parents

Acknowledgement

I derive my esteemed pleasure in expressing my deep sense of gratitude to Professor D. C. Agrawal for suggesting the problem, supervising the work and being a potential source of inspiration at each stage of this investigation. I am deeply indebted to him for his inspiring guidance, meticulus attention, constructive crticism and giving a new shape to this work. The completion of this thesis has been possible, only due to his intellectual support. I hope that his work and his example would continue to inspire me during my entire career in future.

I thank to Mr. Pawan (Phase Device Ltd., ACES, IIT, Kanpur) for helping dielectric measurements of all my samples at GHz frequency range using network analyser.

I also thank to Mr. Soumen Roy for providing a software for lattice parameter calculation.

I sincerely appreciate the companionship of my labmates Atanuda, Banashree, Santosh, Sarika and also exlabmates subhasisda, Soumen, Pankaj and Indraneel, for providing a better work culture inside the lab. My special thank to Mr. V.V. Mishra.

I wish to thank all my oriya friends Panda, Bhujbal, Tanmay, Maharana, Aditya, Rashmi, Manoj, Sasmita, Sangeeta, Lulu, Biswamber, Bhaskar Bhai, Parasar Bhai, Biswa Bhai, Gauranga Bhai, Pranab Bhai, Girija, Pabi, Pratap, Suprem, Raghu Bhai, Mahapatra Sir and my classmates Akash, Prasad, Anirban, Bala, Gopal who made my stay in the campus cherishable one.

I would like to thank all the non-teaching staffs of Materials Science Programme and Advanced Center for Materials Science for their cooperation during the course of my work.

The foremost contribution in acquiring knowledge and shaping my ideas todate comes from the faith, hope and pride of my family members. It was their love which kept me in going and words would fail to express feelings of indebtedness to them. I, therefore, offer my sincere silence words of acknowledgement to them.

Rasmi R. Das

IIT, Kanpur

Abstract

In this study we have aimed at the development of compositions for dielectric ceramic coaxial resonators having low dielectric constant, low dielectric loss (high Q) and high temperature stability. The study has been carried out on $Mg_{0.95}Ca_{0\ 05}TiO_3$ (MTCT) modified by the addition of Al_2O_3. The dielectric constant ($\simeq 21$) of MTCT is perhaps the lowest amongest all the high Q microwave dielectric ceramics in use today for DR application. Addition of Al_2O_3 in different amounts to MTCT leads to the formation of major phase of $MgAl_2O_4$ and some other phases in small amounts. Thus the main phases present in the sintered samples are $MgTiO_3$, $MgAl_2O_4$, and $CaTiO_3$ with small amounts of Al_2O_3, TiO_2, Mg_2TiO_4, $MgTi_2O_5$ and Al_2TiO_5. The lattice parameters of $MgTiO_3$ decreases with addition of Al_2O_3 indicated that some Al^{3+} is going in solid solution in $MgTiO_3$. This is in agreement with the published results. Also the lattice parameter of $MgAl_2O_4$ first increases, reaches a maximum and then decreases upon addition of TiO_2.

The dielectric constant decreases as the content of $MgAl_2O_4$ increases. This is in agreement with logarithmic mixture rule. The temperature coefficient of resonant frequency (TCF) value is increased with $MgAl_2O_4$ content. The quality factor attains a maxium value ($\simeq$ 3400 at 9.67 GHz) at 0.6 $MgAl_2O_4$, and goes to minimum ($\simeq$ 1200 at 11 GHZ) at the composition 0.8 $MgAl_2O_4$. The decrease in Q value at higher $MgAl_2O_4$ (≥ 0.8) content is due to the low density and the presence of microcracks, which cause high loss. The composition at 0.6 $MgAl_2O_4$ has the best properties in the whole composition range. The dielectric constant of 12.4, quality factor $Q \simeq 3400$ at 9.67 GHz and TCF $\simeq -26$ ppm/^oC have been

obtained for this composition. While the dielectric constant and Q are within acceptable range, the TCF is highly negative. Tailoring of temperature stable material has been done by the variation of $CaTiO_3$ content in the system 0.35 $(Mg_{1-y}Ca_yTiO_3)$ - 0.65 $(MgAl_2O_4)$. The composition range $0.086 \leq y \leq 0.143$ has been investigated. The TCF value changes from -16 to +18 ppm/^oC at 13 MHz and -20 to +33 ppm/^oC at $\sim$ 10 GHz. The TCf value of -4.7 ppm/^oC (at 13 MHz) has been obtained with the composition having $y = 0.1$ where as the same ($y = 0.1$) composition has $\epsilon_r \simeq 21$, $Q \simeq 2500$ and TCF $\simeq +10 ppm/^oC$ at 9.25 GHz.

Contents

List of Figures x

List of Tables xii

1 Introduction 1
1.1 General 1
1.2 Parameters of Dielectric Materials 7
1.3 Microwave Measurements of Complex Permittivity ϵ_r and quality factor Q . 9
1.4 Review of Microwave Dielectric Materials 13
1.4.1 $MgTiO_3$ - $CaTiO_3$ 14
1.4.2 BaO-TiO_2 system 14
1.4.3 (Zr,Sn)TiO_4 system 15
1.4.4 Complex Perovskites ($AB'_{1/3}B''_{2/3}O_3$) 20
1.4.5 BaO-RE_2O_3-TiO_2 system 21
1.5 Statement of the Problem 22

2 Experimental Procedure 24
2.1 Sample Preparation 24
2.1.1 Specification of the starting materials as on the labels 24
2.1.2 Loss in Weight on Heating of the Starting Materials 25
2.1.3 Batch Composition, Calcination and Pressing 26
2.1.4 Binder Removal and Sintering 27
2.2 Characterization 27
2.2.1 Density and Phases 27
2.2.2 Dielectric Properties 27
2.2.3 Lattice Parameter Determination 30
2.2.4 Microstructure Studies by Scanning Electron Microscope (SEM) . . . 32

3 Results and Discussion 33
3.1 Optimization of Calcination Temperature 33
3.1.1 Phases in the Calcined Powders 35
3.1.2 Density Determination 35

3.2 Properties of Sintered Samples 51
3.3 Optimization of Dielectric Parameters in MTA(v) system 66
3.4 Lattice Parameter 71
3.5 Microstructure 77

4 Conclusion 82

References 84

Appendix 90

A Weight calculation for a particular batch 90

B Density calculation of a mixed phase system 93

C Predicted data for optimization of dielectric properties 95

D Software for lattice parameter calculation 98

List of Figures

1.1 (a) Coaxial line. The electromagnetic wave propagates in the space between the inner and outer conductor and is entirely enclosed in the lateral direction. (b) Rectangular waveguide. Here again wave propagation is only possible in the longitudinal direction [1]. 3

1.2 (a) Stripline. A strip conductor is sandwiched between two ground planes and is held in place by two layers of dielectric material. (b) Microstrip. The strip conductor here is readily accessible for making connections than symmetrical stripline (a). (c) The microstripline is the electrical equivalent of a twin-ware transmission line in which the second conductor situated at the image of the strip conductor in the ground plane. (d) Suspended stripline. The field of the strip conductor, unlike that in (a) and (b), is largely in air. (e) Coplanar waveguide. (f) Slotline. The r.f. electric field appears across the slot, and slotline is therefore suitable for the connection of parallel impedances [1]. . . 4

1.3 (a) Experimental arrangement for measurement of complex permittivity in Hakki-Coleman configuration. (b) Schematic diagram of measuring cavity [13]. 11

1.4 Example of frequency spectrum measured with the network analyser. The modulus of the ratio S_{21} of the voltage at terminals 2 and 1 is plotted in dB as a function of frequency [2]. 12

1.5 Solid solution formation region in the system ZrO_2-TiO_2-SnO_2 at 1250 to 1350 ^oC [15]. 17

1.6 Temperature coefficient of resonant frequency of ZTS ceramics as function of Sn content [3]. 18

1.7 Quality factor of ZTS dielectric resonator as a function of Sn content [3]. . . 19

2.1 (a) Schematic diagram of sample holder, (b) Schematic arrangement for dielectric constant and TCC measurement. 28

3.1 Particle size distributions of (a) MTA(0.4) and (b) MTA(0.6), powders calcined at 1150^oC and ground in mortar pestle. 34

3.2 X-ray diffractogram from calcined powder MTA(0). 47

3.3 X-ray diffractogram from calcined powder MTA(0.2). 48

3.4 X-ray diffractogram from calcined powder MTA(0.6). 49

3.5 X-ray diffractogram from calcined powder MTA(0.98). 50
3.6 Variation of density with volume fraction of $MgAl_2O_4$ 53
3.7 X-ray diffractograms of sintered pellet MTA(0). 55
3.8 X-ray diffractograms of sintered pellet MTA(0.2). 56
3.9 X-ray diffractograms of sintered pellet MTA(0.4). 57
3.10 X-ray diffractograms of sintered pellet MTA(0.6). 58
3.11 X-ray diffractograms of sintered pellet MTA(0.8). 59
3.12 X-ray diffractograms of sintered pellet MTA(0.98). 60
3.13 Subsolidus phase equilibrium diagram of the MgO-Al_2O_3-TiO_2 system at 1300 ^oC. A and B refer to the compositions of the two coexisting spinel phases. Abbreviations used include: Psb=pseudobrookite, s.s.=solid solution, sp=spinel, MT=$MgTiO_3$, Cor=corundum ($\alpha - Al_2O_3$) [49]. 61
3.14 Variation of dielectric constants (a) predicted, (b) measured, (c) corrected for density vs volume fraction of $MgAl_2O_4$. 63
3.15 Temperature coefficient of resonant frequency is function of $MgAl_2O_4$ content. 64
3.16 The Q.f value of MTA ceramics as a function of $MgAl_2O_4$ content, (Calcination temperature 1150 ^oC, sintering temperature 1400 ^oC). 65
3.17 Variation of TCF (ppm/^oC) of MTA(0.65) system with $CaTiO_3$ content. . . 68
3.18 Variation of Q.f of MTA(0.65) system with $CaTiO_3$ content. 69
3.19 Variation of dielectric constant of MTA(0.65) system with $CaTiO_3$ content. . 70
3.20 Variation of lattice parameter $a(A^o)$ of $MgTiO_3$ with $MgAl_2O_4$ content. . . . 72
3.21 Variation of lattice parameter $c(A^o)$ of $MgTiO_3$ with $MgAl_2O_4$ content. . . . 73
3.22 c/a of $MgTiO_3$ vs $MgAl_2O_4$ content. 74
3.23 Variation of lattice parameter of $MgAl_2O_4$ with different MTA(v) compositions. 75
3.24 Variation in the unit cell size of the spinel solid solutions. Open circles show individual meesurements and their size shows the estimated accuracy of measurement [49]. 76
3.25 SEM micrographs of compositions (a) MTA(0), (b) MTA(0.2), (c) MTA(0.4), (d) MTA(0.6), (e-f) MTA(0.8), (g) MTA(0.9). 81

List of Tables

1.1 Dielectric properties of some microwave dielectrics. 13
1.2 Dielectric properties of Magnesium Titanate and Calcium Titanate ceramics at 7 GIIz frequency [11]. 14

2.1 Linear coefficient of thermal expansion for various phases. 29

3.1 Standard X-ray data of $MgTiO_3$ phase. 36
3.2 Standard X-ray data of $CaTiO_3$ phase. 37
3.3 Standard X-ray data of $MgAl_2O_4$ phase. 38
3.4 Standard X-ray data of $MgTi_2O_5$ phase. 39
3.5 Standard X-ray data of Mg_2TiO_4 phase. 40
3.6 Standard X-ray data of Al_2TiO_5 phase. 41
3.7 Standard X-ray data of Al_2O_3 phase. 42
3.8 Standard X-ray data of rutile TiO_2 phase. 43
3.9 Standard X-ray data of MgO phase. 44
3.10 X-ray data from Table 3.1 to 3.9 combined in the order of ascending 2θ . . . 45
3.11 Phases in the calcined powders. Abbreviations include: MT=$MgTiO_3$, CT=$CaTiO_3$, MA=$MgAl_2O_4$, M_2T=Mg_2TiO_4, MT_2=$MgTi_2O_5$, AT=Al_2TiO_5, s=small, t=trace, BM=ball milling. 46
3.12 Density of pellets sintered at 1400 ^oC, 2hrs from powders calcined for 4 hrs at different temperatures. 51
3.13 Properties of MTA(v) samples sintered at 1400 ^oC, 2hr. 52
3.14 Comparison of phases in our samples with data in reference [49]; the first line in each row is the composition of our samples and the second line is the nearest composition for which data is available. 54
3.15 Dielectric properties of $(Mg_{1-y}CayTiO_3)_x$ - $(MgAl_2O_4)$ at x = 0.4 (volume fraction of MA = 0.65). 67
3.16 Lattice parameters of $MgTiO_3$ (hexagonal) system. 71
3.17 Lattice parameters of $MgAl_2O_4$ (cubic) system 71

A.1 Mole fraction to volume fraction conversion data 91

B.1 Theoretical density of all MTA(v) system. 94

C.1 ϵ_r and TCF data of $MgTiO_3$, $CaTiO_3$ and $MgAl_2O_4$ system. 95
C.2 ϵ_r and TCF data of $Mg_{0.95}Ca_{0.05}TiO_3$ system 96
C.3 Predicted values of ϵ_r and TCF in the system 0.35 $(Mg_{1-y}Ca_yTiO_3)$−0.65 $(MgAl_2O_4)$. 97

Chapter 1

Introduction

1.1 General

The electric circuits with which we are mostly familiar operate at low frequencies. In these circuits the stray elements for a circuit component are very small e.g. a capacitance is nearly fully capacitive and has negligible inductance or resistance. Thus the capacitance is thought to be concentrated in the capacitor, inductance in the inductor and the resistance in the resistor. These circuits are therefore called circuits with lumped components.

At higher operating frequencies, effects not important at the lower frequencies need to be taken into account. These are: (i) the stray elements become more important and the magnitude of these is not known exactly. (ii) the transit time of the signal in the circuit is no longer negligible as compared to the reciprocal of the frequency and, alternately, the wavelength approaches the dimension of the circuit elements. (iii) electromagnetic (em) radiation occures.

In microwave (>1 GHz) circuits, the energy is transmitted through special transmission lines in which the electromagnetic field is bounded in the transverse direction so that no radiation occures. The transmission line here has a capacitance and inductance distributed along its length. Thus the circuit elements in microwave circuits are refered to as distributed.

The most common configuration of the microwave transmission lines are coaxial lines and the rectangular wave guide (Fig. 1.1). The electromagnetic wave propagates in the space inside the the transmission line. The accompanying current flows in a thin "skin" on the surface of the conducting wall. The electrical behaviour of these transmission lines can be very accurately calculated and the uncertainties due to strays are not present.

In the early days, the microwaves were being generated and amplified only by thermoionic valves. With the advent of semiconductors for this purpose, it became necessary to devise microwave transmission lines and components which were less bulky as compared to coaxial or rectangular waveguides. For the transmission of microwaves, planar wave guides have taken the place of cavity wave guides. These consists of thin metal strips on a dielectric substrate. Many configuration of planar wave guides are possible of which the microstripline is the more frequently used (Fig. 1.2) [1].

Two of the most important components needed in microwave circuits for applications such as broadcasting via satellite and mobile telephones are resonators (for maintaining the frequency of the circuit in the specified band) and filters. Upto 1980's these components used to be relatively large cavity resonators made of invar or copper. Invar waveguide is used in the applications where high temperature stability is required. In general, copper waveguide is used in applications where lower temperature stability can be tolerated. It is also less expensive to fabricate. The size of these waveguide resonators is not compatible with microstrip or stripline integrated circuits [2]. All the requirements, high Q, high temperature stability and small dimensions can only be met by the use of dielectric ceramic resonators, which can be smaller because the permittivity of ceramic is higher than that of air. The quality of resonator depends upon the dielectric properties of material at microwave frequency. Two types of resonators are presently in use. These are coaxial $\frac{\lambda}{4}$ resonators for use with frequencies upto 3 GHz and solid rod dielectric resonators for use upto 30 GHz. The coaxial dielectric resonators (CDR) need to be electroded where as the dielectric resonators

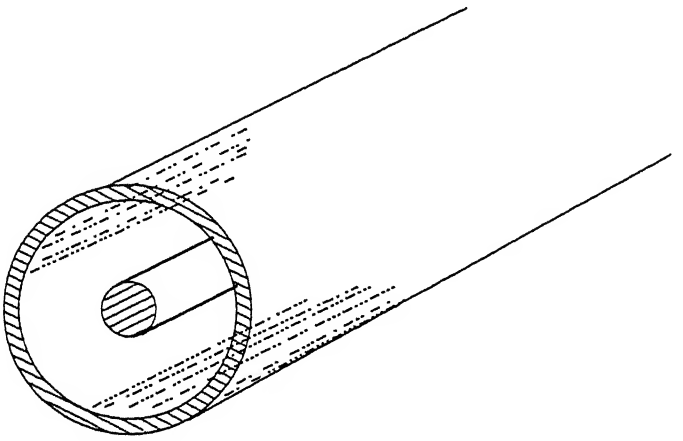

a

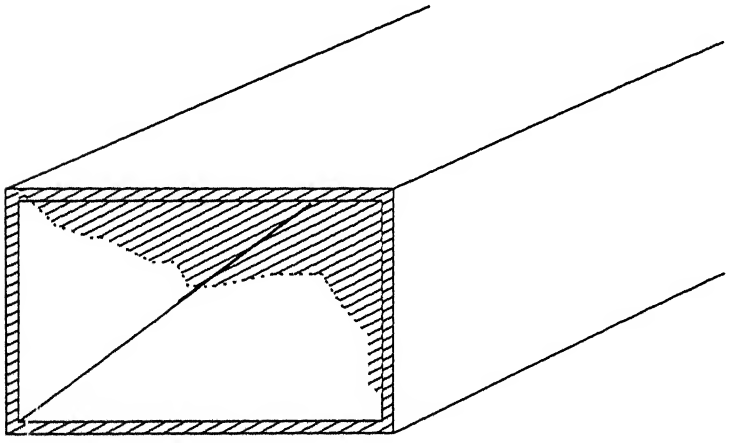

b

Figure 1.1: (a) Coaxial line. The electromagnetic wave propagates in the space between the inner and outer conductor and is entirely enclosed in the lateral direction. (b) Rectangular waveguide. Here again wave propagation is only possible in the longitudinal direction [1].

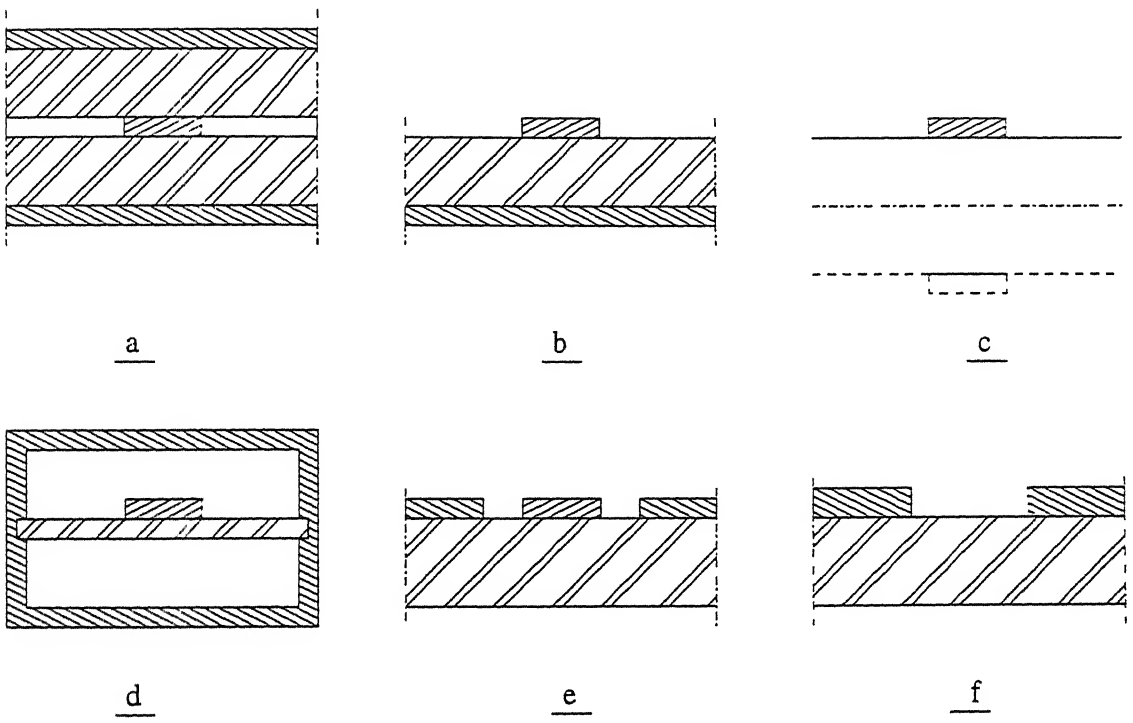

Figure 1.2: (a) Stripline. A strip conductor is sandwiched between two ground planes and is held in place by two layers of dielectric material. (b) Microstrip. The strip conductor here is readily accessible for making connections than symmetrical stripline (a). (c) The microstripline is the electrical equivalent of a twin-ware transmission line in which the second conductor situated at the image of the strip conductor in the ground plane. (d) Suspended stripline. The field of the strip conductor, unlike that in (a) and (b), is largely in air. (e) Coplanar waveguide. (f) Slotline. The r.f. electric field appears across the slot. and slotline is therefore suitable for the connection of parallel impedances [1].

(DR) are used in unelectroded condition. As the electrode material has finite conductivity, the quality factor (Q) of CDR is limited to $\leq$ 1500. The DR do not need electroding so their Q is limited only by the Q of the material.

In CDR, the no load Q (Q_0) depends on the $\tan\delta$ of the material, the electrical conductivity of the metal electroding, CDR cross sectional dimension and the ratio of the inner and outer diameters. At frequency above > 1 GHz, the CDR dimension become too small for easy manufacturing and applications. As the dimension (length 'l') of a CDR is given by [3]

$$l = \frac{\lambda_0}{4}\frac{1}{\sqrt{\epsilon_r}} \tag{1.1}$$

the dielectric constant ϵ_r of the material needs to be decreased to bring back up the size. This is beneficial in other respects also: (a) the temperature coefficient of dielectric constant TCK and hence the temperature coefficient of resonant frequency TCF decreases as ϵ_r decreases (b) the resonant modes of the resonator become fewer and more separated leading to less interference, better tuning (c) Q of the resonator increases because of larger size (d) it is easier to manufacture components with reproducible properties. As the allowed frequency range for communication moves towards higher frequencies, it becomes important to develop materials for CDR with low ϵ_r but high Q ($\geq$ 2500) and near zero TCF.

In the high-K dielectric ceramics used for microwave resonators the dissipation factor increase with frequency above 1 GHz, so that there may be problems in obtaining suitable dielectrics for use near 100 GHz. In this case lower permittivities may give satisfactory components. The source of loss at higher frequency range has been attributed to the infrared absorption bands due to ionic polarization which may be very small in low K ceramics [4]. In addition to their use in CDR's, the low-K dielectric ceramics are frequently used for other components and devices in electronic circuits at frequencies above 1 GHz. Low-K dielectric ceramic also find a application as multilayer substrates in insulating two conductors in hybrid

circuits since low permittivity minimises coupling between components and conductors on the substrate surface.

In last two decades, the development of large-scale integration (LSI) and very large-scale integration (VLSI) has promoted the generation of multilayer substrates to fulfil the demand of electronic systems for reduced size, higher integration density and better reliability.

The requisite properties of any candidate material for multilayer substrates are the following [5]:

(1) High electrical resistivity, such that the substrate acts as a perfect insulator.

(2) Low dielectric constant, which reduces the signal delay time 'T_d' (i.e. $T_d \propto \frac{\sqrt{\epsilon_r}}{c}$).

(3) Low dissipation factor ($\tan\delta$), which reduces the loss of the signal.

(4) The sintering temperature of substrates should be $< 1000^oC$ inorder to use Pd-Ag alloy, Au or Cu as conductors. These have comparatively low electrical resistivities, as well as less fabrication costs.

(5) the coefficient of thermal expansion of substrates should be very less and close to that of silicon (3.6 - 4 ppm/^oC) to avoid "thermal stresses caused by the thermal expansion mismatch between the Si chips and substrates".

(6) High thermal conductivity. The thermal conductivity of the substrates is very important, particularly for high output power devices.

(7) Good mechanical properties.

(8) Stable chemical properties.

A low dielectric constant is favorable when used for a substrate, because it reduces the time delay of electronic signals during propagation in the conductor which is fabricated on the substrate. The signal delay time 'T_d' is related with the dielectric constant through the relation [6]:

$$T_d = L\frac{\sqrt{\epsilon_r}}{C} \tag{1.2}$$

Where 'T_d' is time delay in nanoseconds, 'ϵ_r' is dielectric constant of that material, C is the speed of light and 'L' is the distance travelled by the signal.

As mentioned earlier , for use at higher frequencies, the resonators are in the form of a piece of a solid ceramic rod. These are termed simply as "dielectric resonator" (DR). The diameter of a DR depends on the wavelength λ_0 and the dielectric constant ϵ_r as [3]

$$D \simeq \lambda_0 \frac{1}{\sqrt{\epsilon_r}} \tag{1.3}$$

Hence it is desirable to use materials with high ϵ_r so as to miniaturize the circuits.

The dielectric properties required for practical microwave filters in DR mode are a high unloaded Q ($\geq$ 3000) and low temperature coefficient of resonant frequency TCF ($\pm 20 ppm/^{\circ}C$). In addition the high dielectric constant (prefarably $\epsilon_r > 30$)is desirable [7, 8].

1.2 Parameters of Dielectric Materials

The properties of an ordinary dielectric material can be specified by a complex dielectric constant ϵ_r. In general ϵ_r is separated by real and imaginary parts;

$$\epsilon_r = \epsilon^{'} - j\epsilon^{''} = \epsilon^{'}(1 - j\tan\delta) \tag{1.4}$$

where $j = \sqrt{-1}$

The dimensionless quantity $\tan\delta$ in equation (1.4), is called the *loss tangent*; it is equal to the power dissipated devided the power stored per cycle and is thus a measure of energy lost in the form of heat when a wave is propagated through the material [9].

According to classical dispersion theory, the frequency dependence of real $\epsilon^{'}$ and imaginary $\epsilon^{''}$ part of complex dielectric constant are given by the following equations [10]:

$$\epsilon^{'}(w) = \epsilon_{\infty} + \sum_{i} \frac{4\pi\rho_i\omega_i^2(\omega_i^2 - \omega^2)}{(\omega_i^2 - \omega^2)^2 + (\gamma_i\omega)^2} \tag{1.5}$$

$$\epsilon''(w) = \sum_i \frac{4\pi\rho_i\omega_i^2\gamma_i\omega}{(\omega_i^2 - \omega^2)^2 + (\gamma_i\omega)^2} \tag{1.6}$$

The summation is over all lattice oscillators. The strength $4\pi\rho_i$, width γ_i, and resonant frequency w_i of each oscillator are called dispersion parameter and ϵ_∞ is the dielectric constant caused by electronic polarization at very high frequency. With the condition $w^2 \ll w_i^2$. the loss tangent corresponding to ith dispersion parameter is given by

$$\tan\delta_i = \frac{\epsilon''}{\epsilon'} = \frac{4\pi\rho_i(\gamma_i\omega)/\omega_i^2}{\epsilon_\infty + \sum 4\pi\rho_i} \tag{1.7}$$

$$\tan\delta = \sum_i \tan\delta_i = \frac{\sum_i 4\pi\rho_i(\gamma_i\omega)/\omega_i^2}{\epsilon_\infty + \sum_i 4\pi\rho_i} = A\omega \tag{1.8}$$

Where $A = \frac{\sum_i 4\pi\rho_i\gamma_i/\omega_i^2}{\epsilon_\infty + \sum_i 4\pi\rho_i}$

According to above description of classical dispersion theory, the relative permittivity is independent of frequency and loss tangent ($\tan\delta$) is propertional to frequency w. Hence, Q decreases with increasing frequency. Therefore it is always convenient to consider $Q.f$ value for each material, as so-called figure of merit [11].

The quality factor 'Q' is an important parameter for every dielectric material which is to be used for electronic device applications. The qualitry factor 'Q' of a dielectric resonator is defined for each resonant mode by [12]

$$Q = \frac{f_r}{\Delta f} = \frac{w}{\Delta w} \tag{1.9}$$

Where f_r is the resonant frequency and Δf is the bandwidtih between the frequencies $f_r \pm \Delta f/2$ for which the amplitude of surface current, the surface charge, electric and magnetic fields is reduced to 0.707 of its value at resonant frequency f_r. The quality factor, in general may be written as

Q = 2π maximum energy stored/energy dissipated per cycle

The temperature coefficient of dielectric constant and resonant frequency are defined by [3]

$$TCK = \frac{1}{K}\frac{\partial K}{\partial T} \tag{1.10}$$

$$TCF = \frac{1}{f_r}\frac{\partial f_r}{\partial T} \tag{1.11}$$

The temperature coefficient of resonant frequency TCF is related to the linear thermal expansion coefficient (α) as well as to the temperature coefficient of relative permittivity TCK of the dielectric. The relaion is [4]

$$TCF = -\frac{TCK}{2} - \alpha \tag{1.12}$$

Since TCC = TCK + α

$$\Rightarrow TCF = -\frac{1}{2}(TCC + \alpha) \tag{1.13}$$

In order to maintain the resonant frequency within tolerable limits, TCF must be within 20×10^{-6} of zero.

1.3 Microwave Measurements of Complex Permittivity ϵ_r and quality factor Q

For the measurement of complex permittivity ϵ_r and quality factor 'Q' of a dielectric material at microwave frequency, the usual arrangement is as shown in Fig. 1.3(a) and Fig. 1.3(b) is the schematic representation of measuring cavity [13]. In a cylindrical sample

microwave resonances are generated whose geometry (wavelength) is comparable with the geometry of resonances in a dielectric resonator. The sample is placed between two conducting plates on both sides. A variable frequency signal is applied from the network analyser (NA) to the sample via a coaxial line and excites a field in it. The signal is returned to the analyser by a second coaxial line.

The permittivity parameter ϵ_r of the dielectric resonator material is obtained from the measured resonance frequency f_r, the geometry of the specimen and the height of the air gap, between the specimen and the top metal plate, which is sensitive to the resonant frequency. The equation required for evaluating the permittivity ϵ_r is given by [14]

$$f_r(GHz) = 36.0\frac{[\frac{1}{h} + \frac{e^{-h_a}}{15} + \frac{3.75}{d}]}{\sqrt{\epsilon_r}} \tag{1.14}$$

Where 'h' and 'd' are the height and radius of dielectric cylinder and h_a is the air gap between the upper plate and cylinder.

The dimension of the specimen are very important to achieve wide separation of modes and to reduce the chances of overlap with higher order modes. The proper aspect ratio (diameter/length) is 2 - 2.5 [13].

Fig. 1.4 shows a frequency spectrum measured with the arrangement of Fig. 1. 3(a). In this figure the transmission parameter S_{21} is plotted against frequency. This spectrum contains transerverse electric (TE_{0np}), transverse magnetic (TM_{0np}) and hybrid modes (HE_{mnp}), where m, n, p are integers relating to the number of periods of the electric or magnetic field in the circumferential, radial and axial directions respectively. It is shown on the plot that the mode with lowest frequency is called HE_{111} mode. Q of material is determined from the shape shown by dotted curves, around the TE_{011} mode. The dotted curve is obtained by the magnification of the peak for TE_{011} mode, in the horizontal direction. The quality factor 'Q' is approximately equal to the ratio of the resonant frequency 'f_r', to the width of the resonance peak, measured $3dB$ below the peak (A value of 3 dB corresponds to power ratio

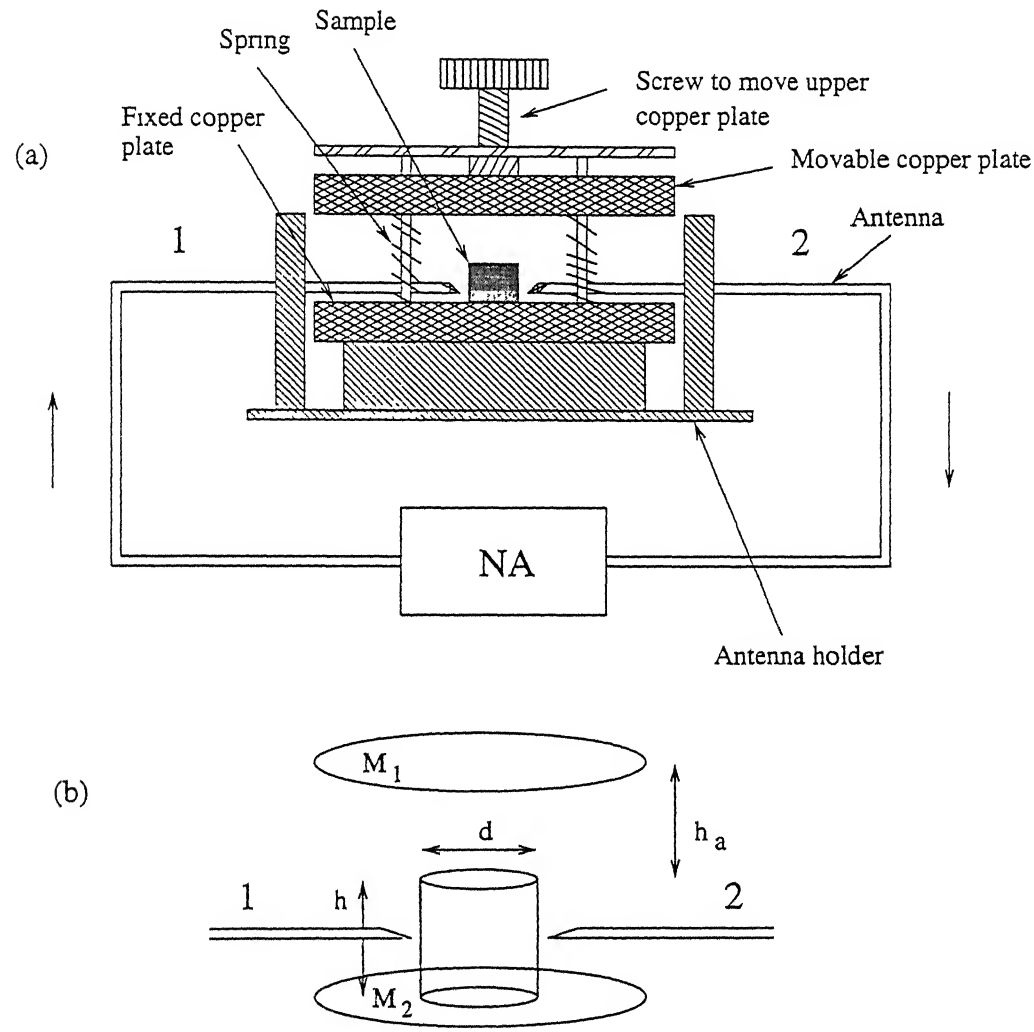

Figure 1.3: (a) Experimental arrangement for measurement of complex permittivity in Hakki-Coleman configuration. (b) Schematic diagram of measuring cavity [13].

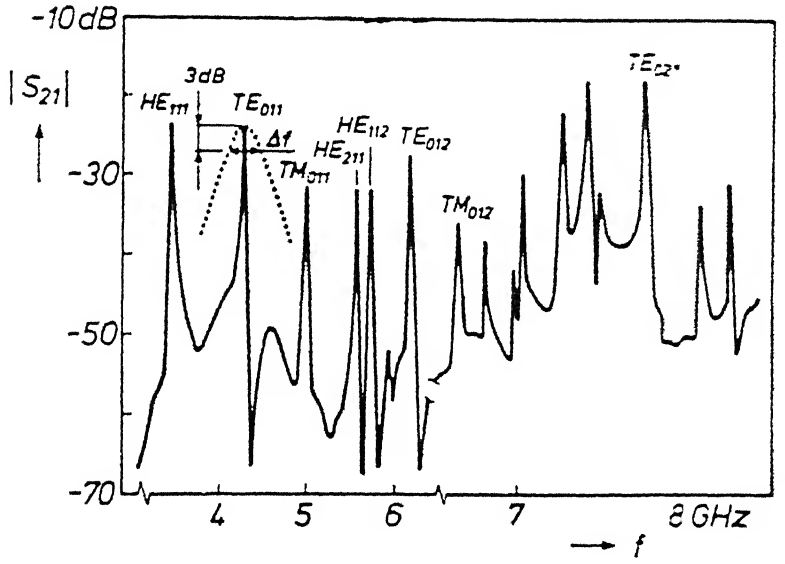

Figure 1.4: Example of frequency spectrum measured with the network analyser. The modulus of the ratio S_{21} of the voltage at terminals 2 and 1 is plotted in dB as a function of frequency [2].

of 0.5) [2].

1.4 Review of Microwave Dielectric Materials

In the recent years, considerably effort has been devoted to the development of materials for dielectric resonators with high ϵ_r and high Q. Search for materials with low ϵ_r but $Q \geq 2500$ and $TCF \simeq 0$ has only recently begun afresh for use in coaxial dielectric resonators as the allowed frequencies for communication purpose have been increase by the regulatory authorities. In the following review we cover mostly the materials for DR for high frequency applications. Among these, a group of materials which are highly technically useful, are shown in Table 1.1.

Table 1.1: Dielectric properties of some microwave dielectrics.

Material	ϵ_r	TCF	Q	f(GHz)	Q.f(GHz)	Reference
$MgTiO_3CaTiO_3$	21	0	8000	7	56000	11
$Ba(SnMgTa)O_3$	25	0	43000	10	430,000	11
$Ba(ZnTa)O_3$	30	0	14000	12	168000	11
$(ZrSn)TiO_4$	38	0	10300	5	51500	15,16
$Ba_2Ti_9O_{20}$	40	0	8000	4	32000	17
BaO-PbO-Nd_2O_3-TiO_2	90	0	5000	1	5000	11
$(BaSr)O$-$Sm_2O_3TiO_2$	80	0	3700	3	11100	11
$CaTiO_3$-$Ca(Al_{1/2}Ta_{1/2})O_3$	46.5	0			27300	18
$(La_{1/2}Na_{1/2})TiO_2$-$Ca(Fe_{1/2}Nb_{1/2})O_3$	58.9	0			14070	19

The details of stochiometry and dielectric properties of some of the important family of dielectrics are described below.

1.4.1 $MgTiO_3$ - $CaTiO_3$

This two phase system is a well known material for microwave dielecric ceramics. The end members have quite different properties, with Q values changing by more than a factor of 10, and the temperature coefficient of resonant frequency (TCF) is far away from stable value zero. In this composition, the partial substitution of magnesium by calcium is known to modify the large negative temperature coefficient of resonant frequency [20] of magnesium titanate ($MgTiO_3$). The dielectric properties of end members are shown in Table 1.2.

Table 1.2: Dielectric properties of Magnesium Titanate and Calcium Titanate ceramics at 7 GHz frequency [11].

	ϵ_r	Q	TCF
$MgTiO_3$	17	$\geq$ 20000	-45
$CaTiO_3$	170	1800	+800

For technical applications, a composition of $(Mg_{0.95}Ca_{0.05})TiO_3$ is usually selected to get a stable temperature compensating system, which yield $TCF \simeq 0$, $\epsilon_r \simeq 21$ and $Q \simeq 8000$at 7 GHz.

All the above results are obtained by conventional mixed ceramic methods. But as reported by Freer [11], the work has been done by Ferrira etal [21] to enhance dielectric properties of this system. They have processed the same composition by chemical route, and the chemically prepared powders pressed isostatically and sintered at moderate temperature (1150 ^oC), yield higher Q values ($\simeq$ 22000 at 7 GHz).

1.4.2 BaO-TiO_2 system

As reported by Wersing [3], $BaTi_4O_9$ was the first microwave dielectric ceramic found to have excellent dielectric properties ($\epsilon_r \simeq 38$, TCF $\simeq$ 15 ppm/^oC, $Q \simeq 5000$ at 2 GHz).

$Ba_2Ti_9O_{20}$ is the successor of the original system $BaTiO_3$, which possessed even better properties.

The microwave dielectric properties of the compound $BaTi_4O_9$ were reported first by Masse etal [22] as $\epsilon_r \simeq 39$, $Q \simeq 2500$ and TCK $\simeq -49$ (TCF $\simeq 18$ ppm/°C). Bryan etal [7] were first to investigated the dielectric properties of ceramics in TiO_2 rich region of BaO-TiO_2. They obtained the compound $Ba_2Ti_9O_{20}$ using carefully controll calcination and sintering conditions, which yielded $\epsilon_r \simeq 40$, TCF $\simeq -2$ ppm/^oC and $Q > 8000$ at 4 GHz.

Although various authors [7, 17, 23] have reported the existence of $Ba_2Ti_9O_{20}$ compound within the TiO_2 rich binary region, their structure data are not compatible. According to phase diagrams, the range of existence of $Ba_{20}Ti_9O_{20}$ and $BaTi_4O_9$ are limited, being 0.818 - 0.819 and 0.798 - 0.799 mole fraction of TiO_2 in BaO-TiO_2 respectively, at 1100 ^oC.

The composition homogeneity of powders also appears to control the formation of $Ba_2Ti_9O_{20}$ phase. The phase formation, kinetic and structural homogeneity is improved in the sol-gel processed $Ba_2Ti_9O_{20}$ compound [24]. A little difference was found between samples prepared by hot pressing and those prepared by sintering when the densities are equal. The sintering temperature reported by all authors were between 1350 - 1450 ^oC for conventional processing. The dielectric loss for all hot-pressed and sintered sample could be lowered by oxidizing heat treatment. A 48 hr annealing at 950 ^oC in O_2, improved Q by 5 to 20 %.

1.4.3 (Zr,Sn)TiO_4 system

The ceramic system based on zirconium titanate have long been used as temperature stable dielectrics [11]. The investigation of solid solution of ZrO-TiO_2-SnO_2 with ZnO was started in 1950's, for the use of temperature stable capacitor [3]. Solid solution formation in the system ZrO_2-TiO_2-SnO_2 has been investigated by Wolfram and Gobel [15] at $1250 < T < 1350^oC$. Single-phase solid solutions of SnO_2 in the $ZrTiO_4$ were found to exist in the

composition zone shown in Fig. 1.5.

There is a structural transition at 1125 ^oC, between the socalled "high-temperature" form having short unit cell parameter, and the "low-temperature" form having a long unit cell parameter. The structural transition is well understood if one takes into account that $\alpha - PbO_2$ structure of $ZrTiO_4$ transforms into the rutile structure of $TiO_2(SnO_2)$ at certain Sn content. As an overview of this system, some important results are shown in Fig. 1.6 and Fig. 1.7, as variation of dielectric properties with Sn content.

The composition having the zero temperature coefficient of resonant frequency (TCF), within the solid solution region is of particular interest of the material for use in microwave frequency. The typical dielectric properties obtained at y = 1, x= 0.25, TCF $\simeq$ 0 and at x = y = 1 - z/2, Q is almost constant for $z < 0.4$ [3]. All the required dielectric properties has been satisfied by one composition $Zr_{0.8}Sn_{0.2}TiO_4$, which yield $\epsilon \simeq 40$, $Q \simeq 5000$ to 10000 with $Q.f > 35000$ upto 10 GHz and $TCF \simeq 0$ [25, 26, 27, 28].

The works of various authors [15, 25, 29] have revealed that the sintering of ZTS is difficult even at a temperature of 1600 ^oC. Thats why some investigators [25, 30] have explored the addition like Fe, La_2O_3, NiO etc. to activate the reaction and densify at some lower temperature (1200-1400 ^oC).

Good quality of ZTS ceramics can be prepared through chemical route. Preparation of ZTS powders by sol-gel technique has also been reported by Hirano et al [27], who have obtained $\epsilon_r \simeq 40$, $TCF \simeq 3$ ppm/^oC, $Q \simeq 5000$, $Q.f \simeq 50,000$, when the densification is > 96%, without any additive, at sintering temperature 1600 ^oC. In that report Hirano mentioned that the dielectric constant in this system was remarkebly dependent upon the relative densities of the sintered bodies and lattice parameters, while 'Q' value is basically affected by the oxygen vacancies in the system. An increase in the relative permittivity with the inclusion of Sn in $ZrTiO_4$ was due to the enhancement of ionic polarization with the increase in lattice parameter i.e. c - axis length.

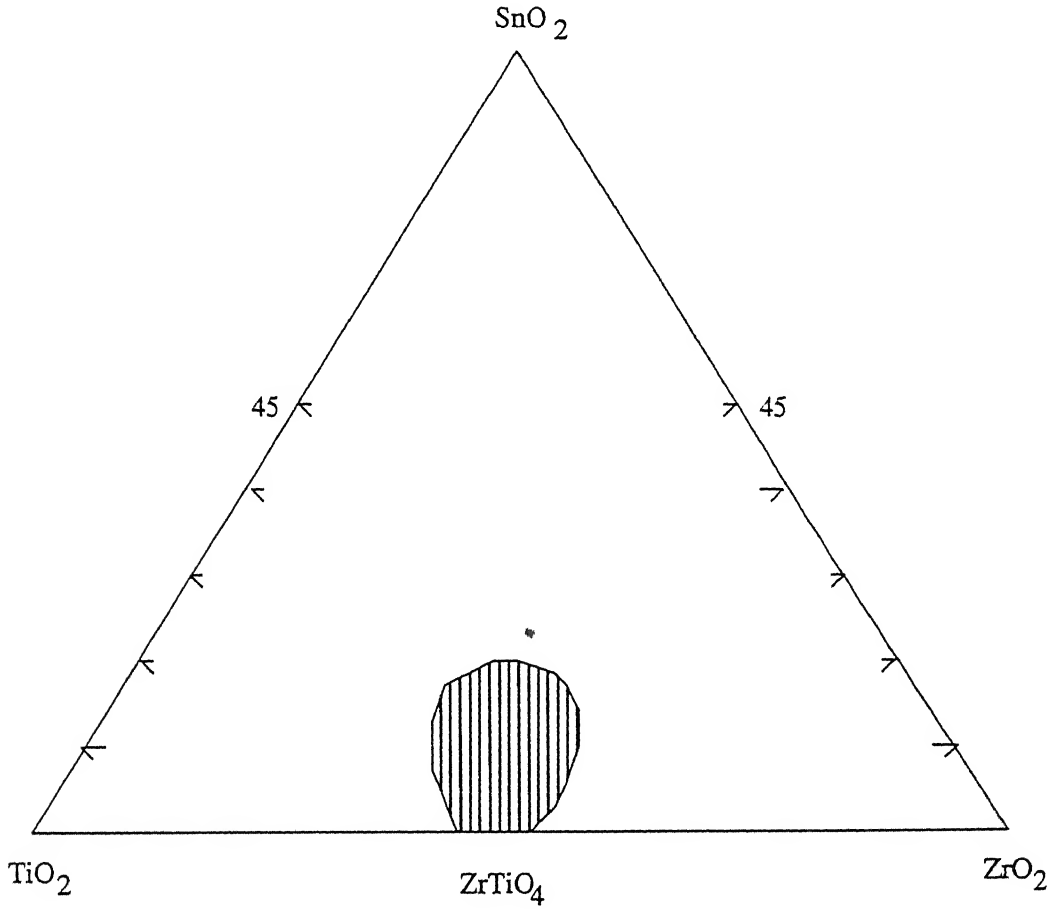

Figure 1.5: Solid solution formation region in the system ZrO_2-TiO_2-SnO_2 at 1250 to 1350 ^oC [15].

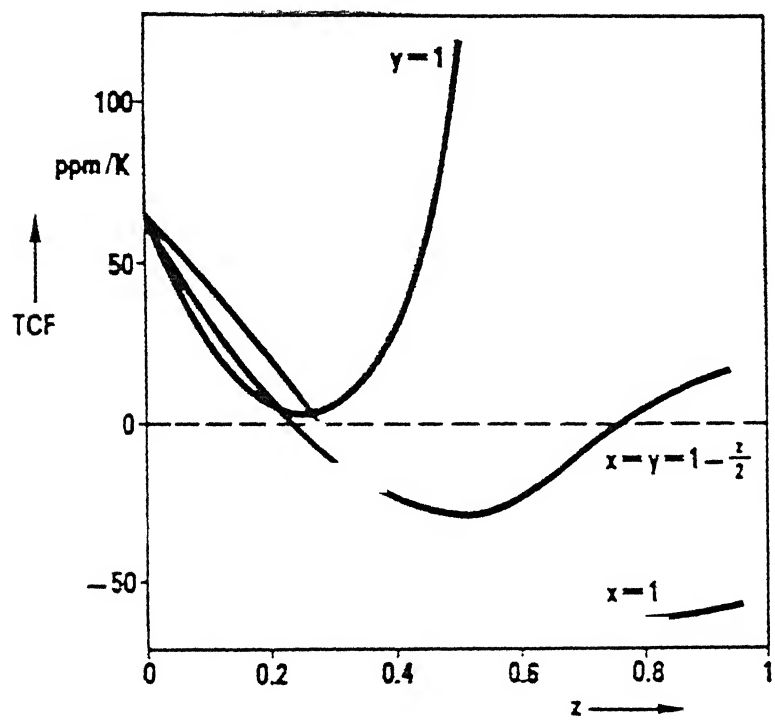

Figure 1.6: Temperature coefficient of resonant frequency of ZTS ceramics as function of Sn content [3].

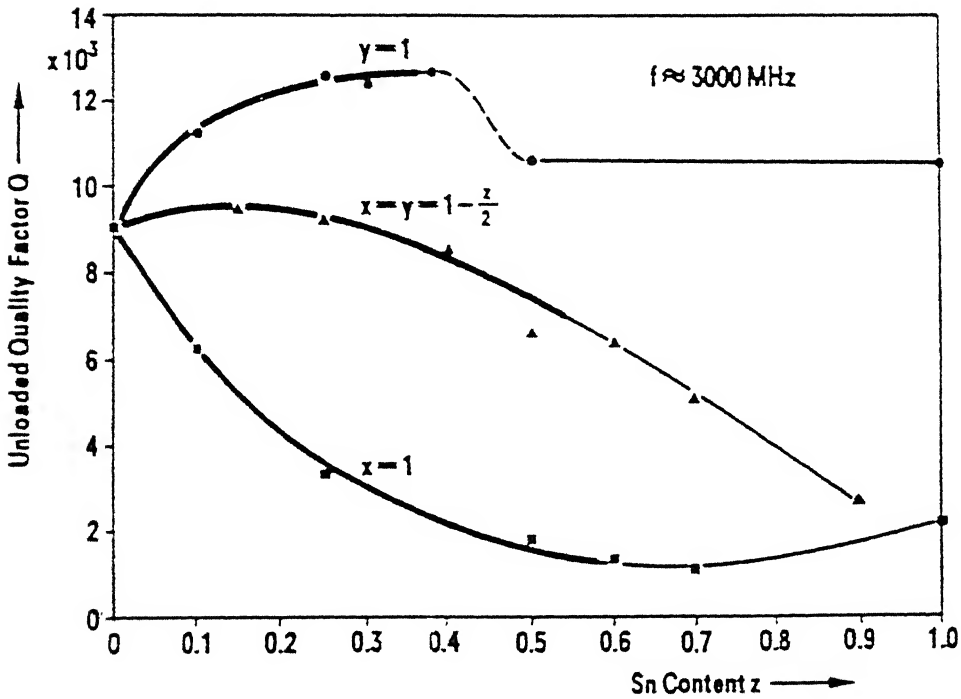

Figure 1.7: Quality factor of ZTS dielectric resonator as a function of Sn content [3].

1.4.4 Complex Perovskites ($AB'_{1/3}B''_{2/3}O_3$)

Microwave dielectric ceramics with complex perovskite structure possess highest available 'Q' values, 10000 – 40000 at 10 GHz and, have relative permittivities in the range 22 - 30 [11]. These systems are technically attractive for use at frequencies of about 10 GHz and higher, due to their extremely higher Q.f products and good temperature stability.

In general one can make a group of all complex perovskites with a general formula $A(B'_{1/3}B''_{2/3})O_3$, where A, B' and B'' can be amongest the following ions :

A : Ba^{2+}, Sr^{2+}

B' : Mg^{2+}, Ca^{2+}, Zn^{2+}, Ni^{2+}, Mn^{2+}, Co^{2+}

B'' : Nb^{5+} or Ta^{5+}

Some of the well known compounds in the perovskite family that have been investigated are as follows [31, 32, 33, 34, 35]

$A = Ba^{2+}$, $B'' = Ta^{5+}$

$Ba(Zn_{1/3}Ta_{2/3})O_3$ (BZT)

$Ba(Mg_{1/3}Ta_{2/3})O_3$ (BMT)

and $A = Ba^{2+}$, $B'' = Nb^{5+}$

$Ba(Ni_{1/3}Nb_{2/3})O_3$ (BNiN)

$Ba(Zn_{1/3}Nb_{2/3})O_3$ (BZN)

Hiroshi [35] reported a wide range of compositions having perovskite structure. Several authors [36] have investigated the dielectric properties of above compound which forms the solid solution with binary compounds and another complex perovskites. The investigated compounds were BZT-$BaZrO_3$ [35], BMT-$BaWO_4$ [37], BMT-$BaSnO_3$ [38], BZN $Ba(Ca_{1/3}Nb_{2/3})O_3$ [39], BZT-SBGT [36] etc.

The microwave properties of the most studied complex perovskites are as follows :

BZT based : $\epsilon_r \simeq 30$, Q.f $\simeq$ 36000 to 21000, $TCF \simeq 0$

BMT based : $\epsilon_r \simeq 24$, $Q.f \simeq 50,000 - 200,000$, $TCF \simeq 0$

BNiN/BCoN, BZN based : $\epsilon_r \simeq 30-34$, $Q.f \simeq 50.000-100,000$, $TCF \simeq 0$

The dielectric properties of perovskites are sensitive to purity, composition, crystallographic structure and microstructure of the material [35, 38]. There are some systems e.g. $Ba(SnMgTa)O_3$, in which the presence of second phase decreases the Q value [35]. High sintering temperature and difficulty in obtaining a single phase are major problem in the preparation of these materials. In order to obtain high Q values, ordering of B-sites appears to be important and long sintering time (60 - 100 hr) is needed to produce highly ordered materials. According to report of Freer [11] the dielectric Q-value changes from 10000 to 1000, in $Ba((MgCo)_{1/3}Nb_{2/3})O_3$ systems as the A-site/ B-site ratio for cations changes slightly by 0.004.

1.4.5 BaO-RE_2O_3-TiO_2 system

In early 1980's investigation were carried out to develop a microwave dielectric having higher relative permittivity. These investigation guided a new family of materials based on BaO-RE_2O_3-TiO_2. According to the report of Wakino [26], the first system in this family was BaO-Nd_2O_3-TiO_2, investigated throughly by Bolton and Kolar [40]. The material in this system posses high relative permittivity and reasonably high Q values. But the temperature stability of this materials is still under active investigation. The ternary compounds in this system which has required microwave dielectric properties are classified into two categories according to their structure.

(i) An orthorhombic structure with compositions 1:1:4 and 1:1:5 of $BaO : Nd_2O_3 : TiO_2$.

(ii) A tungsten bronze structure, with the general formula $Ba_{6-3x}Re_{8+2x}Ti_{18}O_{54}$, with solid solubility range $0.3 < x < 0.7$ [41] and suitable dielectric properties obtained in the composition range of x = 0.5 to 0.7 in the solid solution [42].

(1) With the conventional processing method the dielectric properties in the system o compounds with orthorhombic structure have a large range, depending on RE used. Variou

authors [43, 44] have reported that more useful dielectric properties, particularly temperature stability, are obtained by using Sm and Nd in composition 1:1:5 of $BaO\text{-}RE_2O_3\text{-}TiO_2$, which yield the following properties.

$\epsilon \simeq 72$ to 78, Q.f $\simeq$ 5500 at 1 GHz with Nd, Q.f $\simeq$ 12000 at 3 - 4 GHz with Sm. and TCF $\simeq 0$.

Some authors [26, 40] have indicated the possibility of obtaining single phase materials in the composition 1:1:4 to give better dielectric properties.

(2) The stochiometry of both composition 1:1:4 and 1:1:5 of $BaO\text{-}Re_2O_3\text{-}TiO_2$ are not compatible [45]. The $BaO\text{-}Re_2O_3\text{-}4TiO_2$ ternary compound corresponds to x = 0.5 in the general formula $Ba_{6-3x}Re_{8+2x}Ti_{18}O_{54}$, a well known resonator material. With this idea, Matveeva et al [46] have reported their work with x = 0.75 and RE = Pr and got a compound $Ba_{3.75}Pr_{9.5}Ti_{18}O_{54}$ which has tungsten bronze structure and whose microwave dielectric properties are useful in solid solution range $0.5 < x < 0.7$ [41]. The relative permittivity 80-90 and $Q.f < 10,000$, and $TCF \simeq 0$ were achieved with this composition and structure. These compounds are under active investigation.

1.5 Statement of the Problem

The above material review covers mostly possible microwave dielectric ceramics having high dielectric constant, high Q and highly temperature stable. Among them $(MgCa)TiO_3$ system has relatively low dielectric constant ($\simeq 21$). To reduce the dielectric constant further, it is necessary to add some low dielectric constant material to the above $(MgCa)TiO_3$ system. The mostly available ceramic material having low dielectric constant are Al_2O_3 ($\sim$ 9.5), $MgAl_2O_4$ ($\sim$ 7.5), berylia ($\sim$ 6.5), stetite ($MgSiO_3$) ($\sim$ 6.5), zircon ($\sim$ 8.8) [47]. Addition of Al_2O_3 to $(MgCa)TiO_3$ is likely to lead to the formation of $MgAl_2O_4$ as a major phase. The addition of Al_2O_3 to $(MgCa)TiO_3$ system with the formation of $MgAl_2O_4$ phase is proposed to be investigated in this work. The phases obtained on addition of different amounts of

Al_2O_3 are to be investigated and the dielectric properties of the resulting samples are to be measured and correlated with other parameters.

Chapter 2

Experimental Procedure

2.1 Sample Preparation

2.1.1 Specification of the starting materials as on the labels

I Magnesium Oxide (MgO)

('Baker Analysed' Reagant)

Formula Weight - 40.3

Appearance - White Powder

Adsorption (FDC Yellow No.4) mg/g - 17.8

Loss in Ignition - 2.1

II Calcium Carbonate,$CaCO_3$, (GR)

(Sarabhai M. Chemicals)

Molecular Weight - 100.09

Appearance - White Powder

III Titanium Oxide,TiO_2, (Anatase)

(Fluka Chemie AG, Switzerland)

Purity > 99%

Formula Weight - 79.00

Appearance - White granular powder

Gluhverlust < 0.5%

IV Alumina, Al_2O_3 (High Purity Alumina)

(Sumutimo Chemical Co., Tokyo)

Type AKP - 50

Molecular Weight - 101.96

Appearance - White granular powder

Particle Size -0.3μm

2.1.2 Loss in Weight on Heating of the Starting Materials

All the four starting materials were weighed separately and kept inside the oven for 15 hrs at 140 ^oC. After removing from the oven, the individual powders were weighed again. By this way the losses due to the absorption of moisture in starting materials was estimated. The moisture absorption in MgO, $CaCO_3$, TiO_2, and Al_2O_3 were (wt %) 3.6 %, 0.1 %, 0.57 % and 0.31 % respectively. Then, a weighed amount of each individual dried powder was heated separately in a furnace at 1200 ^oC for 4 hrs. From the weight of powders before and after heating, the loss in heating to high temperature (1200 ^oC) was obtained. High temperature losses in MgO. $CaCO_3$, TiO_2 and Al_2O_3 were 25.23 %, 43.91 %. 0.4 % and 0.41 % respectively. The loss in $CaCO_3$ (i.e. 43.91 %) was expected due to removal of CO_2 from $CaCO_3$. These losses were taken into account during the preparation of a particular batch.

2.1.3 Batch Composition, Calcination and Pressing

Samples were prepared so as to yield mixtures of $Mg_{0.95}Ca_{0.05}TiO_3$ with different volume fractions (0, 0.2, 0.4, 0.6, 0.8, 0.8, 0.9, 0.98 and 1.0) of $MgAl_2O_4$. These volume fractions were converted to mole fractions (as shown in Appendix A) so that the composition could be represented by the formula $((Mg_{0.95}Ca_{0.05})TiO_3)_x$ - $(MgAl_2O_4)_{1-x}$. The calculations of the required amounts of each powder for a particular composition is elaborated in Appendix A. For the preparation of a batch, the calculated amounts of the starting powders were taken. Then the powders were mixed in mortar pestle for 15-20 minutes. For proper mixing, some amount of propanol was added to the mixture and mixing was continued in the mortar pestle for another 40-45 minutes. After mixing with propanol, the resulting paste, still in the mortar, was dried in an oven for 2 hrs at 90 ^oC. It was ground for 5 to 10 minutes before calcination.

The above dried material was calcined for 4 hr at various temperatures (i.e. 1100, 1150, 1200 ^oC) separately. The powder was kept in a platinum crucible covered by a perforated Al_2O_3 lid. The heating and cooling rates were 5 ^oC per minute. The weight of material was measured before and after the calcination, to confirm that there is no significant weight loss beyond what is expected. All the possible precautions were taken during material transfer. In order to avoid the loss, the material was weighed with the crucible, without transferring.

The above calcined powder was ground in mortar pestle for 5-10 minute. Then 1% PVA solution (1gms of PVA in 100 ml distilled water) was added as a binder to the above material in amounts of 1 vol % / mass (x ml PVA solution to x gm of calcined powder). The PVA solution was mixed with the calcined powder, in the mortar pestle, for 20-25 minutes. Then it was dried for 40 minute, inside the oven at 90 ^oC, until nearly dry. The binderized powder was passed through a seive of size 70-80 mesh to get it in the form of granules.

Preweighed amount of powder was pressed into pellets. Mostly the amount of powder taken was about 1.75 gm which produced a sintered pellet 6 mm thick. The powder was

pressed into cyllindrical pellets (12 mm dia × 7.5 to 8 mm length) in a hydraulic hand press using high chromium steel die. Pressure was applied steadily and slowly; after attainment of maximum load of 24 KN, 2 minutes were allowed before release of load in order to homogenize the pressure. The pressure used was thus 212 MPa.

2.1.4 Binder Removal and Sintering

The pellets as prepared above were heated to 600 ^oC at 3 $^oCmin^{-1}$ and held for 3 hrs for the removal of binder.

For sintering a furnace with silicon carbide heating elements was used. Two to three pellets were placed on an alumina plate. The pellets were separated by fused alumina from the plate. The plate with the pellets was raised into the furnace. The soak time of sintering was 2 hrs at 1400 ^oC. The heating and cooling rates were 5 $^oCmin^{-1}$.

2.2 Characterization

2.2.1 Density and Phases

The crystalline phases in the calcined powders and sintered pellets were determined by X-ray powder diffraction with monochromatic (Ni filter) $CuK\alpha$ radiation (Reich Seifert Iso-Debyefley 2002, $\lambda = 1.5405\ A^o$). The densities of sintered pellets were calculated by measuring the geometrical dimensions and the mass of the pellets.

2.2.2 Dielectric Properties

For dielectric constant measurement at 13 MHz, 1mm thick disks with parallel faces were sliced from the pellets using a low speed diamond saw. Both side of the disks were coated with a silver paste (Eltecks Corporation, Bangalore, 1228). The silver paste was cured at 120 ^oC for 2 hrs.

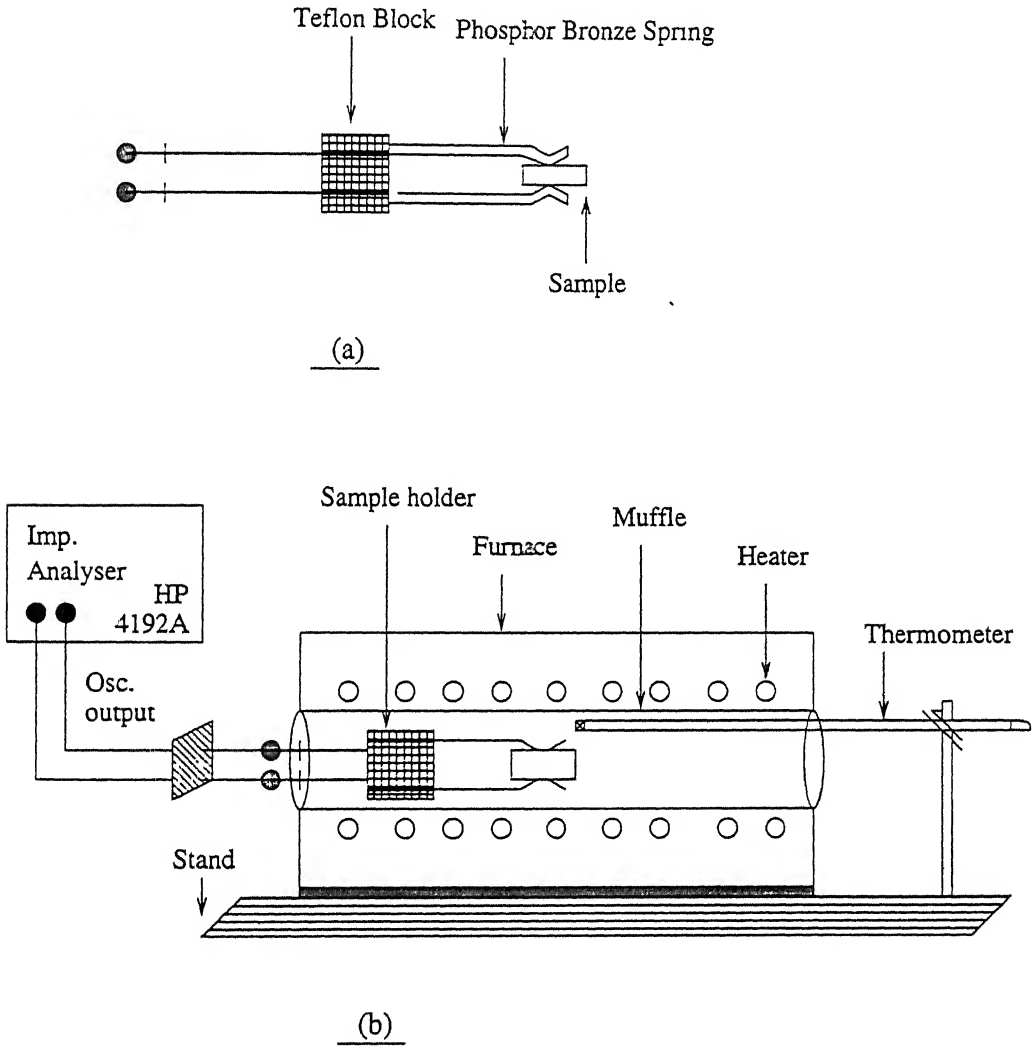

Figure 2.1: (a) Schematic diagram of sample holder, (b) Schematic arrangement for dielectric constant and TCC measurement.

Table 2.1: Linear coefficient of thermal expansion for various phases.

Si.No.	Phases	α	Ref.
1	$MgTiO_3$(MT)	7.5 - 8.5	50
2	$CaTiO_3$(CT)	9	50
3	$MgAl_2O_4$(MA)	6.6	50

The silver plated disk was held in a holder shown in Fig - 2.1 and its capacitance at 13 MHz measured using impedance analyser (Model HP 4192A). The relative permittivity was calculated using the formula :

$$c = \epsilon_r \epsilon_0 \frac{\pi d^2}{4t} \Rightarrow \epsilon_r = \frac{4ct}{\pi \epsilon_0 d^2} \tag{2.1}$$

Where ϵ_0 is permittivity of free space, c is capacitance of the disk and 't' and 'd' are the thickness and diameter of the sample respectively. The impedance analyser was also used for the measurement of temperature coefficient of capacitance (TCC). The TCC was measured from room temperature to 75 - 80 ^oC. It was calculated by the formula

$$TCC = \frac{1}{C(T_1)} \frac{C(T_2) - C(T_1)}{T_2 - T_1} \tag{2.2}$$

Where $C(T_1)$ and $C(T_2)$ are the capacitances at room temperature T_1 and at a higher temperature T_2 (75-80 ^oC). The temperature coefficient of resonant frequency (TCF) was calculated by using the relation [4]

$$TCF = -\frac{1}{2}(TCC + \alpha) \tag{2.3}$$

Where α is the linear coefficient of thermal expansion. The value of α for various phases are given in Table 2.1

The quality factor (Q) and dielectric constant of each sample were also measured at mi-

crowave frequencies (5 to 10 GHz), by using a parallel-plate method combined with network analyser and a computer (at ACES, IIT Kanpur). The measurement procedure is described in chapter - 1. For the measurement of quality factor, the sample diameter to thickness ratio was maintained between 2 - 2.5 . The dielectric constant measured at 13 MHz by impedance analyser and at 5 to 10 GHz with network analyser were found to have nearly same values within the experimental error.

2.2.3 Lattice Parameter Determination

For lattice parameter determination only the high angle peaks ($2\theta > 55^o$) were used [48]. The peaks were indexed using the standard X-ray data. The lattice parameter of both the cubic and rhombohedral (hexagonal) systems were calculated as follows.

Cubic System ($MgAl_2O_4$)

The general formula used for lattice parameter calculation of cubic system is

$$a = \frac{\lambda}{2\sin\theta}\sqrt{h^2 + k^2 + l^2} \tag{2.4}$$

Where 'a' is lattice parameter and 'θ' is diffraction angle, λ is wavelength of X-ray radiation and hkl are miller indices of diffracting planes.

For all angles above 55^o, lattice parameter 'a' values were calculated and then these calculated values were plotted against $\cos^2\theta$. The most accurate value 'a_0' was found by extrapolating the plot to a value of $\cos^2\theta \simeq 0$, as θ approaches 90^o.

Rhombohedral System ($MgTiO_3$)

$MgTiO_3$ has rhombohedral crystal structure. As is well known [48] the lattice points of rhombohedral cell may also be reffered to a hexagonal cell. From the X-ray diffractogram, first the lattice parameters (a_H, c) of the equivalent hexagonal lattice are determined. In

the standard data file these lattice parameters based on hexagonal lattice are given. The parameters (a_R, α) of rhombohedral system can be determined by using the following rlation.

$$a_R = \frac{1}{3}\sqrt{3a_H^2 + c^2} \tag{2.5}$$

$$\sin\frac{\alpha}{2} = \frac{3}{2}\sqrt{3 + (c/a_H)^2} \tag{2.6}$$

But in general, the formula used for lattice parameter calculation in hexagonal systems are

$$a_H = \frac{\lambda}{\sin\theta}\sqrt{\frac{(h^2+k^2+l^2)}{3} + \frac{l^2}{4}\left(\frac{c}{a}\right)^2} \tag{2.7}$$

$$c = \frac{\lambda}{sin\theta}\sqrt{\left(\frac{c}{a}\right)^2\frac{(h^2+k^2+l^2)}{3} + \frac{l^2}{4}} \tag{2.8}$$

The accurate lattice parameters in this system were obtained by succesive approximations. At first the approximate values a_1 and c_1 of the lattice parameters from the positions of two highest angle lines, were calculated. The approximate axial ratio c_1/a_1 was then calculated and used in equation (2.7) to determine an 'a' value for each highest-angle line on the pattern. These values of 'a' were then extrapolated against $cos^2\theta$ to find a more accurate value of a, say a_2. By the similar way the value of c_2 was calculated. Then by using the ratio of c_2/a_2, the whole process of calculation of 'a' and 'c' was repeated. This repeated process was continued for five succesive times to get more accurate value of 'a' and 'c'. The calculation was done, using a computer programme given in Appendix D.

2.2.4 Microstructure Studies by Scanning Electron Microscope (SEM)

For the study of microstructure, the sintered pellets of different compositions were polished to $0.25\mu m$. The procedure of polishing of samples are as follows.

(i) Polished with SiC ($2\mu m$) powder with water, on glass plate, for 30 minutes.

(ii) Polished with $Al_2O_3(1\mu m)$ powder with water, on glass plate, for 30 minutes.

(iii) Polished with diamond paste ($3\mu m$) with hifin fluid, on glass plate, for 30 minutes.

(iv) Polished with diamond paste ($3\mu m$) with hifin fluid, on micro polishing cloth, for 30 minutes.

(v) Polished with diamond paste ($1\mu m$) with hifin fluid, on micro polishing cloth, for 30 minutes.

(vi) Polished with diamond paste ($0.25\mu m$) with hifin fluid. on micro polishing cloth, for 30 minutes.

The polished pellets were cleaned with acetone by using ultrasonic dismembrator. After cleaning, the pellets were etched chemically by using a $1HF : 1HNO_3$ solution and then thermally etched at 1300 ^oC for 20 minutes. The etched samples were coated with Au-Pd by sputtering. Finally the microstructure were observed by scanning electron microscopy (SEM).

Chapter 3

Results and Discussion

In the present study synthesis of $((Mg_{0.95}Ca_{0.05})TiO_3)_x - (MgAl_2O_4)_{1-x}$ ceramics abbreviated henceforth as MTA(v), where v is the corresponding volume fraction of $MgAl_2O_4$). using the mixed powder route and their characterization have been carried out. The results are presented in this chapter together with relevent discussion.

The present study can be categorized into three parts. In the first one, optimization of calcination temperatures of MT and MTA powders is covered. The second part comprises of the processing of different compositions, varying from MT to $MgAl_2O_4$. In the third and final part, the characterization studies on the synthesized systems using X-ray diffraction (XRD), scanning electron microscope (SEM) and dielectric measurements are covered.

3.1 Optimization of Calcination Temperature

Powders of various compositions were calcined at different temperatures for 4 hours each as discussed in Chapter-2. The calcined powders were ground in a mortar pestle for 20 - 30 minutes, before further processing. Fig 3.1(a) and (b) show particle size distributions of the calcined powders of two compositions $MgAl_2O_4$ (0.4 and 0.6), after calcination at 1150 ^oC and after grinding in the mortar pestle. The powders calcined at 1100 ^oC and 1200 ^oC had similar particle size distributions. Apart from minor variations there is not much difference

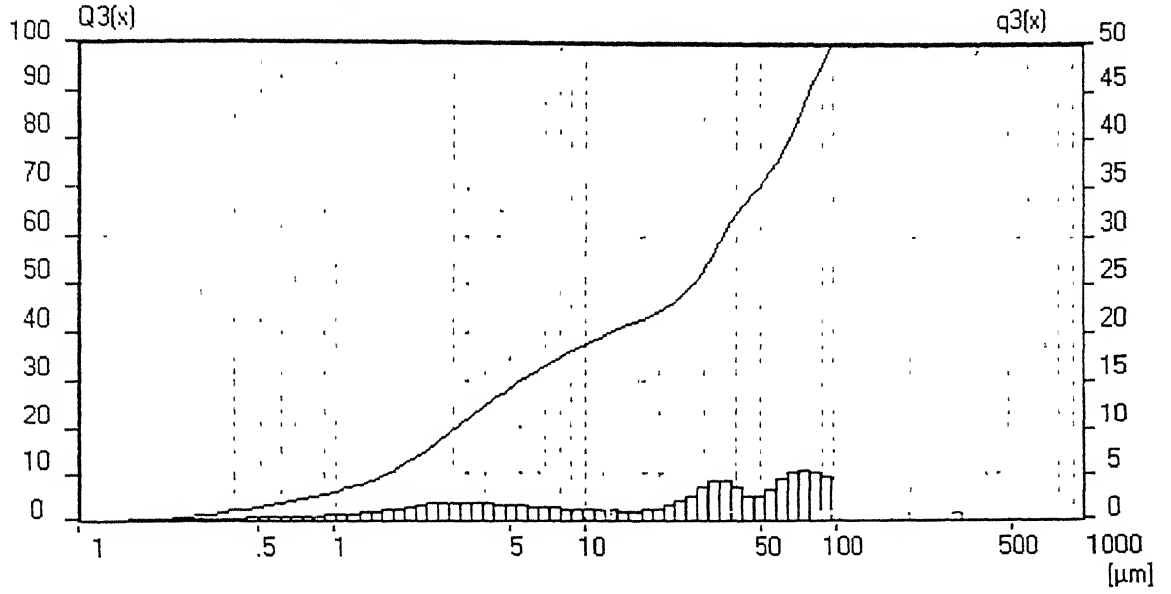

(a)

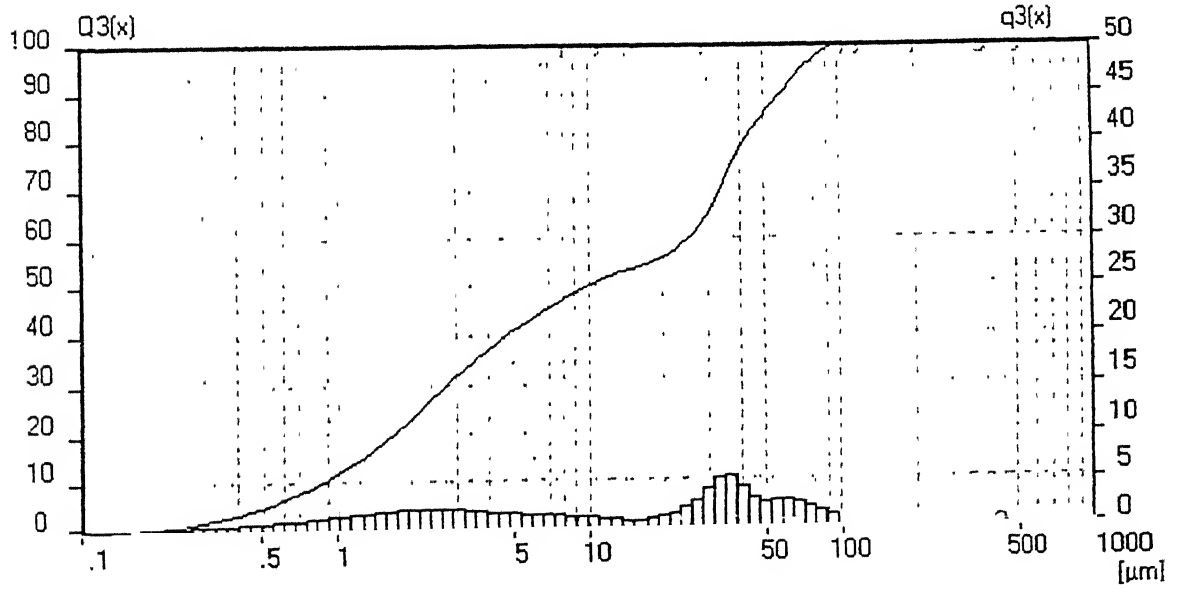

(b)

Figure 3.1: Particle size distributions of (a) MTA(0.4) and (b) MTA(0.6), powders calcined at 1150^oC and ground in mortar pestle.

in the particle size distributions. The distribution is flat with average particle size (d_{50}) of about $10\mu m$.

3.1.1 Phases in the Calcined Powders

Phases in the calcined powders were determined from the X-ray diffractograms using the standard X-ray data, for the various possible phases like $MgTiO_3$, $CaTiO_3$, Mg_2TiO_4, $MgTi_2O_5$, Al_2TiO_5, $MgAl_2O_4$, Al_2O_3, TiO_2, MgO. This data is reproduced in Table 3.1 to 3.9. All the X-ray data from Table. 3.1 - 3.9 is combined in an ascending order of 2θ in Table. 3.10.

The phases obtained in the powders of different compositions calcined under different conditions are shown in Table 3.11. $MgTiO_3$ and $CaTiO_3$ phases are obtained in all the compositions upto a volume fraction of 0.8 of $MgAl_2O_4$. At higher aluminate contents these phases progressively disappear and increased amounts of $MgAl_2O_4$, MgO and Al_2O_3 are obtained. Even for an aluminate content less than 0.8, the reaction is not complete and unreacted Al_2O_3 and TiO_2 are present. In addtion trace amounts of Mg_2TiO_4 (M_2T) are obtained at these compositions. Few representative X-ray charts are shown in Fig. 3.2 - 3.5.

3.1.2 Density Determination

Sintered pellets were prepared from these calcined powders (sintering temperature 1400 ^oC, 2hrs) and their densities determined. These are given in Table 3.12. The theoretical densities of all compositions are given in Appendix B.

From the results given in Table 3.11, it is seen that the highest density is obtained when the calcination temperature 1150 ^oC. Hence this temperature was used for calcination for all compositions.

Table 3.1: Standard X-ray data of $MgTiO_3$ phase.

06-0494 Wavelength= 1.54056 1

$MgTiO_3$

Magnesium Titanium Oxide

Geikielite, syn

2θ	Int	h	k	l	2θ	Int	h	k	l
19.112*	30	0	0	3	94.050*	2	1	1	12
21.238*	30	1	0	1	96.079*	2	4	0	4
24.012*	45	0	1	2	95.757*	2	1	0	13
32.877*	100	1	0	4	101.456	6	3	1	8
35.495*	55	1	1	0	105.405	4	0	1	14
40.643*	70	1	1	3	105.983	6	3	2	4
43.253*	10	2	0	2	107.493	6	4	1	0
49.154*	40	0	2	4	110.833	4	4	1	3
50.403*	4	1	0	7	112.576	2	0	4	8
53.614*	55	1	1	6					
55.901*	6	2	1	1					
56.981*	12	0	1	8					
62.082*	30	2	1	4					
63.164*	6	0	2	7					
63.724*	40	3	0	0					
67.201*	2	3	0	3					
68.962*	2	2	0	8					
71.109*	14	1	0	10					
71.563*	8	1	1	9					
74.622*	4	2	1	7					
75.134*	10	2	2	0					
78.373*	4	2	2	3					
79.194*	2	1	3	1					
80.041*	6	1	2	8					
82.051*	6	0	2	10					
84.448*	12	1	3	4					
87.639*	10	3	1	5					
87.956*	10	2	2	6					
90.890*	2	0	4	2					
92.740*	14	2	1	10					

Sys.: Rhombohedral S.G.: $R\bar{3}$ (148)

a: 5.054 b: c: 13.898 A: C: 2.7499

α: β: γ: Z: 6 mp:

Ref: Ibid

Dx 3.895 Dm: 4.050 SS/FOM: F_{30}=45(.0155, 43)

ε: nωβ: 2.31 εγ 1.95 Sign: - 2V:

Ref: Dana's System of Mineralogy, 7th Ed., I. 535

Color: Colorless

Pattern taken at 26 C. Optical data on specimen from Ceylon.

CAS #: 1312-99-8. Spectroscopic analysis of sample: <0.1%

Ca: <0.01% Cu, Fe, Si; <0.0001% Ba, Mn. Corundum group.

Ilmenite subgroup PSC: hR10. Mwt. 120.20. Volume[CD]. 307.44.

Table 3.2: Standard X-ray data of $CaTiO_3$ phase.

22-0153 Wavelength= 1.54056

CaTiO3

Calcium Titanium Oxide

Perovskite, syn

Rad. CuKα1 λ 1.5405 Filter: Mono d-sp:

Cut off Int. Diffract. I/Icor. 2.60

Ref: Natl. Bur. Stand. (U.S.) Monogr. 25, 9, 17 (1971)

Sys: Orthorhombic S.G.: Pnma (62)

a 5.4405 b 7.6436 c 5.3812 A 0.7118 C 0.7040

α β γ Z 4 mp

Ref: Ibid

Dx 4.036 Dm 4.030 SS/FOM: F_{30}=49(.0152, 40)

εα. ηωβ: 2.38 εγ: Sign. 2V:

Ref: Winchell, Elements of Optical Mineralogy, 2, 92 (1951)

Color: Yellowish white
Pattern taken at 25 C. Prepared by mixing equimolar amounts of CaO + TiO2 and pelletizing at 5000 pounds per inch -2. The pellets were heated to 1000-1200 C for 4 hours in an oxidizing atmosphere. Perovskite group, perovskite subgroup. Tungsten used as an internal stand. PSC: oP20. Mwt: 135.98
Volume[CD] 223.78

2θ	Int	h	k	l	2θ	Int	h	k	l
23.242*	14	1	0	1	63.380*	1	0	3	3
26.009*	3	1	1	1	65.463*	1	3	3	1
32.914*	40	2	0	0	68.979*	3	4	0	0
33.140*	100	1	2	1	69.452*	11	2	4	2
34.980*	1	2	1	0	69.848*	5	0	0	4
36.993*	1	2	0	1	70.218*	2	4	1	0
37.232*	2	1	0	2	71.463*	1	4	0	1
38.905*	4	2	1	1	72.311*	1	1	0	4
39.080*	7	0	3	1	73.077*	1	2	5	1
40.662*	6	2	2	0	73.241*	1	1	5	2
40.971*	4	0	2	2	74.130*	1	3	4	1
42.590*	2	1	3	1	75.527*	1	3	1	3
44.141*	2	2	2	1	77.131*	1	1	2	4
44.369*	1	1	2	2	78.781*	2	4	0	2
47.541*	50	0	4	0	79.171*	7	1	6	1
48.929*	2	2	3	0	79.907*	1	4	3	0
49.041*	3	2	1	2	80.334*	1	2	5	2
52.005*	1	2	3	1	80.570*	1	2	1	4
52.164*	1	1	3	2	83.024*	1	1	3	4
52.357*	1	0	1	3	84.822*	1	3	5	1
53.243*	2	3	0	1	85.024*	1	3	3	3
53.546*	3	1	4	1	85.218*	1	1	5	3
53.784*	2	1	0	3	88.086*	2	4	4	0
54.722*	3	3	1	1	88.895*	2	0	4	4
55.186*	1	1	1	3	89.327*	1	4	3	2
58.887*	14	3	2	1	92.068*	1	0	7	1
59.052*	16	2	4	0	92.448*	1	5	0	1
59.303*	25	0	4	2	93.620*	1	5	1	1
60.501*	1	2	3	2	95.272*	1	4	2	3
61.898*	1	1	4	2	95.635*	1	3	2	4
63.192*	1	0	5	1	97.135*	1	5	2	1

2θ	Int	h	k	l
97.516*	3	4	4	2
97.606*	4	3	6	1
98.056*	5	1	6	3
98.393*	6	1	2	5
103.036	1	5	3	1
107.297	2	4	0	4
107.444	1	0	8	0
108.503	1	4	1	4
111.695	1	5	4	1
112.225	1	4	2	4
113.042	1	5	1	3
113.419	1	3	7	1
116.344	1	6	0	0
116.898	1	5	2	3
117.459	4	3	6	3
117.775	4	3	2	5

Table 3.3: Standard X-ray data of $MgAl_2O_4$ phase.

21-1152 Wavelength= 1.5405

MgAl2O4

Magnesium Aluminum Oxide

Spinel, syn

Rad. CuKa1 λ. 1.5405 Filter Mono d-sp

Cut off Int : Diffract. I/Icor · 1.70

Ref· Natl Bur. Stand (U.S.) Monogr. 25, 9, 25 (1971)

Sys Cubic S.G.: Fd3m (227)

a 8.0831 b: c: A· C

α, β: γ: Z: 8 mp:

Ref. Ibid.

Dx: 3.579 Dm: SS/FOM: F_{29}=58(.0151, 33)

εα· ηωβ· 1.718 εγ: Sign: 2V·

Ref· Ibid

Color: Colorless
Pattern taken at 25 C. The sample was furnished by H.R. Shell, Bureau of Mines, College Park, MD, USA. CAS #: 1302-67-6. Shell used a carbon electrode furnace and removed an excess of MgO with hot HCl after crushing. Spinel group, spinel subgroup. Silver used as an internal stand. PSC: cF56. Mwt: 142.27. Volume[CD]· 528.12

2θ	Int	h	k	l
19.029*	35	1	1	1
31.271*	40	2	2	0
36.852*	100	3	1	1
38.524*	4	2	2	2
44.832*	65	4	0	0
55.658*	10	4	2	2
59.370*	45	5	1	1
65.241*	55	4	4	0
68.640*	4	5	3	1
74.130*	4	6	2	0
77.323*	8	5	3	3
78.403*	2	6	2	2
82.642*	6	4	4	4
85.759*	2	5	5	1
90.974*	6	6	4	2
94.096*	12	7	3	1
99.344*	8	8	0	0
107.904	2	6	6	0
111.226	8	7	5	1
112.317	2	6	6	2
116.919	6	8	4	0
120.504	2	9	1	1
121.697	<2	8	4	2
126.763	<2	6	6	4
130.733	8	9	3	1
138.066	18	8	4	4
142.981	<2	7	7	1
152.681	2	10	2	0
160.645	12	9	5	1

Table 3.4: Standard X-ray data of $MgTi_2O_5$ phase.

35-0792 Wavelength= 1.54056

MgTi2O5

Magnesium Titanium Oxide

Rad.: CuKa1 λ: 1.5405 Filter: Graph Mono. d-sp. Diffractometer

Cut off: Int.: Diffract. I/Icor.:

Ref: Natl. Bur. Stand. (U.S.) Monogr. 25. 21. 87 (1984)

Sys.: Orthorhombic S G.: Bbmm (63)

a: 9.7501(6) b: 9.9802(6) c: 3.7483(3) A: 0.9769 C: 0.3756

α: β: γ: Z: 4 mp:

Ref: Ibid.

Dx: 3.644 Dm. SS/FOM: F_{30}=113(.0078, 34)

Color: Gray
Peak height intensity. The mean temperature of data collection was 23.9 C. CAS #. 12032-35-8. The sample was prepared from basic magnesium carbonate and Ti O2 by repeated heatings with periodic grinding. Final reaction temperature was 1500 C and the sample was quenched in water. $\sigma(I_{obs})$= ±4. A tetragonal phase has been reported. Pseudobrookite. Fe2 O5 Ti type. Silicon. fluorophlogopite used as an internal stands. PSC. oC32. To replace 20-694. Mwt. 200.10. Volume[CD]: 364.74

2θ	Int	h	k	l	2θ	Int	h	k	l
17.763*	20	0	2	0	57.392*	6	6	1	0
18.173*	32	2	0	0	58.596*	5	2	6	0
20.255*	4	2	1	0	59.673*	37	2	3	2
25.436*	100	1	0	1	59.840*	20	4	5	0
26.983*	5	1	1	1	60.245*	25	5	3	1
31.208*	9	1	2	1	61.682*	8	1	6	1
32.559*	80	2	3	0	61.860*	3	0	4	2
35.974*	1	0	4	0	62.479*	3	4	0	2
36.558*	20	3	0	1	63.696*	5	6	3	0
36.845*	9	4	0	0	65.075*	7	2	4	2
37.267*	18	1	3	1	65.493*	11	4	2	2
37.692*	2	3	1	1	68.013*	7	3	6	1
37.949*	2	4	1	0	68.200*	3	4	6	0
40.579*	21	2	4	0	68.501*	4	2	7	0
41.208*	22	4	2	0	69.177*	13	4	3	2
44.573*	2	1	4	1	71.390*	5	1	7	1
45.903*	12	3	3	1	71.699*	10	2	5	2
46.129*	31	4	3	0	72.210*	3	5	5	1
48.548*	38	0	0	2	72.332*	3	7	0	1
49.294*	18	2	5	0	73.017*	6	7	1	1
52.077*	4	0	2	2	75.140*	9	7	2	1
52.243*	20	2	0	2	75.347*	5	6	5	0
52.756*	3	1	5	1	76.271*	2	0	8	0
52.894*	3	5	0	1	76.524*	8	0	6	2
53.125*	1	2	1	2	77.320*	<2	3	7	1
53.737*	4	5	1	1	77.506*	<2	4	7	0
55.156*	16	0	6	0	77.707*	<2	6	0	2
55.647*	3	2	2	2	78.414*	3	6	1	2
56.245*	18	5	2	1	78.663*	3	7	3	1
56.583*	3	6	0	0	79.443*	4	2	6	2

2θ	Int	h	k	l
81.176*	2	8	2	0
82.872*	3	3	0	3
83.084*	3	1	3	3
83.343*	2	3	1	3
83.489*	2	7	4	1
83.931*	3	6	3	2
87.657*	3	3	8	1
87.821*	2	4	8	0
88.845*	3	3	3	3

Table 3.5: Standard X-ray data of Mg_2TiO_4 phase.

25-1157 Wavelength= 1 54056

Mg2Ti04

Magnesium Titanium Oxide

Qandilite, syn

Rad CuKa1 λ: 1 5405 Filter: Mono d-sp:

Cut off: Int. Diffract. I/Icor: 2.10

Ref: Natl. Bur. Stand (U S.) Monogr. 25, 12, 25 (1975)

Sys: Cubic S.G.: Fd3m (227)

a 8 4409 b c: A C

α: β: γ: Z: 8 mp

Ref: Ibid.

Dx: 3 545 Dm: SS/FOM. F_{24}=87(.0099, 28)

Color: Colorless

Pattern taken at 25 C Prepared by heating together Ti 02 and Mg C 03 at 1380 C, grinding and reheating. Spinel group. spinel subgroup. Tungsten used as an internal stand. PSC: cF56. To replace 3 858. Mwt: 160 51. Volume[CD]: 601.40

2θ	Int	h	k	l
18 179*	45	1	1	1
29 899*	20	2	2	0
35.250*	100	3	1	1
36.883*	2	2	2	2
42 823*	60	4	0	0
46 890*	<1	3	3	1
53 143*	6	4	2	2
56 629*	30	3	3	3
62.165*	50	4	4	0
65.349*	3	5	3	1
70 502*	1	6	2	0
73 500*	6	5	3	3
74 512*	2	6	2	2
78.419*	5	4	4	4
81.336*	2	5	5	1
86.137*	1	6	4	2
89.007*	9	7	3	1
93.782*	5	8	0	0
101 484	1	6	6	0
104.422	6	7	5	1
105 420	1	6	6	2
109 402	3	8	4	0
112 483	1	9	1	1
117.775	1	8	8	4

Table 3.6: Standard X-ray data of Al_2TiO_5 phase.

41-0258 Wavelength= 1.54056

Al2TiO5

Aluminum Titanium Oxide

2θ	Int	h	k	l	2θ	Int	h	k	l
18.394*	15	0	2	0	62.088*	6	4	5	3
18.800*	66	2	0	2	62.346*	17	2	3	2
26.299*	29	2	2	0	62.386*	19	5	3	1
26.524*	100	1	0	1	64.176*	4	4	6	1
28.115*	6	1	1	1	64.642*	1	3	4	2
32.484*	3	1	2	1	65.206*	3	4	0	2
33.724*	88	2	3	0	66.062*	1	6	3	0
37.983*	9	3	0	1	67.978*	4	2	4	2
38.103*	16	4	0	0	68.197*	5	5	4	1
38.756*	6	1	3	1	68.397*	5	4	2	2
39.153*	1	3	1	1	70.782*	3	6	0	0
39.271*	2	4	1	0	70.861*	2	4	6	0
42.047*	19	2	4	0	71.217*	3	2	7	0
42.506*	8	3	2	1	71.550*	<1	6	4	0
42.625*	18	4	2	0	72.280*	1	4	3	2
46.312*	1	1	4	1	74.336*	2	1	7	1
47.667*	15	3	3	1	74.913*	3	2	5	2
47.773*	31	4	3	0	75.149*	2	5	5	0
50.793*	27	0	0	2	75.202*	2	7	0	1
51.107*	10	2	5	0	75.972*	3	7	1	1
54.270*	18	3	4	1	78.205*	3	7	2	1
54.347*	14	4	4	0	78.362*	3	6	5	2
54.460*	9	0	2	2	79.400*	<1	0	8	0
54.619*	4	2	0	2	80.024*	1	6	6	2
54.861*	2	1	5	1	80.396*	1	3	7	1
57.256*	11	0	6	0	80.672*	1	4	7	0
58.125*	2	2	2	2	80.841*	2	1	0	2
58.397*	13	3	2	1	81.932*	2	7	3	1
58.635*	7	6	0	0	81.932*	2	6	1	2
59.488*	3	6	1	0	82.252*	1	3	1	0
60.810*	3	2	6	0	83.102*	1	2	6	2
62.001*	6	6	2	0	83.335*	1	5	6	1
62.001*	6	3	5	1	84.460*	1	8	2	0

Rad: CuKa1 λ: 1.5405 Filter: Graph Mono d-sp: Diffractometer

Cut off: 15.0 Int.: Diffract. I/Icor.:

Ref: Syvinski, W., McCarthy, G., North Dakota State University, Fargo, North Dakota, USA. ICDD Grant-in-Aid, (1989)

Sys: Orthorhombic S.G.: Bbmm (63)

a: 3.439(2) b: 9.647(2) c: 3.5929(1) A: 3.9784 C: 0.3724

α: β: γ: Z: 4 mp: 2133

Ref: Ibid.

Dx: 3.692 Dm: SS/FOM: F30=147(.0059, 35)

Color: Tan

Peak height intensity. Sample prepared by mixing stoichiometric amounts of anatase and amorphous Al2 O3 and heating twice to 1573 K with one intermediate regrinding. Sample contained small amounts of rutile and corundum. Average relative standard deviation in intensity of the ten strongest reflections for three specimen mounts is 13%. Preferred orientation may be observed on the (230) and higher order reflections. Cell parameters refined from cell data by Holcombe and Coffey as: orthorhombic, a=3.591, b=9.429, c=9.626. S.G.=Cmcm(63), Z=4. Kennedyite type. Silicon used as an internal stand. PSC: oC32. Mwt: 181.86. Volume[CD]: 327.16.

2θ	Int	h	k	l
86.477*	<1	6	6	0
87.053*	1	7	4	1
87.439*	1	1	3	3
87.821*	1	6	3	2
88.120*	<1	8	3	0
89.899*	<1	3	2	3

Table 3.7: Standard X-ray data of Al_2O_3 phase.

10-0173

Wavelength= 1.54056

Al2O3

Aluminum Oxide

Corundum, syn

Rad.: CuKa1 λ: 1.5405 Filter: Ni Beta.M d-sp:

Cut off: Int.: Diffract. I/Icor.: 1.00

Ref: Natl. Bur. Stand. (U.S.), Circ. 539, 9, 3 (1960)

Sys.: Rhombohedral S.G.: R3c (167)

a: 4.758 b c: 12.991 A: C: 2.7303

α: β: γ: Z: 6 mp: 2050

Ref: Ibid

Dx: 3.989 Dm: 4.050 SS FOM: F_{30}=50(.0186, 32)

εα: 1.7604 ηωβ: 1.7666 εγ: Sign: - 2V:

Ref: Dana's System of Mineralogy, 7th Ed., I, 520

Color: Blue, colorless, yellow

Pattern taken at 26 C. Sample annealed at 1400 C for four hours in an Al2O3 crucible. Spectroscopic analysis showed <0.1% K, Na, Si, <0.01% Ca, Cu, Fe, Mg, Pb; <0.001% B, Cr, Li, Mn, Ni. Also called: ruby. Also called: sapphire. Al2O3 type. Corundum group, corundum subgroup. Also called: alumina. Also called: diamonite.PSC: hR10. Mwt: 101.96. Volume[CD]: 254.70.

2θ	Int	h	k	l	2θ	Int	h	k	l
25.584*	75	0	1	2	109.832	<1	1	2	11
35.136*	90	1	0	4	111.029	4	3	1	8
37.784*	40	1	1	0	114.126	4	2	2	9
41.683*	<1	0	0	6	116.141	14	3	2	4
43.362*	100	1	1	3	116.630	4	0	1	14
46.183*	2	2	0	2	117.901	3	4	1	0
52.551*	45	0	2	4	120.283	<1	2	3	0
57.518*	80	1	1	6	122.071	4	4	1	2
59.767*	4	2	1	1	124.647	2	0	4	8
61.164*	6	1	2	2	127.731	12	1	3	10
61.344*	8	0	1	8	129.916	4	3	0	12
66.547*	30	2	1	4	131.148	4	2	0	14
68.196*	50	3	0	0	136.162	22	1	4	8
70.357*	2	1	2	5	142.396	4	1	1	15
74.266*	4	2	0	8	145.208	11	4	0	10
76.880*	16	1	0	10	149.287	7	0	5	4
77.227*	8	1	1	9	150.244	14	1	0	16
80.692*	8	2	2	0	152.445	13	3	3	0
83.217*	<1	3	0	6					
84.375*	6	2	2	3					
85.181*	2	1	3	1					
86.375*	6	3	1	2					
86.461*	4	1	2	8					
89.018*	8	0	2	10					
90.662*	4	0	0	12					
91.201*	8	1	3	4					
95.260*	14	2	2	6					
98.407*	2	0	4	2					
101.092	12	2	1	10					
102.768	<1	1	1	12					
103.345	4	4	0	4					
109.522	<1	3	2	1					

Table 3.8: Standard X-ray data of rutile TiO_2 phase.

21-1276 Wavelength= 1.5405

TiO2

Titanium Oxide

Rutile, syn

Rad CuKa1 λ 1.5405 Filter: Mono d-sp

Cut off Int Diffract. I/Icor 3.40

Ref: Natl Bur Stand (U.S.) Monogr 25, 7 83 (1969)

Sys Tetragonal S.G.: $P4_2/mnm$ (136)

a 4.5933 b: c: 2.9592 A C 0.6442

α β γ Z 2 mp

Ref: Ibid

Dx: 4.250 Dm 4.230 SS/FOM: F_{30}=107(.0088, 32)

εα. 2.9467 nωβ: 2.6505 εγ: Sign. + 2V

Ref Dana's System of Mineralogy, 7th Ed., I. 575

Color: White
Pattern taken at 25 C. Sample obtained from National Lead Co., South Amboy, NJ, USA. No impurity over 0.001%. Two other polymorphs, anatase (tetragonal) and brookite (orthorhombic), converted to rutile on heating above 700 C. Optical data on specimen from Dana's System of Mineralogy, 7th Ed., I 555. Opaque mineral optical data on specimen from Sweden R3R%=20.3. Disp.=Std., VHN100=1132-1187. Ref.: IMA Commission on Ore Microscopy QDF. Pattern reviewed by Syvinski, W., McCarthy, G., North Dakota State Univ, Fargo, ND, USA ICDD Grant-in-Aid (1990). Agrees well with experimental and calculated patterns. Additional weak reflections [indicated by brackets] were observed. Naturally occurring material may be reddish brown. 02 Ti type. Rutile group, rutile subgroup. Also called titania. Tungsten used as an internal stand. PSC tP6. Validated by calculated pattern. Mwt: 79.90. Volume[CD]: 62.43.

2θ	Int	h	k	l
27.446*	100	1	1	0
36.085*	50	1	0	1
39.187*	8	2	0	0
41.225*	25	1	1	1
44.050*	10	2	1	0
54.322*	60	2	1	1
56.640*	20	2	2	0
62.740*	10	0	0	2
64.038*	10	3	1	0
65.478*	2	2	2	1
69.008*	20	3	0	1
69.788*	12	1	1	2
72.408*	2	3	1	1
74.409	1	[3	2	0]
76.508*	4	2	0	2
79.819*	2	2	1	2
82.333*	6	3	2	1
84.358*	4	4	0	0
87.461*	2	4	1	0
89.555*	8	2	2	2
90.705*	4	3	3	0
95.272*	6	4	1	1
96.014*	6	3	1	2
97.173*	4	4	2	0
98.511	<1	[3	3	1]
105.095	2	4	2	1
106.015	2	1	0	3
109.402	2	1	1	3
116.222	4	4	0	2
117.522	4	5	1	0
120.054	8	2	1	3
122.783	8	4	3	1
123.655	8	3	3	2
131.841	6	4	2	2
136.542	8	3	0	3
140.044	12	5	2	1
143.107	2	4	4	0
155.856	2	5	3	0

Table 3.9: Standard X-ray data of MgO phase.

45-0946

MgO

Magnesium Oxide

Periclase, syn

Rad CuKa1 λ 1.5405 Filter Ge Mono d-sp Diffractometer

Cut off Int: Diffract I/Icor: 1.0

Ref: Kern A., Doetzer, R., Eysel, W.
Mineralogisch-Petrographisches Inst., Univ. Heidelberg, Germany., ICDD Grant-in-Aid (1993)

Sys: Cubic S.G.: Fm3m (225)

a	b	c	A	C
4.2112				
α	β	γ	Z	mp
			4	

Ref. Ibid

Dx: 3.585 Dm: 3.560 SS/FOM: F_{10}=101(.0099, 10)

Color: Colorless
Integrated intensities. MgO (Heraeus, 99.99 %) annealed in open Au crucible at 800 C for 1 week. Validated by calculated pattern 43-1022. Cl Na type, Halite group, periclase subgroup. Silicon used as an internal stand. PSC: cF8. To replace 4-829. Mwt: 40.30. Volume[CD]: 74.68

2θ	Int	h	k	l
36.936*	4	1	1	1
42.916*	100	2	0	0
62.302*	39	2	2	0
74.689*	5	3	1	1
78.628*	10	2	2	2
94.018*	8	4	0	0
105.730	2	3	3	1
109.761	19	4	2	0
127.279	14	4	2	2
143.745	4	5	1	1

Table 3.10: X-ray data from Table 3.1 to 3.9 combined in the order of ascending 2θ

2 theta	Intensity	h	k	l	Phases
17.730	23	0	2	0	$MgTi_2O_5$
18.179	45	1	1	1	Mg_2TiO_4
18.210	24	2	0	0	$MgTi_2O_5$
18.394	15	0	2	0	Al_2TiO_5
18.800	66	2	0	0	Al_2TiO_5
19.052	35	1	1	1	$MgAl_2O_4$
19.112	30	0	0	3	$MgTiO_3$
21.238	30	1	0	1	$MgTiO_3$
23.390	40	1	0	0	$CaTiO_3$
24.012	45	0	1	2	$MgTiO_3$
25.281	100	1	0	1	TiO_2
25.478	100	1	0	1	$MgTi_2O_5$
25.584	75	0	1	2	Al_2O_3
26.399	29	2	2	0	Al_2TiO_5
26.524	100	1	0	1	Al_2TiO_5
28.115	8	1	1	1	Al_2TiO_5
29.899	20	2	2	0	Mg_2TiO_4
31.271	40	2	2	0	$MgAl_2O_4$
32.551	72	2	3	0	$MgTi_2O_5$
32.877	100	1	0	4	$MgTiO_3$
33.152	100	1	1	0	$CaTiO_3$
33.724	68	2	3	0	Al_2TiO_5
35.250	100	3	1	1	Mg_2TiO_4
35.495	55	1	1	0	$MgTiO_3$
36.651	15	3	0	1	$MgTi_2O_5$
36.922	10	4	0	0	$MgTi_2O_5$
36.946	10	1	0	3	TiO_2
37.237	16	1	3	1	$MgTi_2O_5$
37.784	40	1	1	0	Al_2O_3
37.800	20	0	0	4	TiO_2
37.982	9	3	0	1	Al_2TiO_5
38.105	10	4	0	0	Al_2TiO_5
38.575	10	1	1	2	TiO_2
40.536	17	2	4	0	$MgTi_2O_5$
40.643	70	1	1	3	$MgTiO_3$
40.990	40	1	1	1	$CaTiO_3$
41.236	21	4	2	0	$MgTi_2O_5$
42.047	19	2	4	0	Al_2TiO_5
42.508	8	3	2	1	Al_2TiO_5
42.628	18	4	2	0	Al_2TiO_5
42.823	60	4	0	0	Mg_2TiO_4
42.916	100	2	0	0	MgO
43.253	10	2	0	2	$MgTiO_3$
43.362	100	1	1	3	Al_2O_3
44.832	65	4	0	0	$MgAl_2O_4$

2 theta	Intensity	h	k	l	Phases
47.568	80	2	0	0	$CaTiO_3$
47.667	15	3	3	3	Al_2TiO_5
47.773	31	4	3	0	Al_2TiO_5
48.049	35	2	0	0	TiO_2
48.610	29	0	0	2	$MgTi_2O_5$
49.154	40	0	2	4	$MgTiO_3$
49.182	20	2	5	0	$MgTi_2O_5$
50.795	27	0	0	2	Al_2TiO_5
51.107	10	2	5	0	Al_2TiO_5
52.232	11	3	4	1	$MgTi_2O_5$
52.367	10	2	0	2	$MgTi_2O_5$
52.551	45	0	2	4	Al_2O_3
53.546	20	2	1	0	$CaTiO_3$
53.614	55	1	1	6	$MgTiO_3$
53.890	20	1	0	5	TiO_2
54.270	18	3	4	1	Al_2TiO_5
54.347	14	4	4	0	Al_2TiO_5
54.460	9	0	2	2	Al_2TiO_5
55.044	14	0	6	0	$MgTi_2O_5$
55.060	20	2	1	1	TiO_2
55.658	10	4	2	2	$MgAl_2O_4$
55.901	6	2	1	1	$MgTiO_3$
56.316	21	5	2	1	$MgTi_2O_5$
56.629	30	3	3	3	Mg_2TiO_4
56.981	12	0	1	8	$MgTiO_3$
57.250	11	0	6	0	Al_2TiO_5
57.518	80	1	1	6	Al_2O_3
59.177	80	2	1	1	$CaTiO_3$
59.370	45	5	1	1	$MgAl_2O_4$
59.609	18	3	5	1	$MgTi_2O_5$
59.726	28	2	3	2	$MgTi_2O_5$
60.328	25	5	3	1	$MgTi_2O_5$
61.164	6	1	2	2	Al_2O_3
61.344	8	0	1	8	Al_2O_3
62.082	30	2	1	4	$MgTiO_3$
62.165	50	4	4	0	Mg_2Ti_4
62.302	39	2	2	0	MgO
62.346	17	2	3	2	Al_2Ti_5
62.688	14	2	0	4	TiO_2
63.724	40	3	0	0	$MgTiO_3$
65.241	55	4	4	0	$MgAl_2O_4$
65.585	12	4	2	2	$MgTi_2O_5$
66.547	30	2	1	4	Al_2O_3
68.196	50	3	0	0	Al_2O_3
69.287	11	4	3	2	$MgTi_2O_5$
69.581	60	2	2	0	$CaTiO_3$

Table 3.11: Phases in the calcined powders. Abbreviations include: MT=$MgTiO_3$, CT=$CaTiO_3$, MA=$MgAl_2O_4$, M_2T=Mg_2TiO_4, MT_2=$MgTi_2O_5$, AT=Al_2TiO_5, s=small, t=trace, BM=ball milling.

Composition	Calcination temperature/ time ($^oC/h$)	Phases
MTA(0) MTCT	1150/4	MT, CT, MT_2, M_2T(t), TiO_2(s)
MTA(0.2)	1150/4	MT, CT, MA, Al_2O_3 (s), TiO_2 (s), M_2T (t), MT_2 (t)
MTA(0.4)	1150/4	MT, CT, MA, Al_2O_3(s), TiO_2 (s), M_2T (t), MT_2 (t), AT (t)
MTA(0.6)	1150/4	MT, CT, MA, Al_2O_3 (s), TiO_2 (t), M_2T (t), MT_2 (t), AT (t)
MTA(0.8)	1150/4	MT, CT(s), MA, Al_2O_3 (s), TiO_2 (t), M_2T (t), MT_2 (t), AT (t)
MTA(0.9)	1150/4	MT (s), CT (t), MA, Al_2O_3, MgO, AT (t)
MTA(0.98)	1150/4	MT (t), CT (t), MA, Al_2O_3, MgO
MTA(1.0)	1150/4	MA, MgO, Al_2O_3,
MTA(1.0)	1390/6	MA, MgO, Al_2O_3,
MTA(1.0) $MgAl_2O_4$	1390/6 BM 1390/6	$MgAl_2O_4$ (MA)

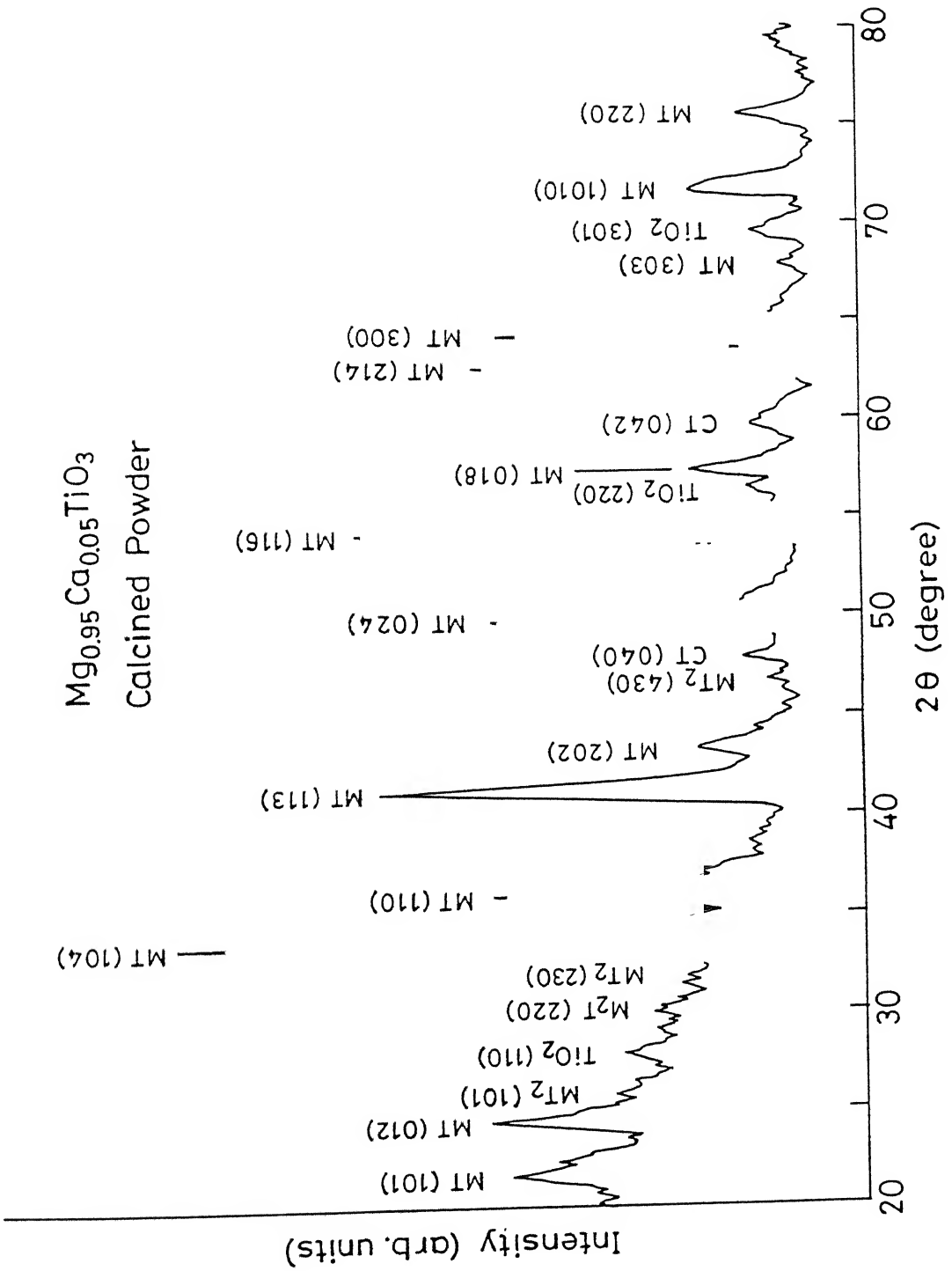

Figure 3.2: X-ray diffractogram from calcined powder MTA(0).

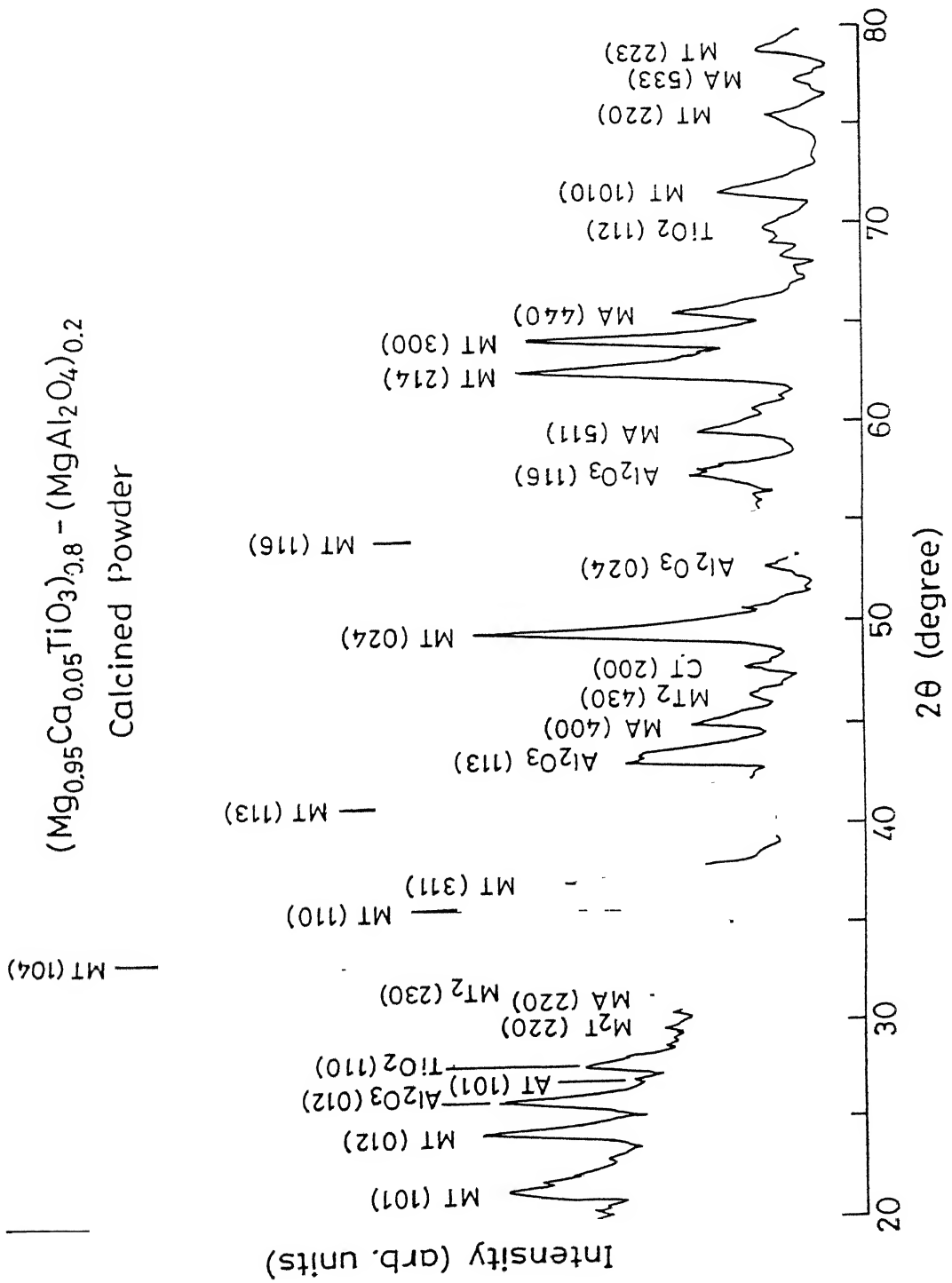

Figure 3.3: X-ray diffractogram from calcined powder MTA(0.2).

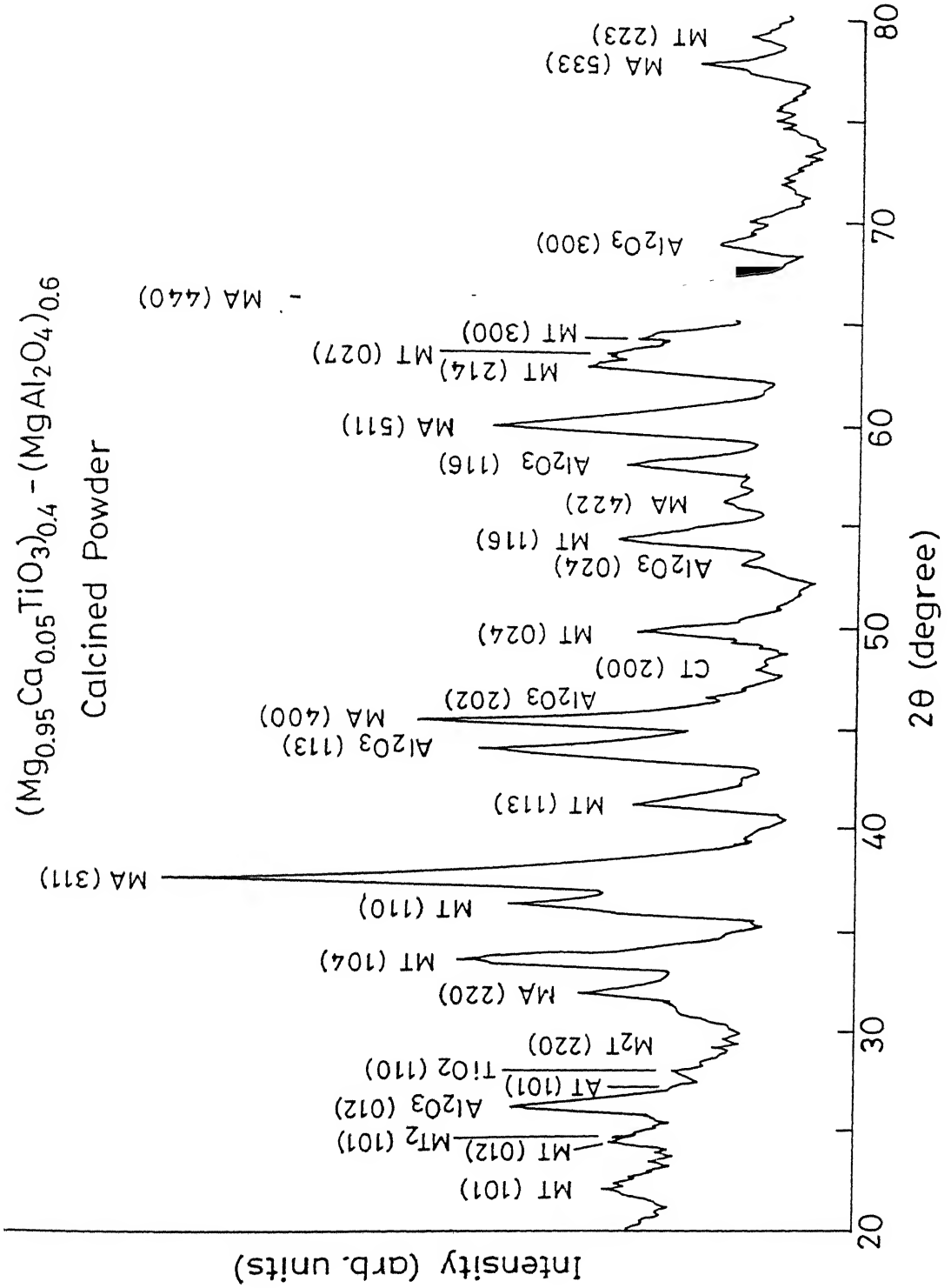

Figure 3.4: X-ray diffractogram from calcined powder MTA(0.6).

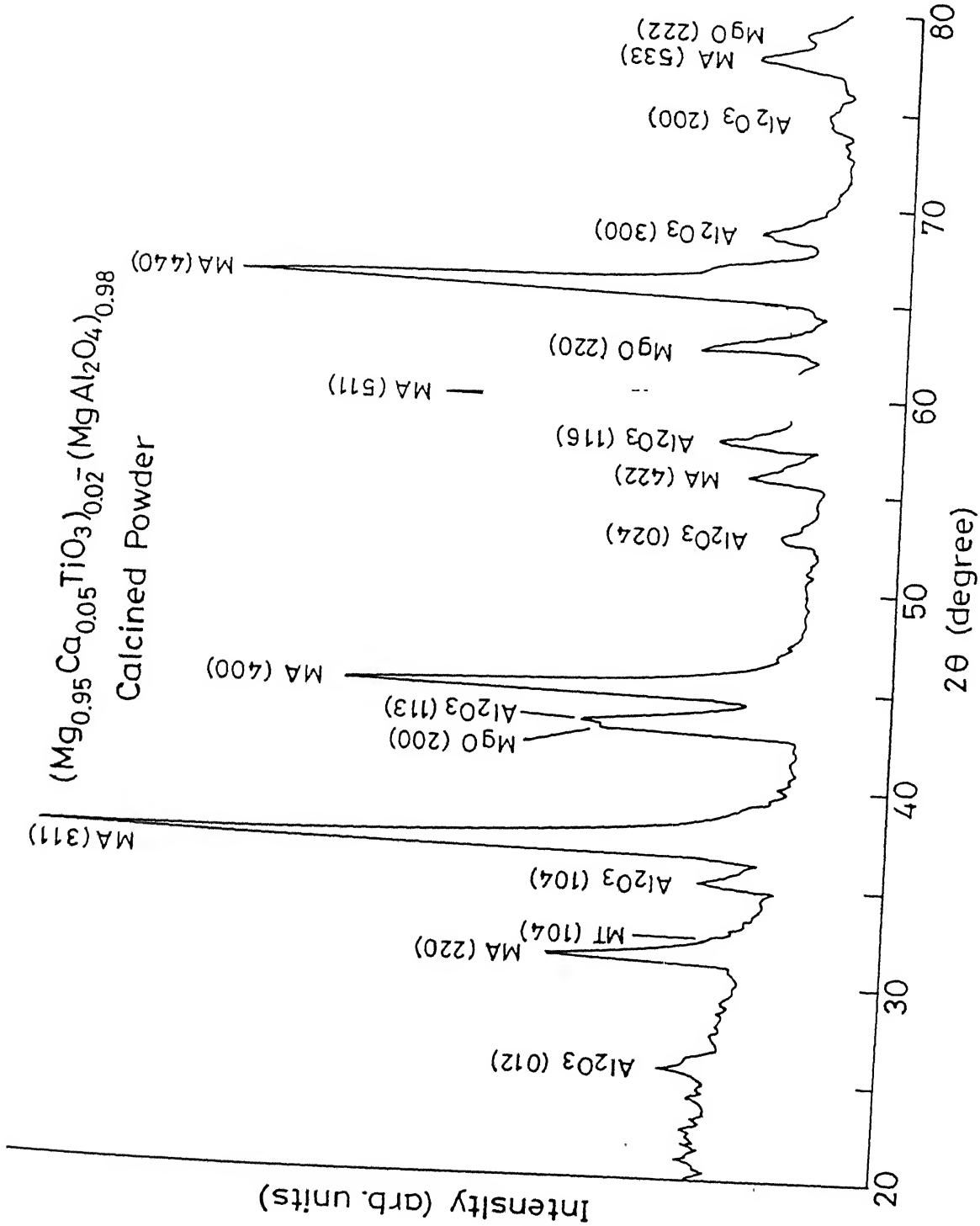

Figure 3.5: X-ray diffractogram from calcined powder MTA(0.98).

Table 3.12: Density of pellets sintered at 1400 ^oC, 2hrs from powders calcined for 4 hrs at different temperatures.

Calcination temperature(^{0}C)	Density gm/cc for volume fraction of MA		
	0	0.4	0.6
1100	89.2, 88.9 89.2	85.4, 85.4	86.9, 86.3 86.9, 85.2
1150	90.6, 90.8 91.0,	89.2, 92.5 91.2, 90.5	91.4, 91.5 91.3
1200	84.2, 84.0 84.6		87.6

3.2 Properties of Sintered Samples

Table 3.13 shows the properties of sintered samples of various compositions sintered at 1400 ^oC for 2 hrs. The density data is plotted in Fig. 3.6. It is seen that the densities of samples containing 0.98 and 1.00 volume fraction of $MgAl_2O_4$ are very low (e.g. 67.5 % and 53.9 % respectively). Also unreacted MgO and Al_2O_3 are present in significant amounts in the sintered samples as shown in Fig 3.12. Increasing the sintering time to 4 hrs, did not lead to any increase in density. It was found that, complete reaction between Al_2O_3 and MgO in $MgAl_2O_4$ composition took place only after calcination at 1390 ^oC for 6 hrs for two times each with an intermediate ball milling step for 4 hrs. However, this powder was too coarse for sintering.

The phases present in the sintered samples were determined in the same manner, as in the calcined powders. Some of the representative X-ray charts are given in Fig 3.7 - 3.12. It is observed that the composition MT contains some trace amount of M_2T phase. All the MTA compositions, upto 0.8 volume fraction contain trace amounts of TiO_2, AT, M_2T and small amounts of Al_2O_3 phases, with the main phases being $MgTiO_3$ and $MgAl_2O_4$. The MTA compositions above 0.9 $MgAl_2O_4$ contain large amounts of MgO and Al_2O_3 as

Table 3.13: Properties of MTA(v) samples sintered at 1400 ^{o}C, 2hr.

Volume fraction of $MgAl_2O_4$ (v)	Calcination Temperature °C /time (hrs)	Phases	Density (% th)	Dielectric constant MHz, GHz	TCF (ppm/°C)	Q	f (GHz)	Q f (GHz)
0.00	1100/4	MT,CT,M_2T(t)	89.2, 89.9, 89 2	18 6, 17 9	-9.3	2500	7 96	19900
	1150/4	MT,CT,M_2T(t),TiO_2(t), MT_2(t)	90 6, 90 8, 91.0	18.5, 18 4	-8 1	2182, 1830	7 99, 7 26	17434, 13286
	1200/4	MT,CT,M_2T(t), MT_2(t)	84 2, 84 0, 84 6	17 1, 16.6	-7	1130	8 21	92777
0.20	1150/4	MT,CT,MA, AT(t),M_2T(t),MT_2(t) Al_2O_3(t),TiO_2(t)	93 2, 92 5, 94 7, 95.3, 94 1, 94 8	16 9, 17 1, 17.4	-10 9	1260 2900	7 67 7 92	9664 22968
0 40	1100/4	MT,CT,MA, M_2T(t),Al_2O_3(s), TiO_2(t)	85 3, 85 3	12 7	- 6 83			
	1150/4	MT,CT,MA,MT_2(t),M_2T(t), Al_2O_3(s), TiO_2(t),AT(t)	92.5, 91 2, 90.5, 89.5	13.4, 14 1	-15 6	1950	8 38	16431
0 60	1100/4	MT,CT,MA, Al_2O_3(s), TiO_2(t),MT_2(t)	86.8, 86 3, 86 8 85 2	10 1	-55 23			
	1150/4	MT,CT, MT_2(t) MA,M_2T(t), AT(t), Al_2O_3(s),TiO_2(t)	91.4, 91.5, 91 3	12 3,12 4	-26 4	3400	9 67	32878
	1150/4,BM, 1150/4	MT,CT, MT_2(t) MA,M_2T(t), AT(t), Al_2O_3(s),TiO_2(t)	95 2, 95.2, 95.4, 95.5	12 7, 12 3	-23 15	1730	9 27	16037
	1200/4	MT,CT,MA, Al_2O_3(s),TiO_2(t), MT_2(t),AT(t)	87.5	10 8	-10			
0.80	1150/4	MT(s),CT(t), MA, Al_2O_3(s). TiO_2(t), AT(t), MT_2(t)	89.5, 90.0, 89.2, 89.8	9.6, 8 5	-33	1200	11 05	13260
0.90	1150/4	MT(s), CT(s), Al_2O_3(s), MA	92.0, 92.2, 91.7, 92.8	9.11, 8.7	-41	1400	11.25	15750
0.98	1150/4	MgO, Al_2O_3, MT(t), MA	66.1, 65.6, 67.5, 67.5	5 75	-67 1			
1.00	1150/4	MgO, Al_2O_3, MA	53.6, 53.6, 53.9					

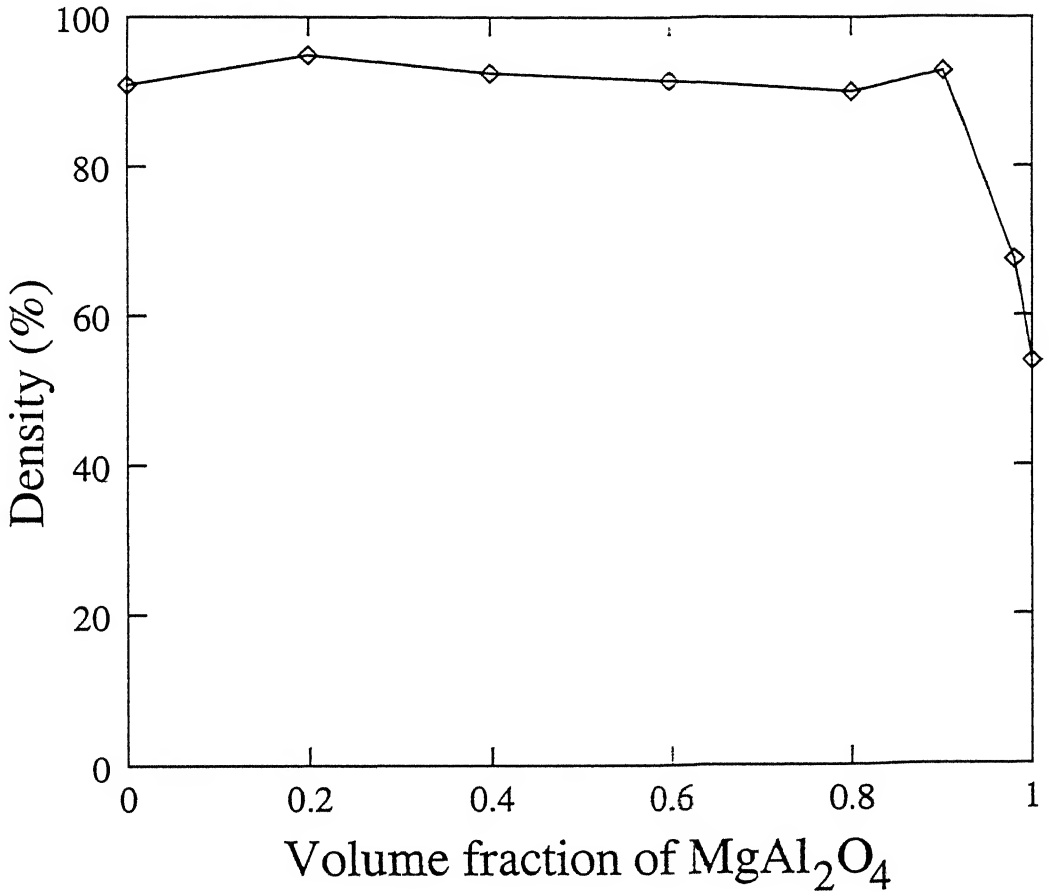

Figure 3.6: Variation of density with volume fraction of $MgAl_2O_4$

Table 3.14: Comparison of phases in our samples with data in reference [49]; the first line in each row is the composition of our samples and the second line is the nearest composition for which data is available.

MA	Wt %			T	Phases
(v)	MgO	Al_2O_3	TiO_2	(^oC)	
0.2	30	50	20	1285	Sp s.s. + $MgTiO_3$ + Psb s.s.
0.4	30	40	30	1285	Sp B + Psb + $MgTiO_3$
0.6	35	25	40	1115	Psb s.s. + Sp s.s.
0.8	30	10	60	1130	Sp s.s. + Psb s.s.

described earlier.

Boden et al [49] have investigated the phase relationship in the system MgO - Al_2O_3 - TiO_2. The subsolidus phase diagram for the system at 1300 ^oC is reproduced in Fig. 3.13. The various phases that are shown are as follows : Psb = Pseudobrookite; $MgTi_2O_5$ and Al_2TiO_5 are both isomorphous with pseudobrookite, Fe_2TiO_5. Here, pseudobrookite denotes a solid solution between $MgTi_2O_5$ (MT_2) and Al_2TiO_5 (AT).

Sp = Spinel; Mg_2TiO_4 and $MgAl_2O_4$ are spinels. They exist in the composition range from Mg_2TiO_4 to A and $MgAl_2O_4$ to B. The points A and B are reffered to as spinel A and spinel B.

The phases expected for various compositions according Fig. 3.13 are given in Table 3.14 and marked by the squares in the same figure. For composition MTA(0.2) and MTA(0.4), acording to Fig. 3.13, the phases should be Psb (Solid Solution of MT_2 and AT), $MgTiO_3$ (MT) and Sp B Experimentally we obtain mostly MT and MA with presence of M_2T, AT, MT_2, TiO_2, Al_2O_3. The Sp B corresponds to MA solid solution. Also it is known that Al_2TiO_5 decomposes to α Al_2O_3 and TiO_2 below 1267 ^oC. Thus the phases obtained are in resonable agreement with those expected from the figures. This is true for the other compositions also.

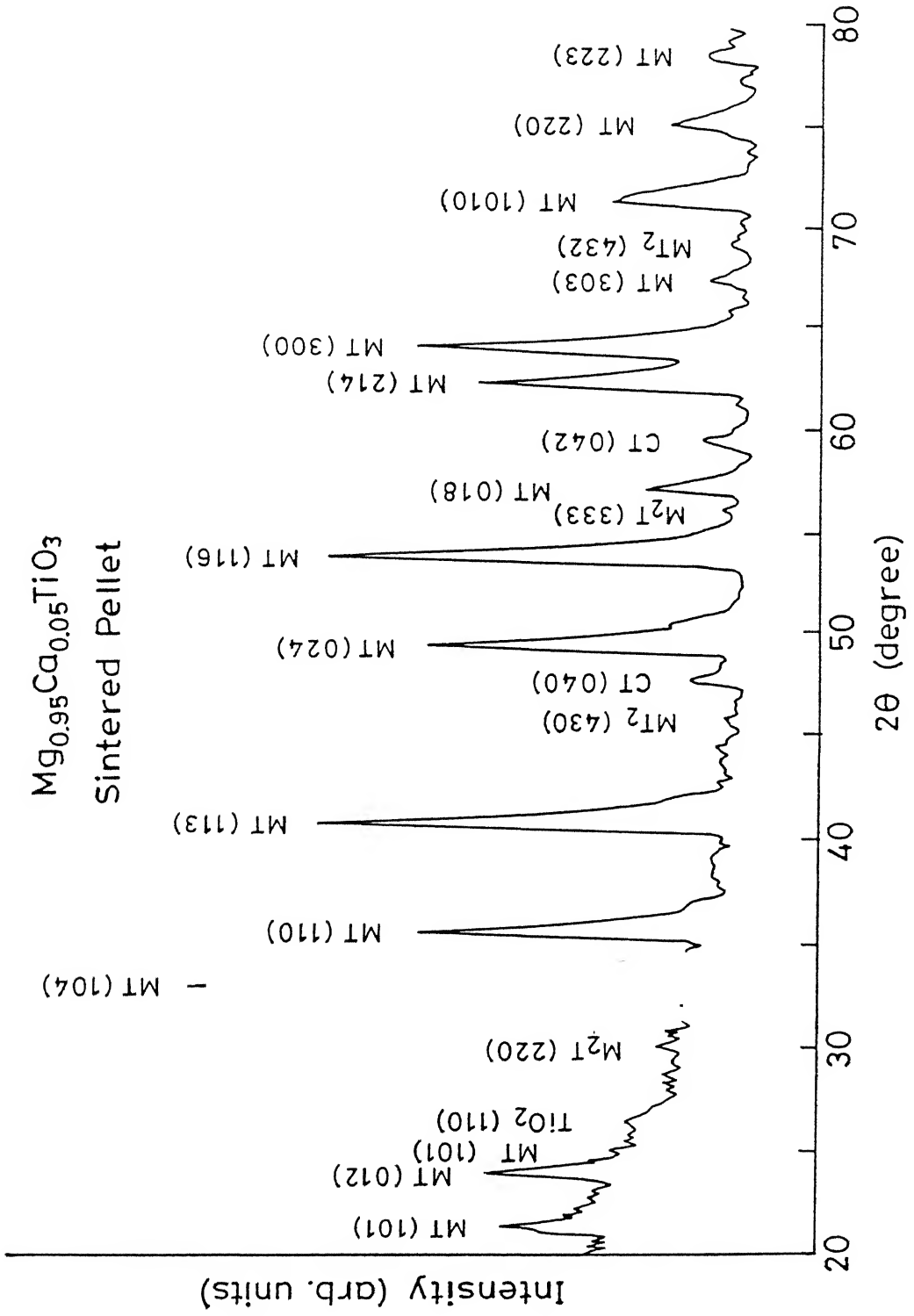

Figure 3.7: X-ray diffractograms of sintered pellet MTA(0).

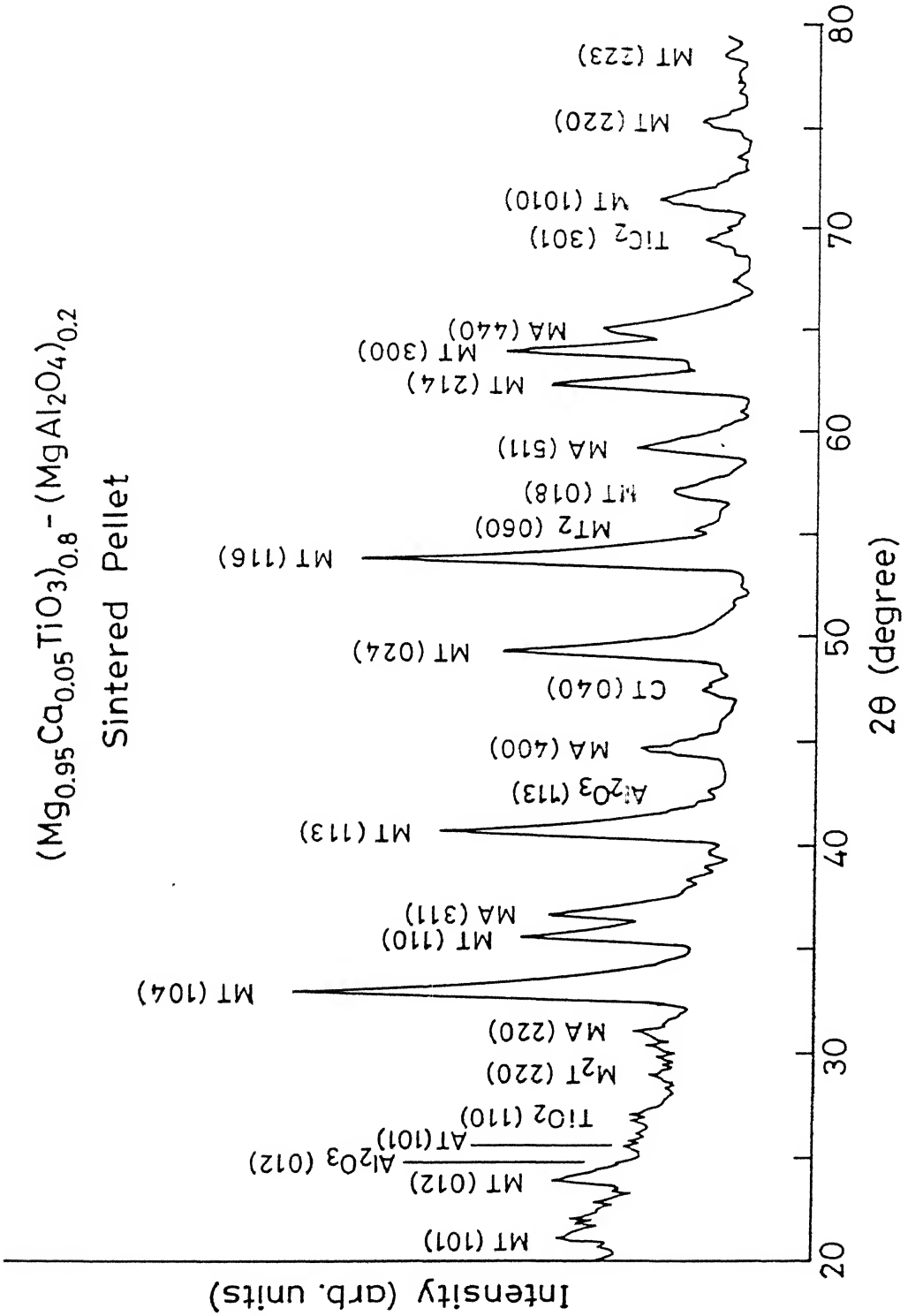

Figure 3.8: X-ray diffractograms of sintered pellet MTA(0.2).

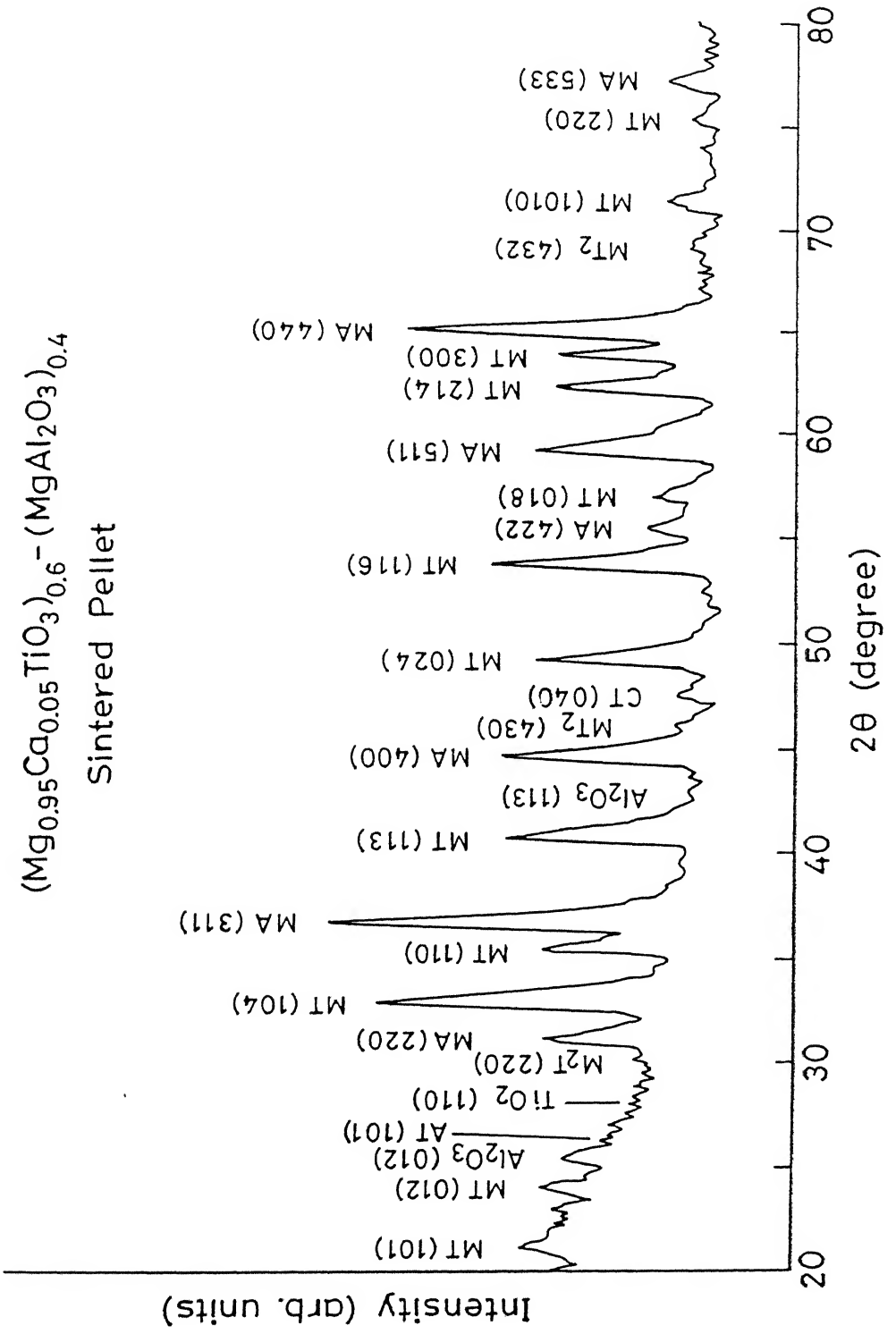

Figure 3.9: X-ray diffractograms of sintered pellet MTA(0.4).

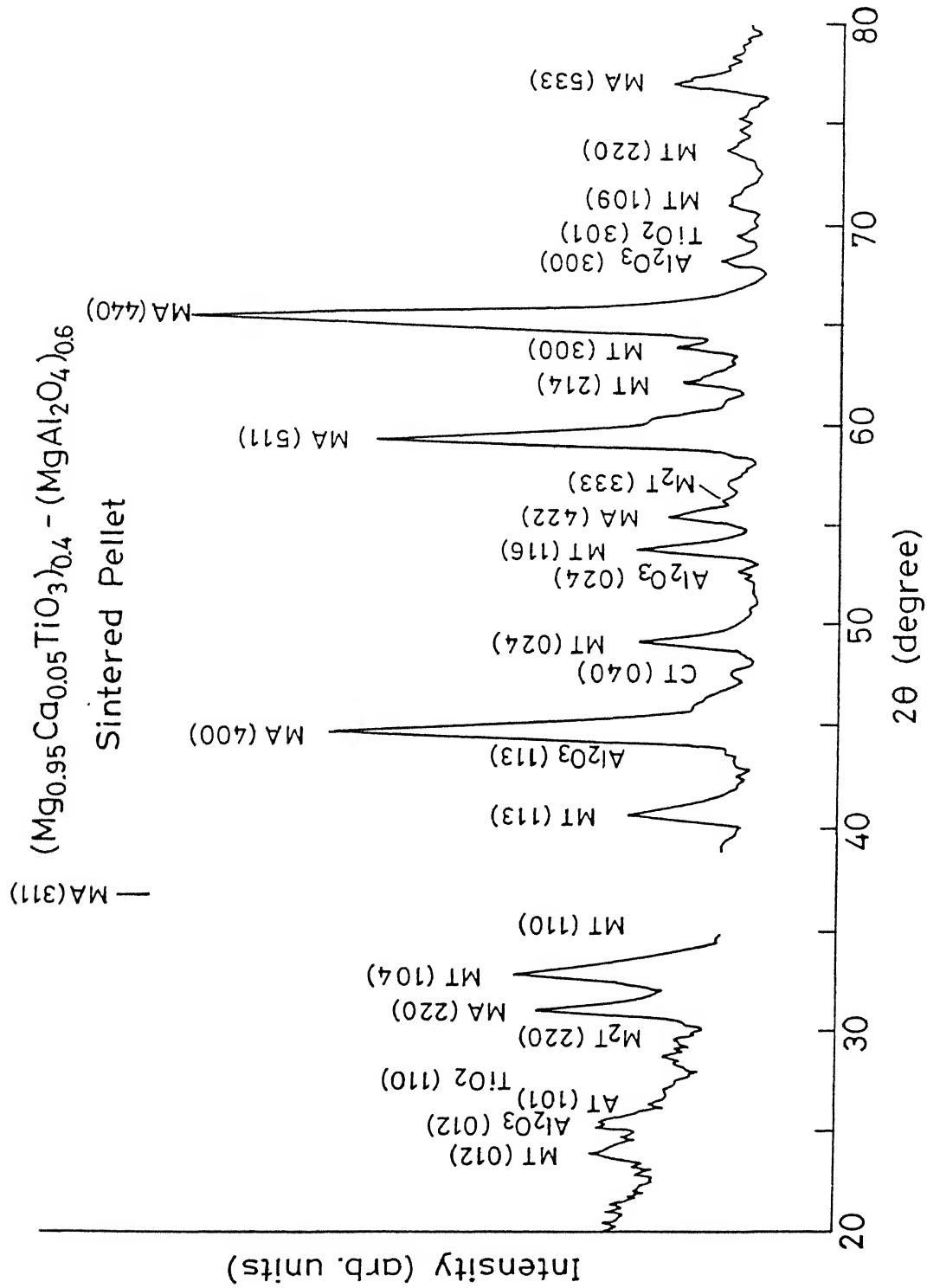

Figure 3.10: X-ray diffractograms of sintered pellet MTA(0.6).

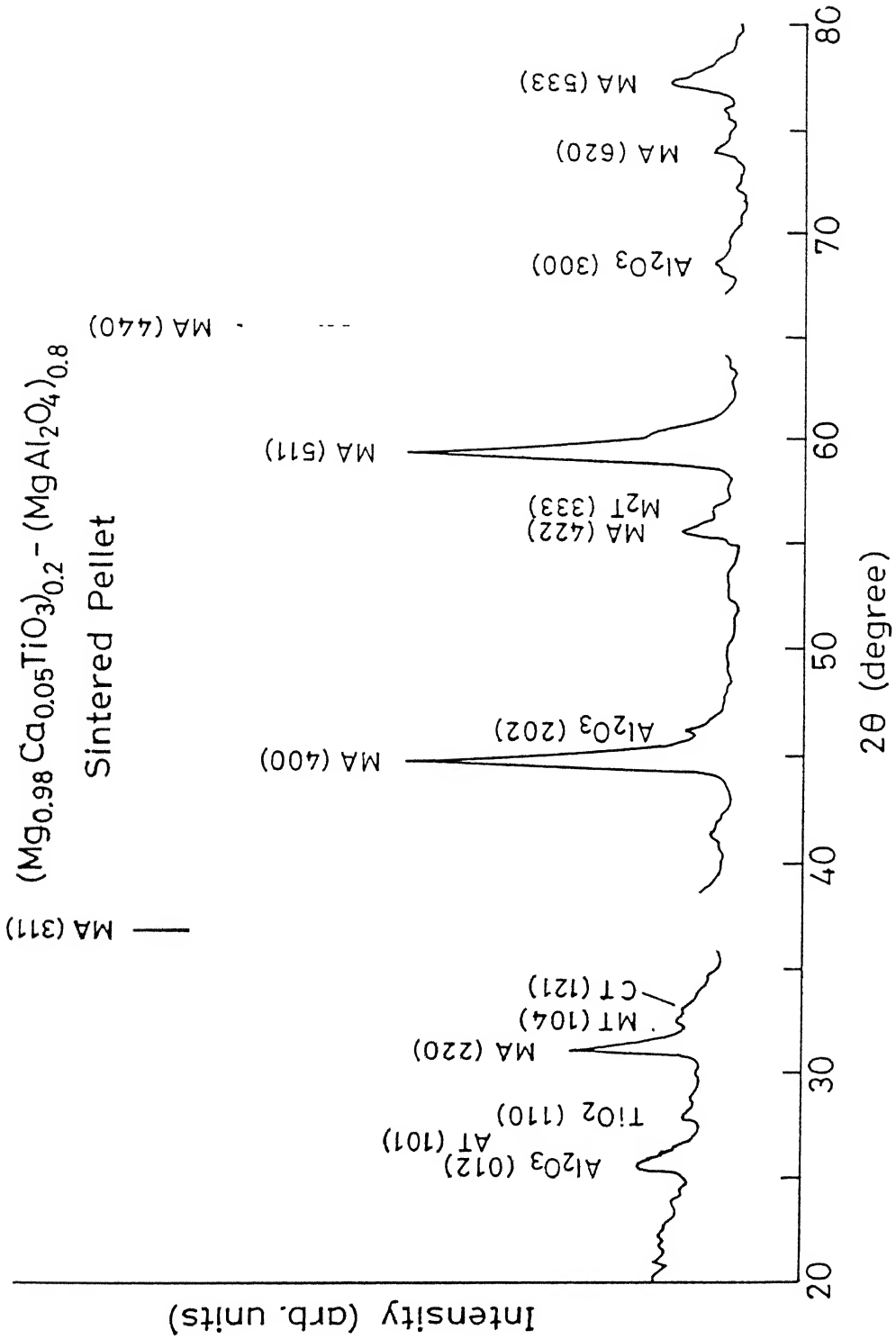

Figure 3.11: X-ray diffractograms of sintered pellet MTA(0.8).

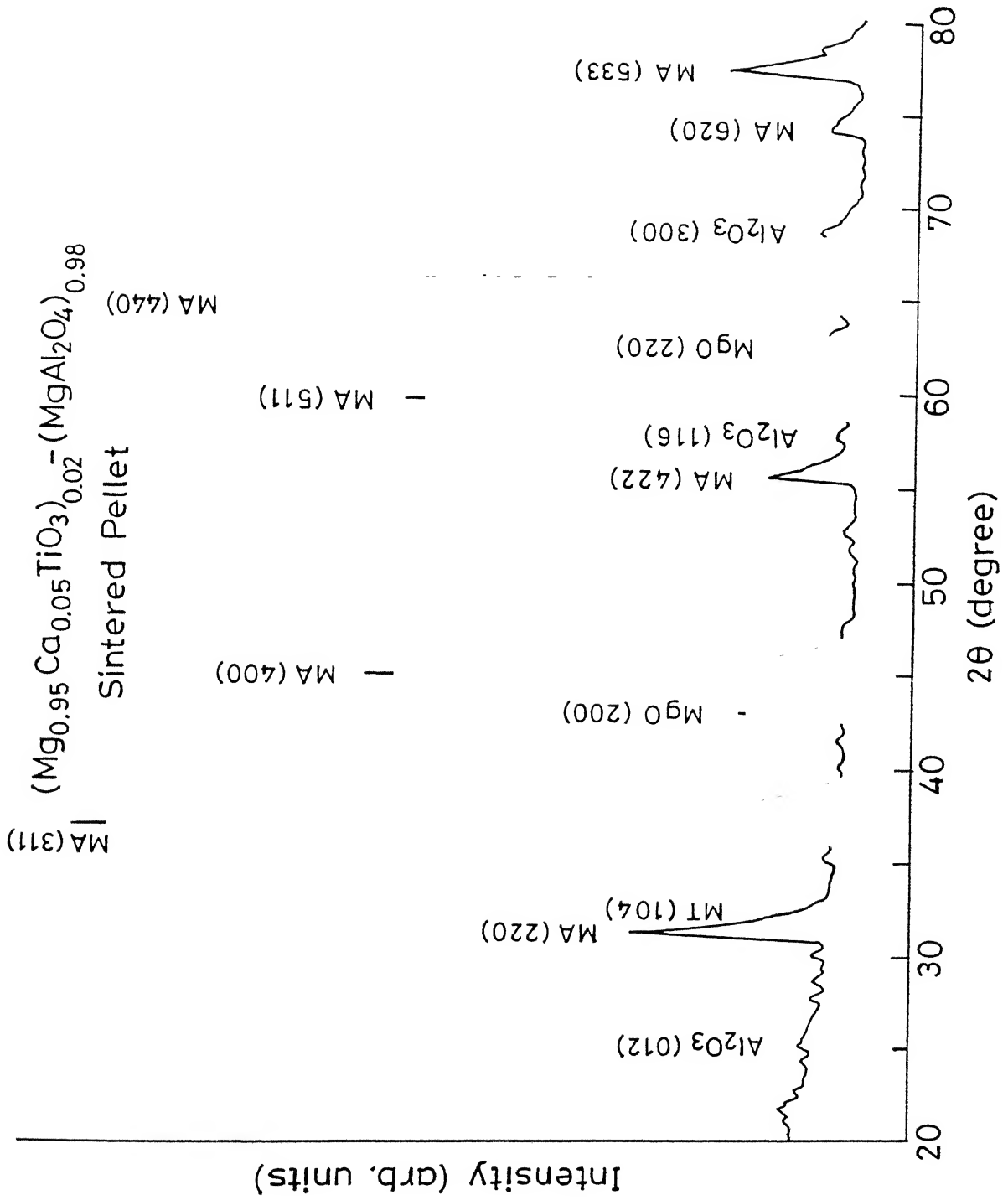

Figure 3.12: X-ray diffractograms of sintered pellet MTA(0.98).

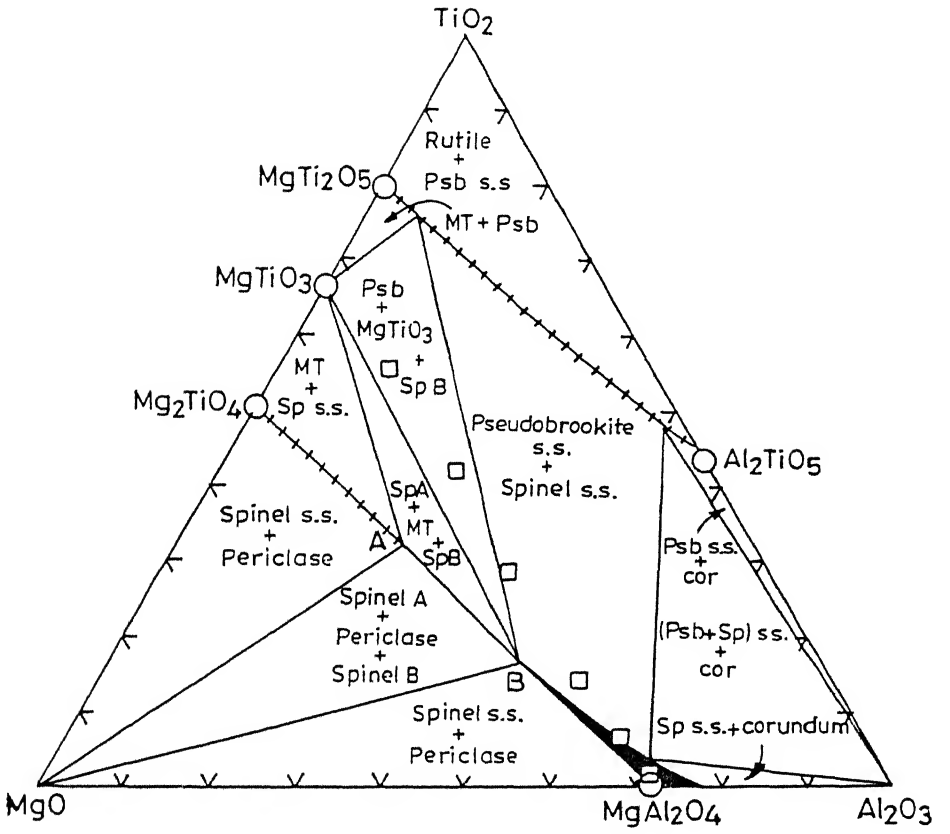

Figure 3.13: Subsolidus phase equilibrium diagram of the MgO-Al_2O_3-TiO_2 system at 1300 ^oC. A and B refer to the compositions of the two coexisting spinel phases. Abbreviations used include: Psb=pseudobrookite, s.s.=solid solution, sp=spinel, MT=$MgTiO_3$, Cor=corundum ($\alpha - Al_2O_3$) [49].

The variation of measured and calculated dielectric constants are shown in Fig. 3.14. For calculation, the dielectric constant of $Mg_{0.95}Ca_{0\,05}TiO_3$ and $MgAl_2O_4$ have been taken to be 21 and 7.5 respectively [11, 4]. The logarithmic mixture rule ($\log \epsilon = v_1 \log \epsilon_1 - v_2 \log \epsilon_2$) is used for calculation. The calculated values have been further corrected for the actual density and the resulting curve is also shown on the same figure. It is observed that the dielectric constant decreases monotonically as the content of $MgAl_2O_4$ phase increases. This trend of decrease in dielectric constant with $MgAl_2O_4$ phase is in agreement with the predictions of the logarithmic mixture rule. There is slight variation of measured dielectric constant, from calculated value. This variation is attributed the presence of small amount of different phases (e.g. M_2T, MT_2, AT, TiO_2, Al_2O_3).

The temperature coefficient of resonant frequency (TCF) data from Table 3.13 is plotted against $MgAl_2O_4$ content for all MTA compositions in Fig 3.15. It is observed that in all compositions, TCF value is negative and as the $MgAl_2O_4$ content increases the TCF increases in the negative direction, first slowly and then rapidly. For a fraction 0.45 of MA the $|TCF|$ is > 20, the limiting acceptable value in practical resonators.

The dielectric loss ($\tan\delta$) of a ceramic system is usually expressed in terms of quality factor Q ($\sim 1/\tan\delta$) and the resonant frequency of the sample (a function of dimension). The quality factor 'Q' of various compositions are given in Table 3.13. Since the resonant frequency is not constant for all the samples, it is more appropriate to consider the product Qf. The variation of Qf is plotted against $MgAl_2O_4$ content (Fig-3.16). It is observed that the Qf values are low, go through a maximum ($\simeq$ 33000) at $\sim$ 0.6 MA and then again decreases as the MA content is further increased. The highest Q.f value 32878 obtained from the composition having volume fraction 0.6 of $MgAl_2O_4$ with 91.5 % theoratical density. At higher aluminate contents (0.8, 0.9), the Q.f values are very small (13260, 15750). This decrease in Q.f values is attributed to microcracks in the samples and low densities, as discussed further in section - 3.5.

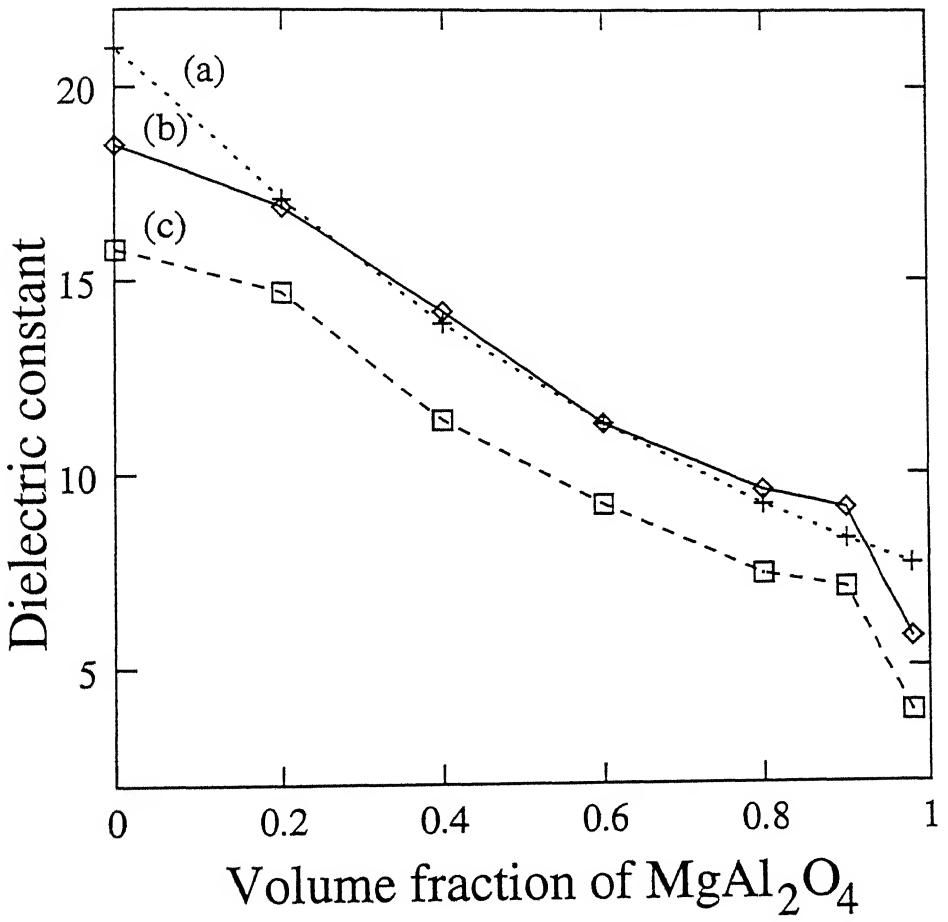

Figure 3.14: Variation of dielectric constants (a) predicted, (b) measured, (c) corrected for density vs volume fraction of $MgAl_2O_4$.

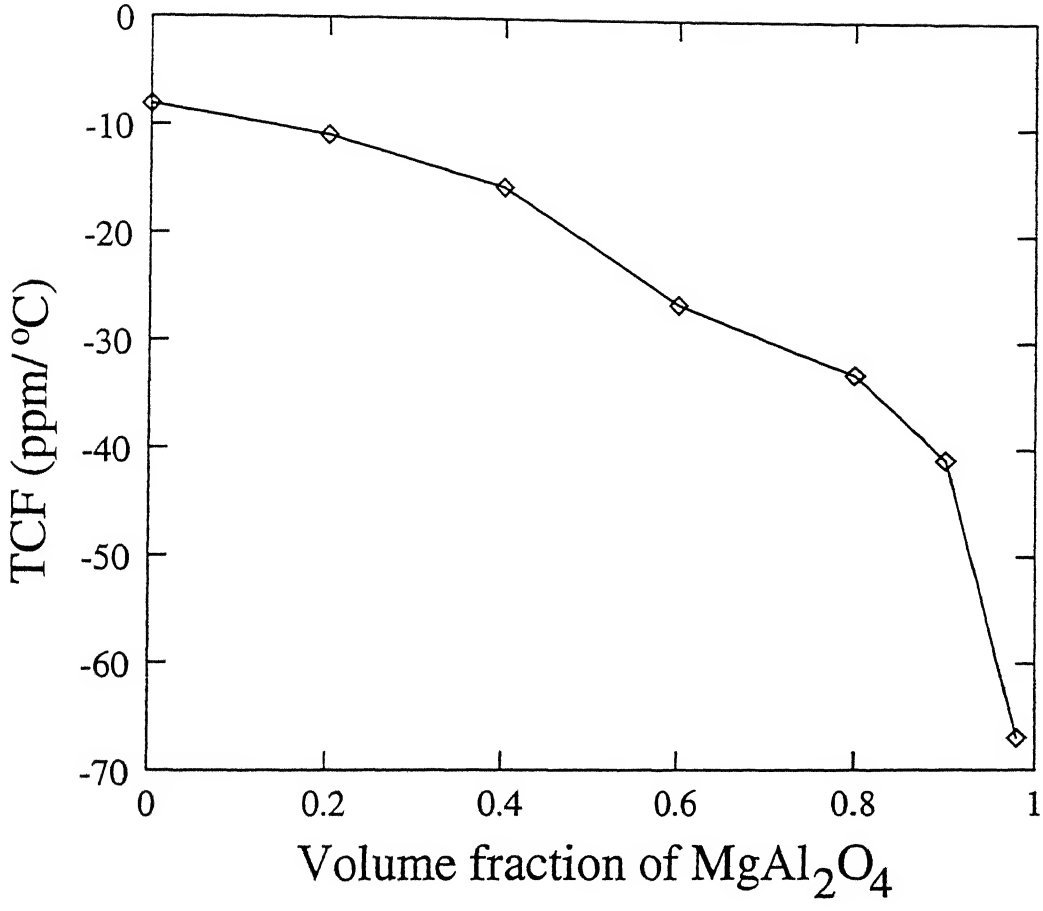

Figure 3.15: Temperature coefficient of resonant frequency is function of $MgAl_2O_4$ content.

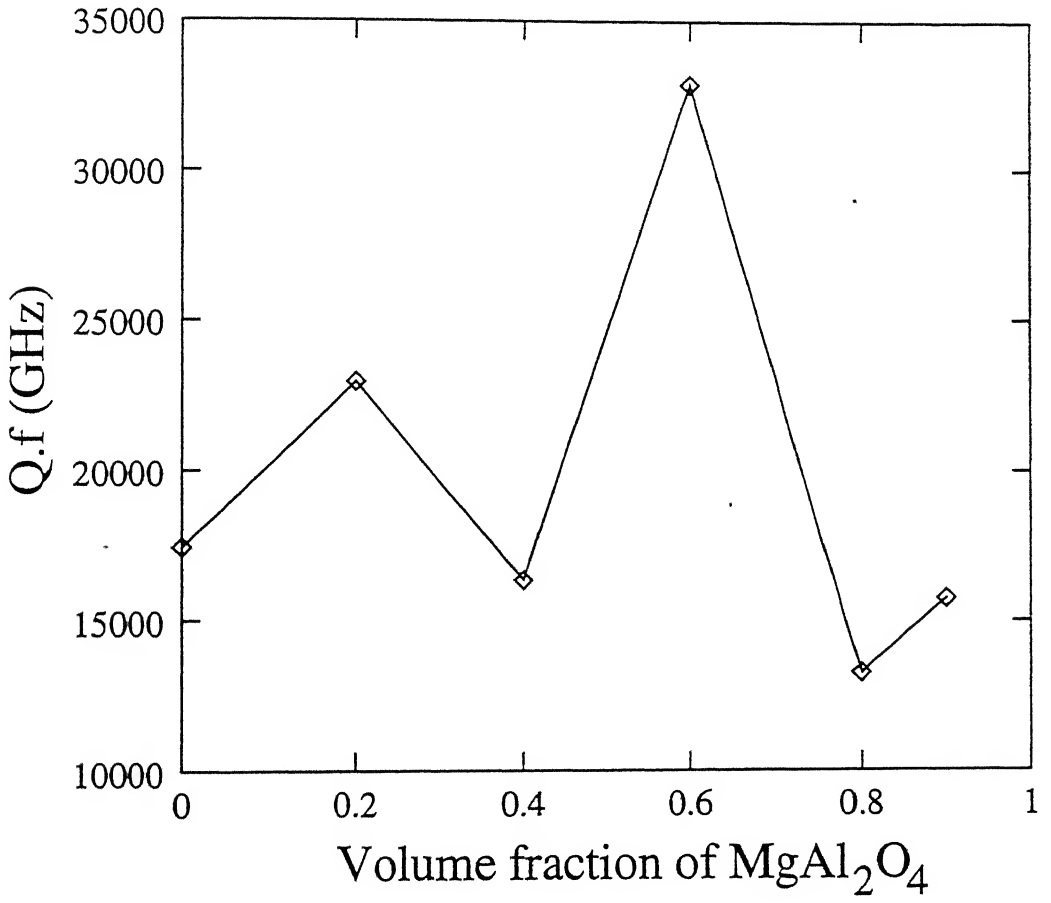

Figure 3.16: The Q.f value of MTA ceramics as a function of $MgAl_2O_4$ content, (Calcination temperature 1150 ^oC, sintering temperature 1400 ^oC).

The Q.f depends strongly on the processing conditions and density. Thus in the case of MTA(0). the Q.f varies from 9277 to 19900 (Table 3.13), depending upon the processing condition and density. Further for this composition, higher value of Q.f ($\sim$ 19900) is obtained at a lower density (89.2 %) as compared to 17434 at 91.2 % density. This may be due to the presence of small amount of TiO_2 phase in the latter sample, which was prepareed from powders calcined at 1150 ^oC (as against 1100 ^oC for the other sample).

Since the composition of MTA(0.6) had highest Q value, with 91.5 % density, effort was made to enhance its density. For this the powder was ball milled before and after the calcination step in a teflon jar. Although the density improved to 95.4 % by this method, the Q.f detereorated to 16037. Hence the process was not pursued further. The reduction in Q is attributed to some teflon carbonaceas product introduced during the ball milling step.

The above results show that low loss, high Q ceramics with good sintered density are obtained in the system MTA when the volume fraction of $MgAl_2O_4$ is 0.6. The composition in the neighbourhood of this point were further investigated to see the effect of simultaneous variation in the amount of $MgAl_2O_4$ and $CaTiO_3$ on the microwave dielectric properties.

3.3 Optimization of Dielectric Parameters in MTA(v) system

To reduce the TCF further, the amount of both $CaTiO_3$ and $MgAl_2O_4$ were varied using the formula $(Mg_{1-y}Ca_yTiO_3)_x$ - $(MgAl_2O_4)_{1-x}$. Last section dealt with the compositions having constant value of y = 0.05 and a range of x ($0 \leq x \leq 1$). In the present set of experiments, the value of x was chosen to be 0.40 to give the volume fraction of $MgAl_2O_4$ to be 0.65, and y was chosen to be between 0.086 to 0.143 instead of 0.05. The reasoning behind these choices is given in Appendix C. The results of these experiments are given in Table - 3.15 and plotted in Figure 3.17 to 3.19. The TCF data from Table - 3.14 is plotted with $CaTiO_3$ content as shown in Fig. 3.17. It is observed that for the y values ($CaTiO_3$

contents) between 0.1 to 0.12 the TCF changes from -4.7 to +15.3. Thus in this system the TCF can be adjusted to near zero by adjusting the amount of $CaTiO_3$. The q.f product of all the new compositions is plotted with $CaTiO_3$ content in Fig. 3.18. From that figure, it is seen that the highest Q.f ($\simeq$ 30464) obtained is at the composition having 0.086 $CaTiO_3$. In the composition at 0.1 $CaTiO_3$ Q.f value is also quitely high. As we increase the $CaTiO_3$ content, Q.f value decreases. For the compositions with near zero TCF and high Q, the dielectric constant is between 12 and 13 (Fig. 3.19).

Table 3.15: Dielectric properties of $(Mg_{1-y}CayTiO_3)_x$ - $(MgAl_2O_4)$ at x = 0.4 (volume fraction of MA = 0.65).

Sl No	Y	Density (%th)	Dielectric Constant		TCF (ppm/°C)		Q	f (GHz)	Q f
			13 MHz	GHz	13 MHz	GHz			
1(a)	0.086	92.5, 92 3 92.3, 92.5	12.03	11 65	-16	-20	2500	9.5	23750
1(b)	0.086	93.7, 93.5 93.5, 93.3	12.3	12.0	-14 9	-20	3200	9 52	30464
2	0.1	94.2, 94.1 94.2, 94.1	12.8	12.7 12.7	-4.7	+10	1500 2500	9.29 9.25	13935 23125
3	0.12	93, 93, 93 93.3, 93.1	13.1	12 6	+15 3	+33	2150	9.14	19651
4	0 143	93.7, 93 8 93.4, 94.3	13 7	13 2	+18 8	+13	1975	8.98	17735

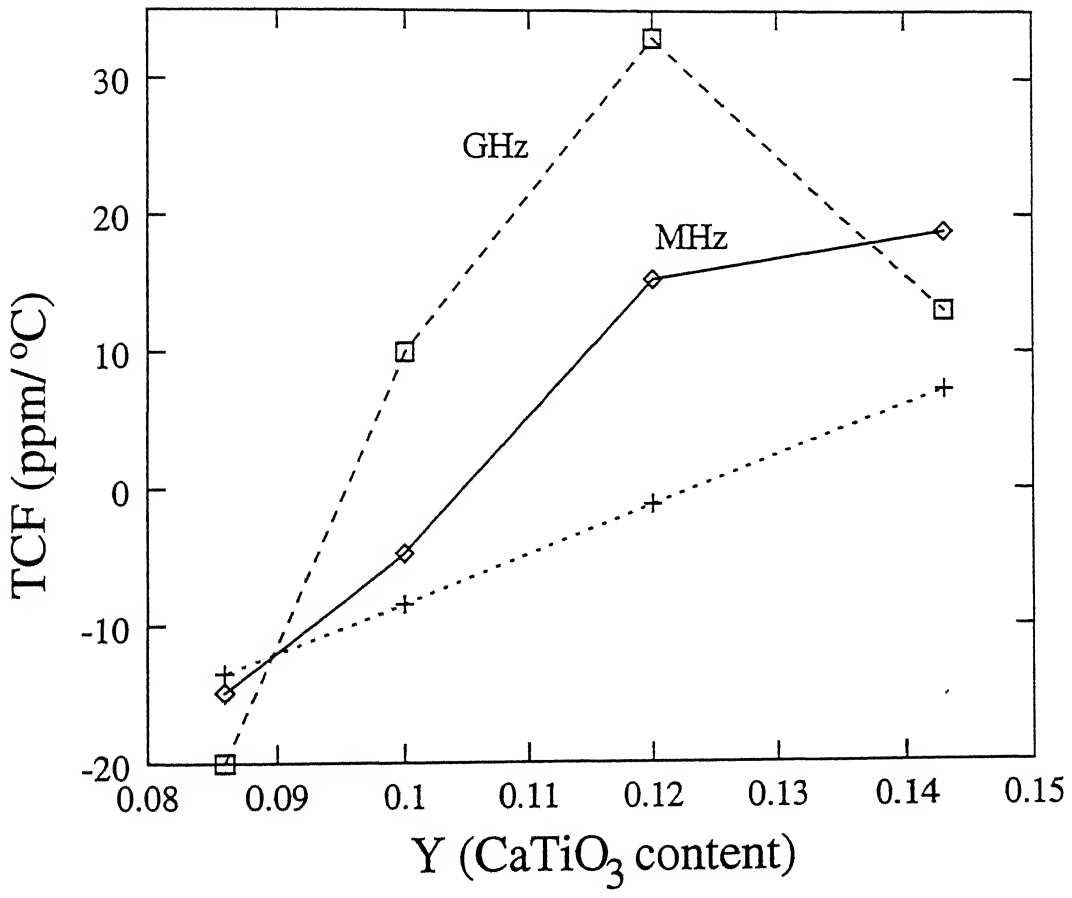

Figure 3.17: Variation of TCF (ppm/^oC) of MTA(0.65) system with $CaTiO_3$ content.

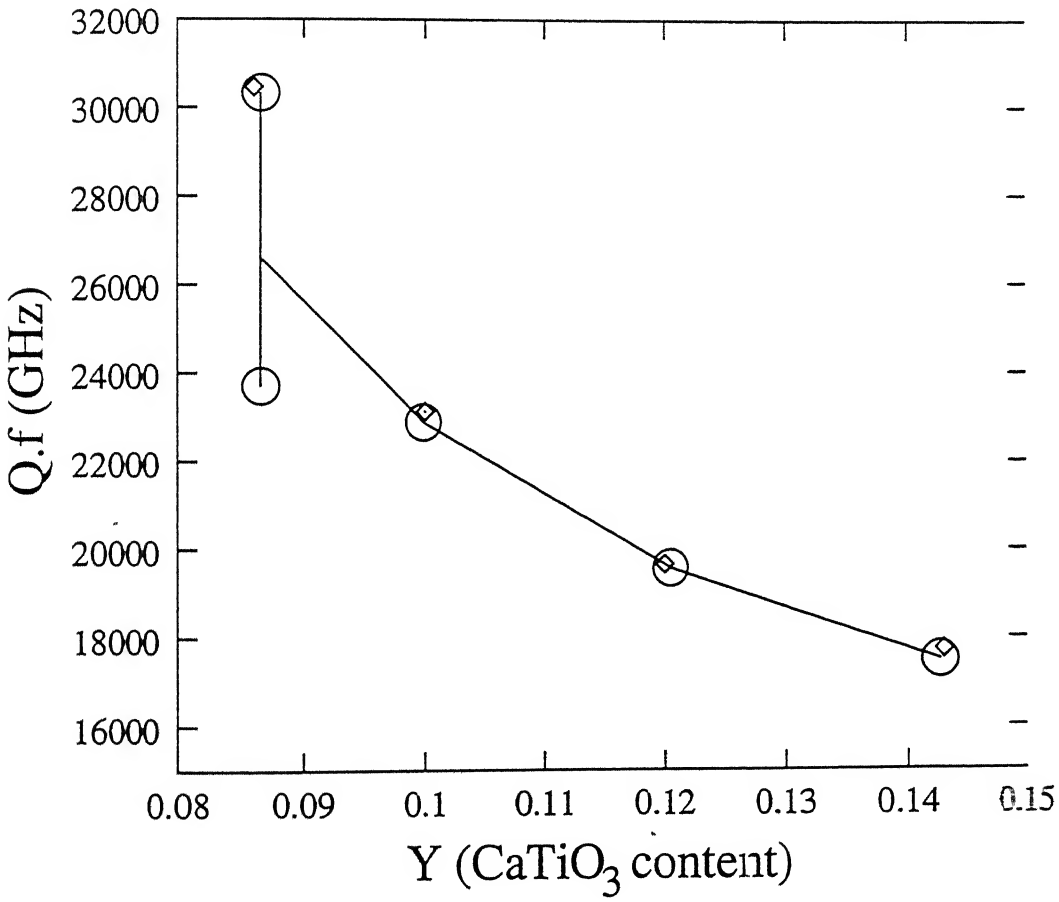

Figure 3.18: Variation of Q.f of MTA(0.65) system with $CaTiO_3$ content

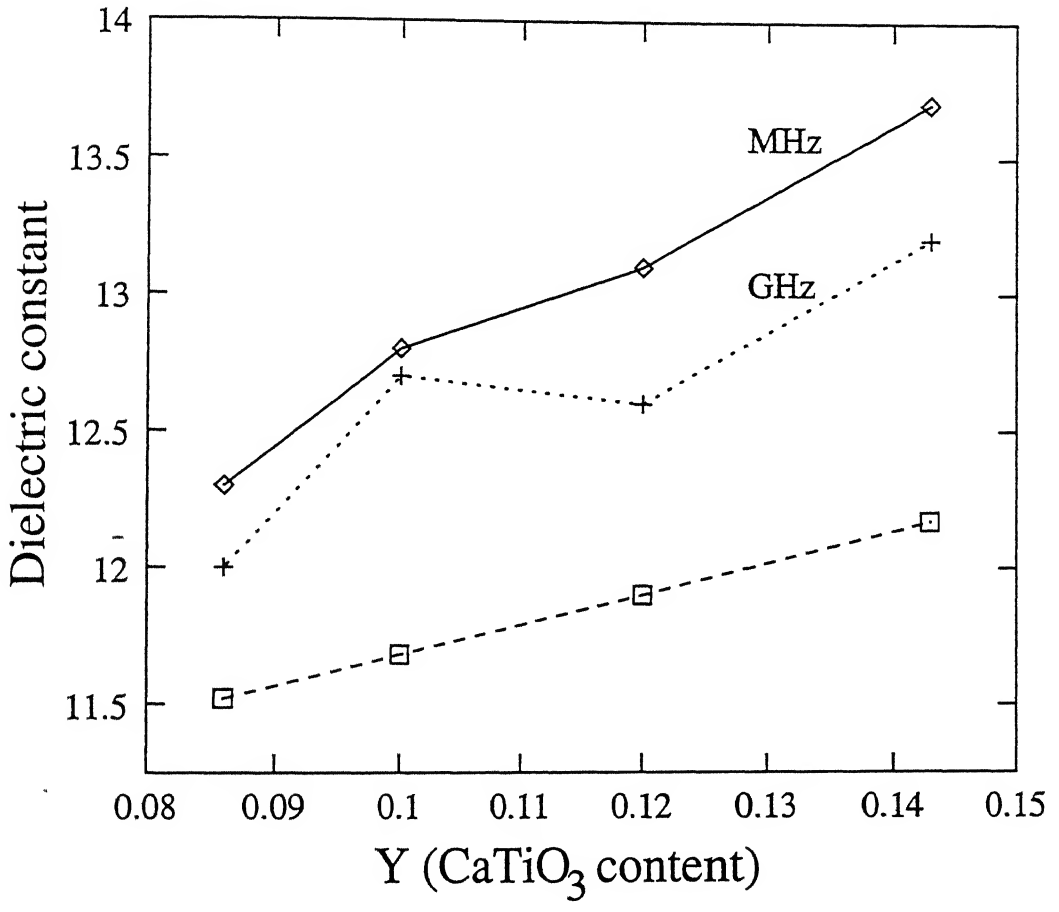

Figure 3.19: Variation of dielectric constant of MTA(0.65) system with $CaTiO_3$ content.

3.4 Lattice Parameter

The investigation of lattice parameters has been directed into two fields of interest :

1. Efforts to determine the systematic crystallographic similarities between related phases.

2. The possibility of using lattice parameter changes with changes of composition as a probe to help clarify the understanding of solid solution formation. The lattice parameters of hexagonal $MgTiO_3$ and cubic $MgAl_2O_4$ are given in Table 3.16 and Table 3.17.

Table 3.16: Lattice parameters of $MgTiO_3$ (hexagonal) system.

MTA(v)	a (A^o)	c (A^o)	c/a
MTA(0)	5.0937	13.9908	2.7466
MTA(0.2)	5.0741	13.9580	2.7508
MTA(0.4)	5.0582	13.9245	2.7528
MTA(0.6)	5.0405	13.8463	2.7470

Table 3.17: Lattice parameters of $MgAl_2O_4$ (cubic) system

MTA(v)	a (A^o)
MTA(0.2)	8.070922
MTA(0.4)	8.081421
MTA(0.6)	8.112471
MTA(0.8)	8.130346
MTA(0.9)	8.119699
MTA(0.98)	8.0541
MTA(1.0)	8.05685

The lattice parameters of both the systems are plotted against volume fraction of $MgAl_2O_4$ (Fig. 3.20 - 3.23). It is observed that, lattice parameter (a,c) of $MgTiO_3$ system goes on decreasing, as $MgAl_2O_4$ content increases. In case of $MgAl_2O_4$, the lattice

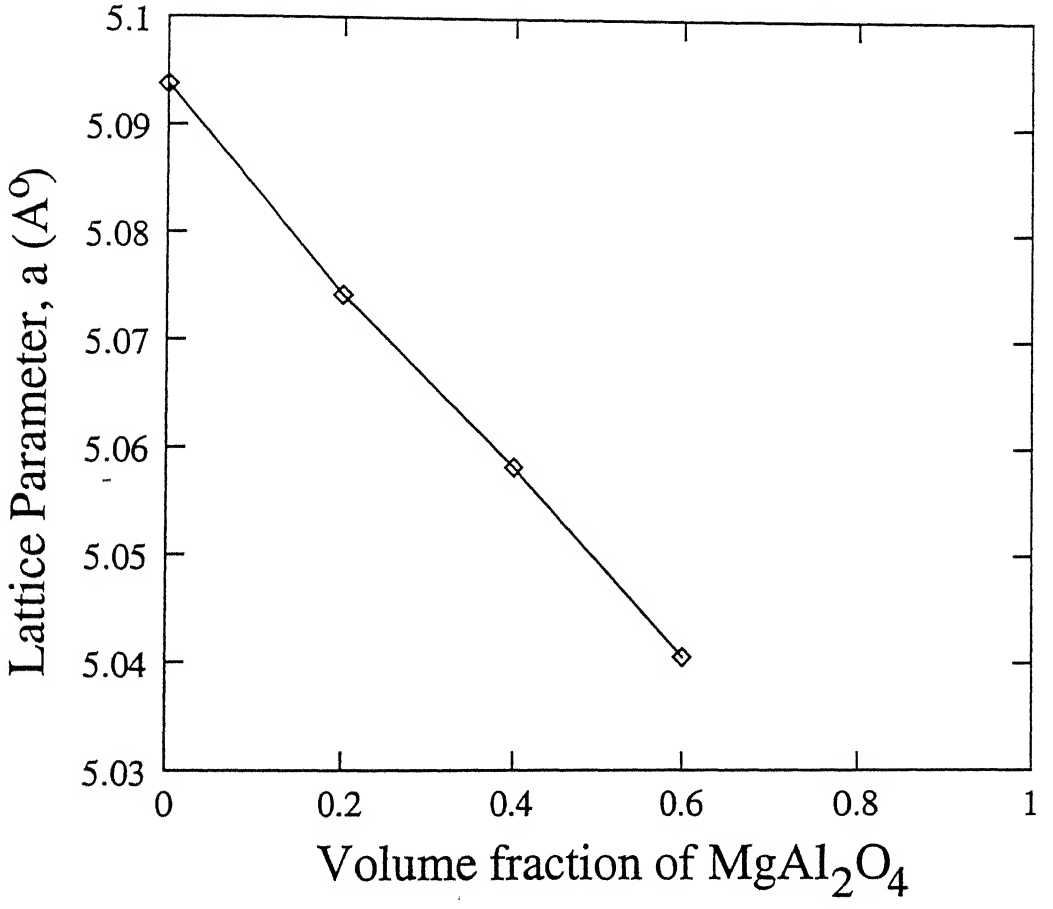

Figure 3.20: Variation of lattice parameter $a(A^o)$ of $MgTiO_3$ with $MgAl_2O_4$ content.

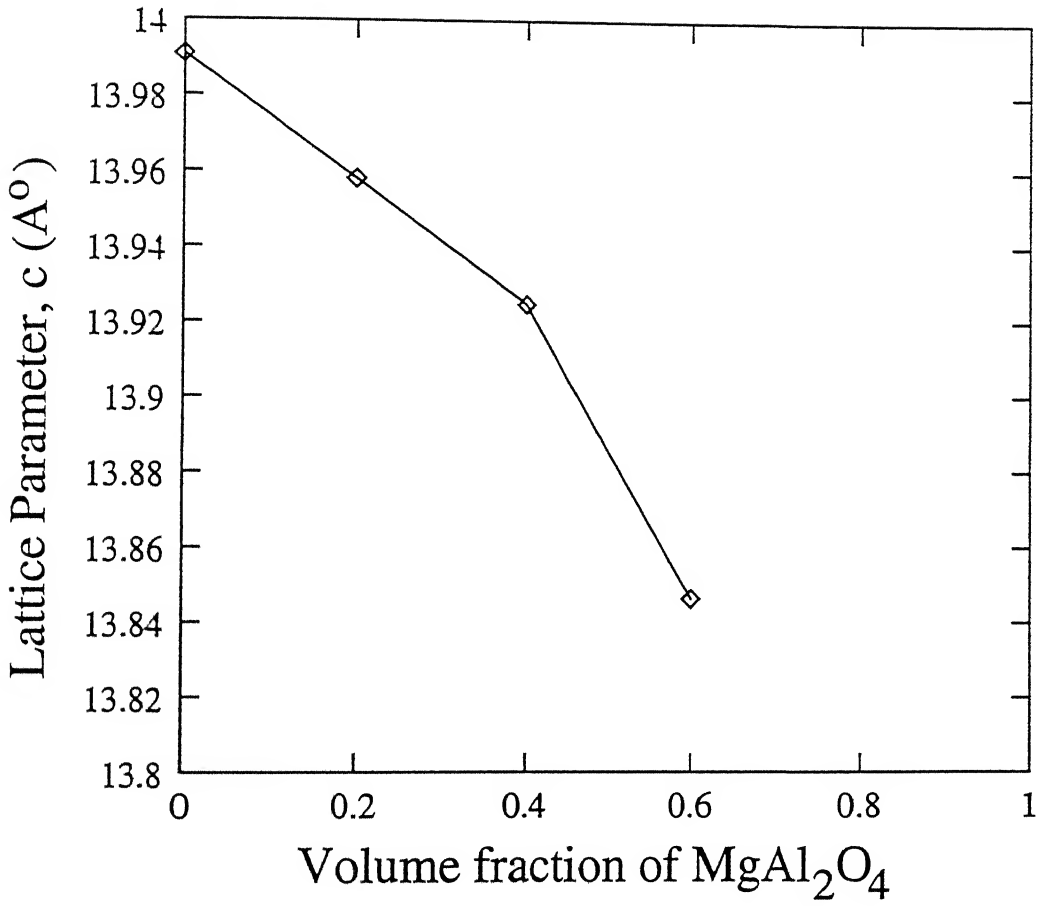

Figure 3.21: Variation of lattice parameter $c(A^o)$ of $MgTiO_3$ with $MgAl_2O_4$ content.

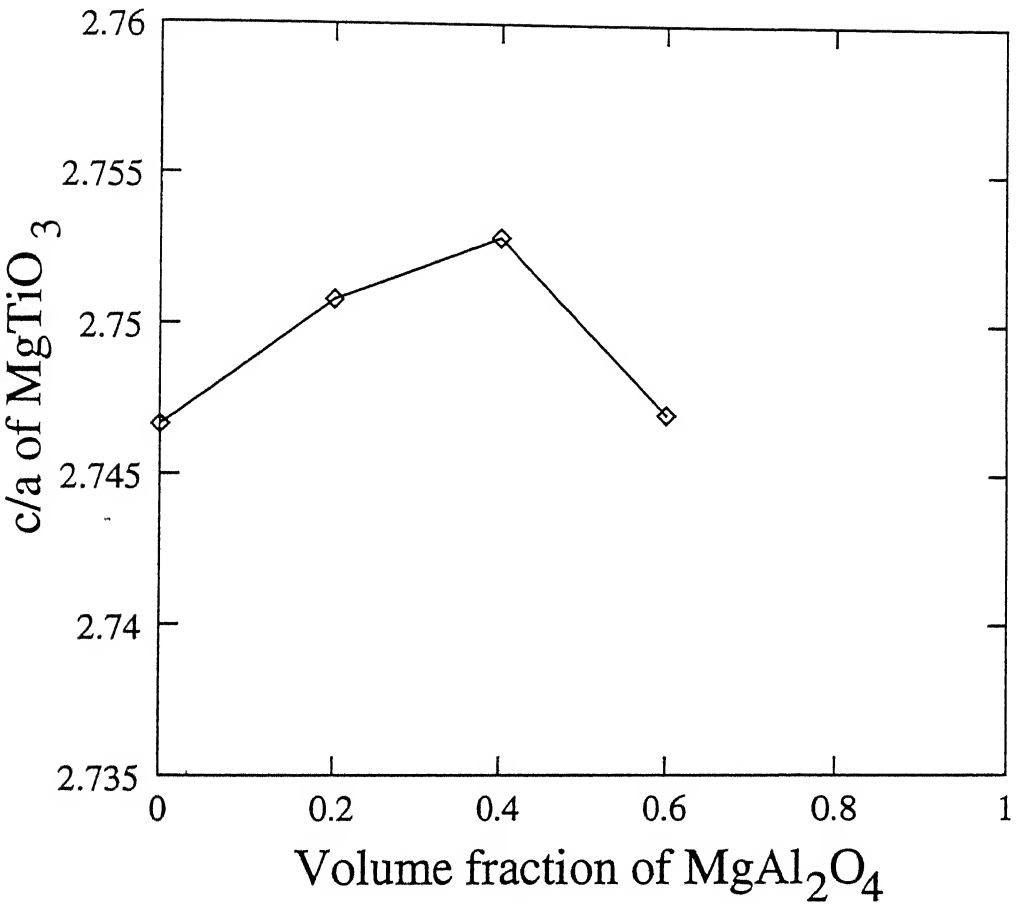

Figure 3.22: c/a of $MgTiO_3$ vs $MgAl_2O_4$ content.

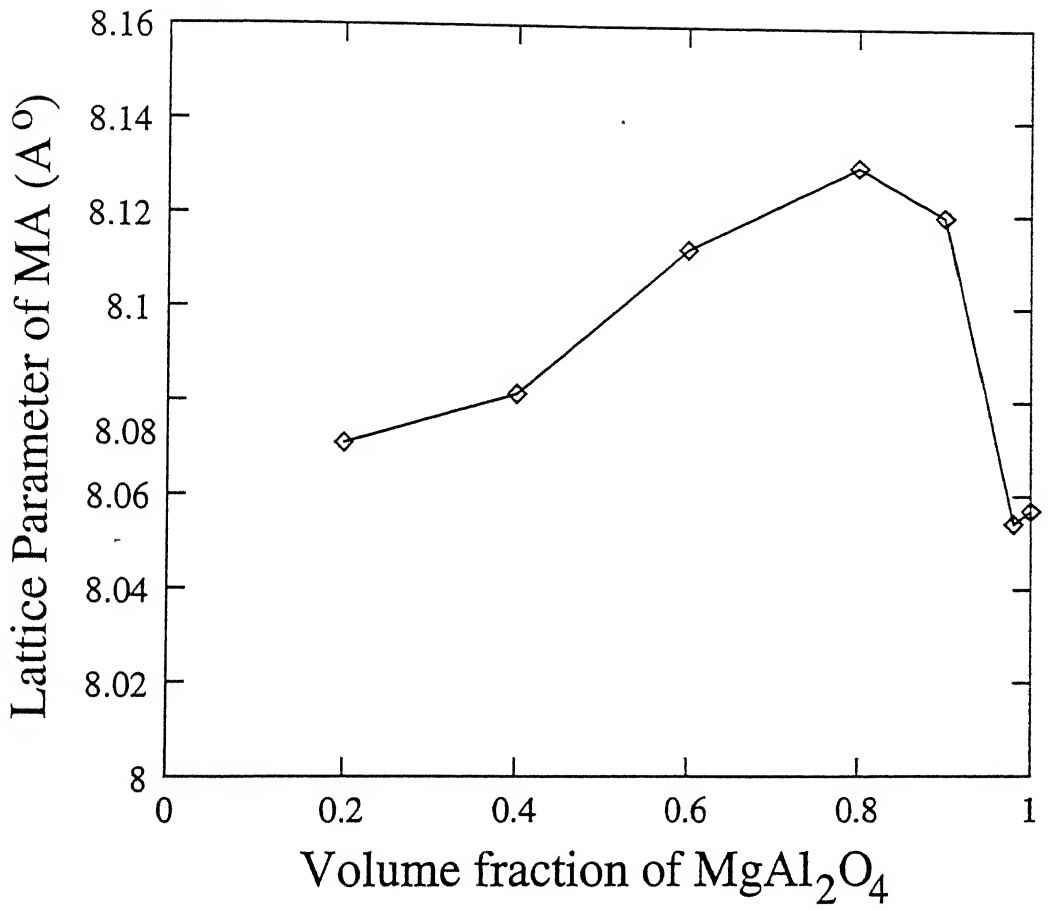

Figure 3.23: Variation of lattice parameter of $MgAl_2O_4$ with different MTA(v) compositions.

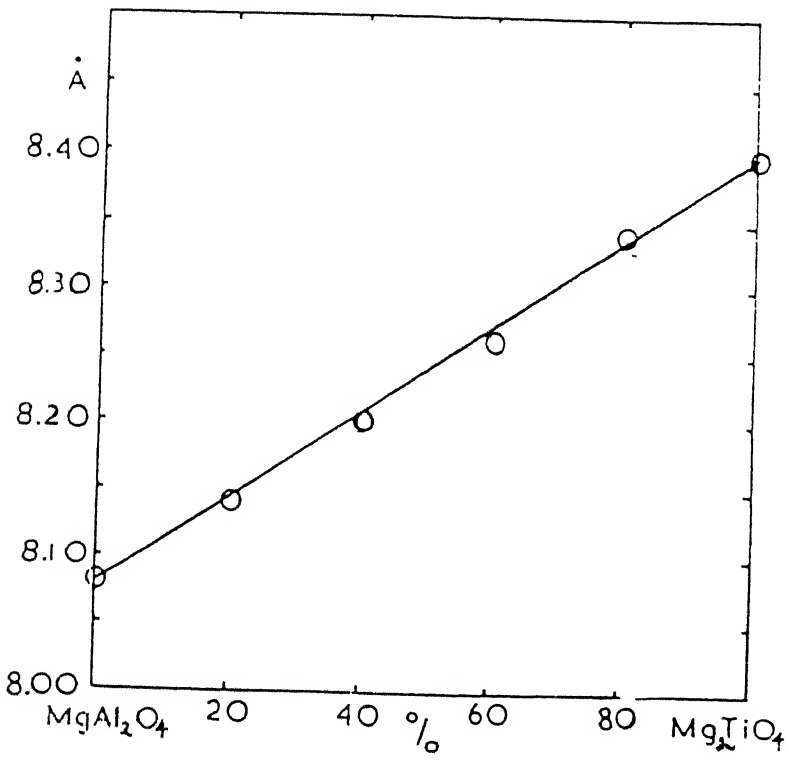

Figure 3.24: Variation in the unit cell size of the spinel solid solutions. Open circles show individual meesurements and their size shows the estimated accuracy of measurement [49].

parameter increases as % $MgAl_2O_4$ in MT-MA system is increased, but after the composition MTA(0.8) it decreases. The decrease in lattice parameters in $MgTiO_3$, is due to $Al^{3}+$ entering substitutional sites in the lattice of $MgTiO_3$.

It is observed that all four of the following substitutions are possible.

(i) $Mg^{2+} + Ti^{4+} = 2\ Al^{3+}$

(ii) $Mg^{2+} + Ti^{4+} = 2\ Al^{3+}$ and $3\ Ti^{4+}$

(iii) $2Al^{3+} = 3\ Mg^{2+}$

(iv) $2Al^{3+} = 3\ Mg^{2+}$ and $3\ Ti^{4+} = 4\ Al^{3+}$

Since the ionic radii of Al^{3+} (0.51 A^o) is smaller than the Ti^{4+} (0.68 A^o), this may decreases the lattice parameter.

Fig. 3.24 [49] shows that the variation of the lattice parameter of $MgAl_2O_4$ as Mg_2TiO_4 dissolves in it. This shows that the lattice parameter increases as the Ti concentrates in $MgAl_2O_4$ increases. Fig 3.23 gives the present result which show that, as the concentration of $MgTiO_3$ increases (from the MA end) the lattice parameter does increases but after ~0.2 volume fraction of $MgTiO_3$, the lattice parameter again decreases. This seems that the solubility of Ti in $MgAl_2O_4$ may be peaking at 0.2 volume fraction of $MgTiO_3$.

3.5 Microstructure

Fig. 3.25(a)-(g) shows the microstructures of the polished surfaces of the samples with different compositions. Due to the lack of availability of enough time on SEM, the definitive identifications of the phases by EDAX analysis could not be done. From the micrographs it can be seen that in the sample with no $MgAl_2O_4$ (Fig. 3.25(a)) large size grains are predominant with smaller number of smaller sized grains. As the phases in the sample are $MgTiO_3$ and $CaTiO_3$ in the ratio 0.95 and 0.05, it can be said that the larger grains are $MgTiO_3$ and smaller grains are $CaTiO_3$. Fig. 3.25(b) and (c) clearly show that the size of $MgTiO_3$ grains decreases as amount of $MgAl_2O_4$ increases. In the sample with 0.6 $MgAl_2O_4$,

the grain sizes of all the constituent phases are similar and uniform. The average grain size, here is less than $5\mu m$. This composition showed the best properties in terms of Q and TCF. As the amount of $MgAl_2O_4$ increases, larger grains appear which should be $MgAl_2O_4$. Microcracks in the samples also appear at high concentration of $MgAl_2O_4$ (Fig. 3.25(f)). The properties degrade as the amount of $MgAl_2O_4$ is increased beyond 0.6 volume fraction of $MgAl_2O_4$.

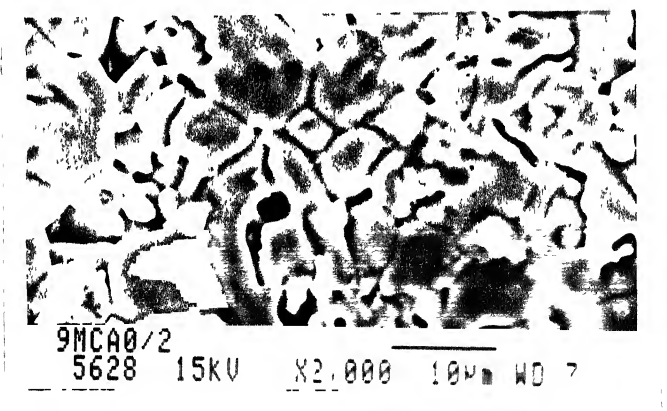

(a)

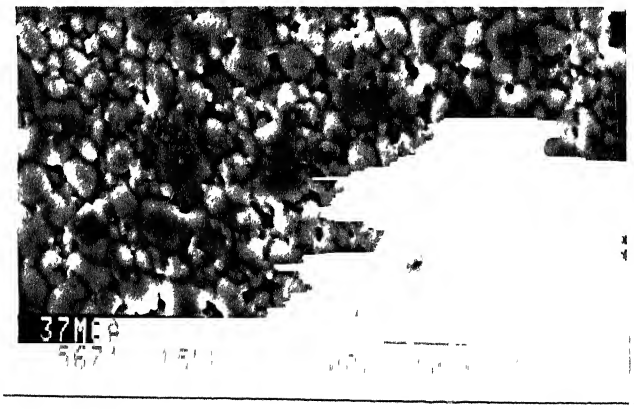

(b)

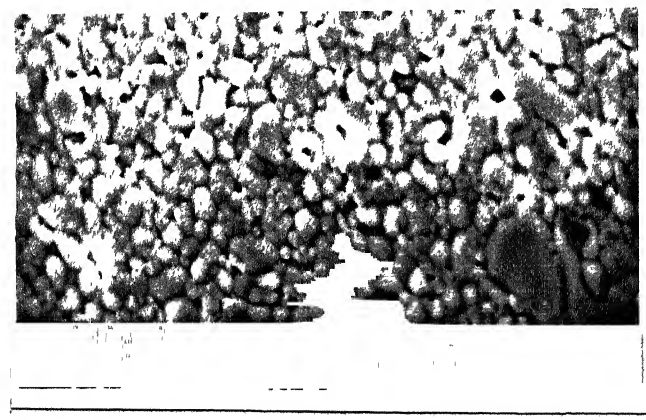

(c)

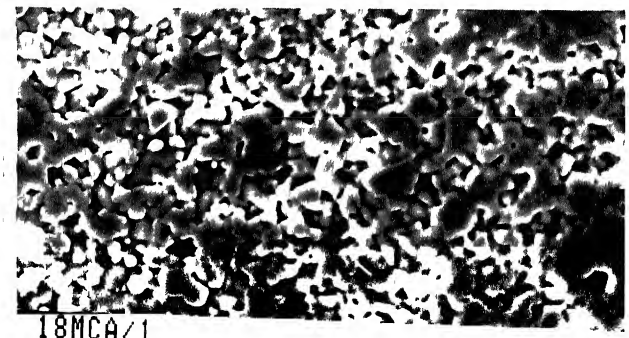

(d)

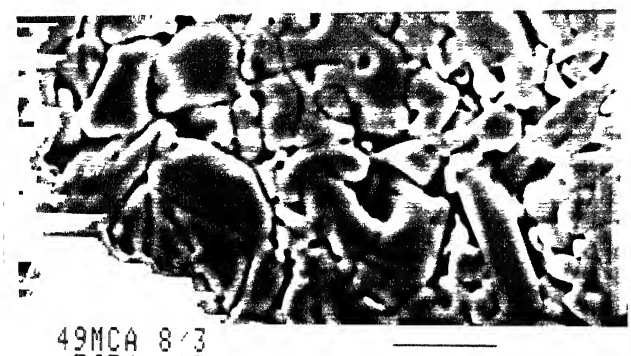

(e)

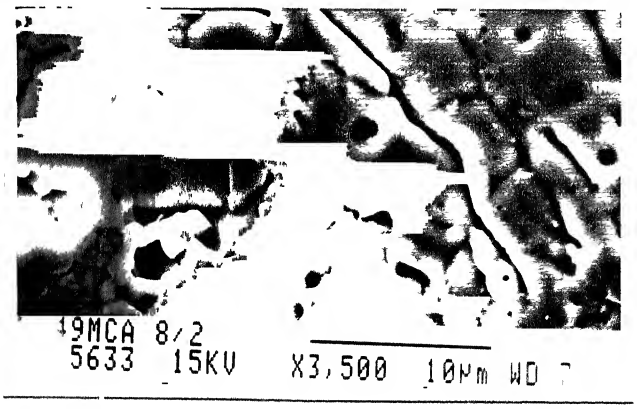

(f)

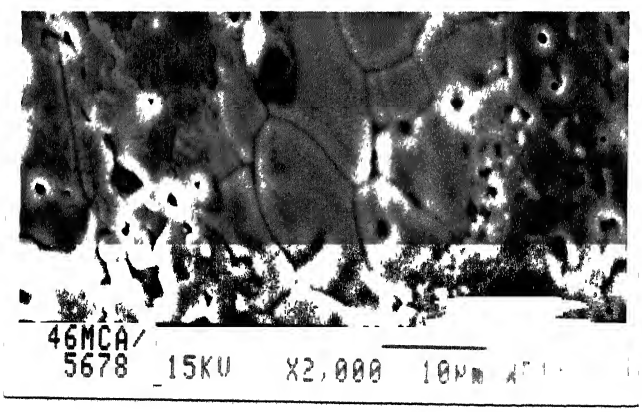

(g)

Figure 3.25: SEM micrographs of compositions (a) MTA(0), (b) MTA(0.2), (c) MTA(0.4), (d) MTA(0.6), (e-f) MTA(0.8), (g) MTA(0.9).

Chapter 4

Conclusion

In this work ceramics in the system $(Mg_{0.95}Ca_{0.05}TiO_3)$ - $(MgAl_2O_4)$ have been investigated with a view to their suitability for application in dielectric resonators. The compositions with volume fraction of $MgAl_2O_4$ 0, 0.2, 0.4, 0.6, 0.8 0.9, 0.98, 1.0 have been studied. The density of all the compositions upto 0.9 $MgAl_2O_4$ was found to be between 90 to 93 % of the theoretical density. Above 0.9 $MgAl_2O_4$, the density drastically goes down decreasing to 53 % for 100 % $MgAl_2O_4$, at a sintering temperature of $1400^oC/2$h. The use of intermediate ballmilling step enhances the density to 95.4 %, but the quality factor is severely reduced. The major phases in the sintered samples were $MgTiO_3$, $CaTiO_3$ and $MgAl_2O_4$. The presence of small amounts of phases TiO_2, Al_2O_3, Mg_2TiO_4, $MgTi_2O_5$ and Al_2TiO_5 also affect the dielectric properties. The decrease in lattice parameter of $MgTiO_3$ with $MgAl_2O_4$ content showed that Al^3+ enters the lattice of $MgAl_2O_4$. The lattice parameter of $MgAl_2O_4$ attains a maxium value at an intermediate composition.

The decrease in the dielectric constant of $(MgCa)TiO_3$ upon addition of $MgAl_2O_4$ is in agreement with the logarithmic mixture rule. There is no systamatic variation of quality factor with increase in the content of $MgAl_2O_4$. At higher $MgAl_2O_4$ (> 0.8) content the quality factor goes down due to poor density and the generation of microcracks in the sintered bodies, which cause high loss. The value of TCF in all the compositions increases

with increase in $MgAl_2O_4$ content. With this investigation, it was seen that the composition at 0.6 $MgAl_2O_4$ has best properties ($\epsilon_r \simeq 12.4$, $Q \simeq 3400$ at 9.67 GHz and TCF $\simeq -26.4$ ppm/^oC). The compositions were further modified by varying the value of y in the formula 0.35 $(Mg_{1-y}Ca_yTiO_3)$ - 0.65 $(MgAl_2O_4)$. Highly temperature stable composition could be obtained by adjusting the value of y. The composition at $y = 0.1$ has $\epsilon_r \simeq 12.7$, $Q \simeq 2500$. and TCF $\simeq +10$ ppm/^oC at 9.67 GHz. This investigation leads to conclusion that the composition 0.35 $(Mg_{0.9}Ca_{0.1}TiO_3)$ - 0.65 $(MgAl_2O_4)$ has suitable dielectric properties for use in dielectric resonator or in coaxial dielectric resonator.

The further works which may be possible on these investigated systems is as follows :

(1) Identification of (particularly in microstructure), quantitative determination and control of the amount of the minor phases. These phases may have significant effect on properties. Further work can be carried out to investigate the control of the amount of these phases and their effect on properties.

(2) Corelation of microstructure with the dielectric properties of investigated systems can be done.

(3) These systems can be processed by the chemical route, which may give better dielectric properties (e.g. low loss) and highly densified material with uniformity in stochiometry.

References

[1] J.H.C. Van Heuven and A.G. Van Nie; "Microwave integrated circuits," *Philips Tech. Rev.*, **32** 294-304 (1971).

[2] G. Lutteke and D. Hennings; "Dielectric resonators for microwave integrated oscillators," *Philips Tech. Rev.*, **43** 35-46 (1986).

[3] W. Wersing; "High frequency ceramic dielectrics and their application for microwave components," **Electronic ceramics**, edited by B.C.H. Steel, Elsevier Applied Science, London, 67-119 (1991).

[4] J.M. Herbert; "**Ceramic dielectrics and capacitors**," Gordon and Breach Science Publishers, Philadelphia, p124-126 (1992).

[5] Jen-Yan Hsu, Nan-Chung Wu and Shu-Cheng Yu; "Characterization of material for low-temperature sintered multilayer ceramic substrates," *J. Am. Ceram. Soc.*, **72**[10] 1861-67 (1989).

[6] B. Schwartz, "Ceramic packaing of integrated circuits," **Electronic ceramics**, edited by L.M. Levinson, Marcel Dekker, Inc., Newyork, p-28 (1987).

[7] H.M. O'Bryan, Jr., and J. Thomson, Jr., J.K. Plourde; "A new BaO-TiO_2 compound with temperature stable high permittivity and low microwave loss," *J. Am. Ceram. Soc.*, **57**[10] 450-453 (1974).

[8] Soichiro Nomura; "Ceramics for microwave dielectric resonator," *Ferroelectrics*, **49** 61-74 (1983).

[9] R.M. Redheffer; "The measurement of dielectric constants," **Technique of microwave measurements**, edited by C.G. Montgomery, McGraw-Hill book company, Inc.. Newyork, p-561 (1947).

[10] K. Wakino, M. Murata and H. Tamura; "Far infrared reflection spectra of $Ba(Zn,Ta)O_3$ - $BaZrO_3$ dielectric resonator material," *J. Am. Ceram. Soc.*, **69**[1] 34-37 (1986).

[11] R. Freer; "Microwave dielectric ceramics - an overview," *Silic. Ind.*, **58**[9-10] 191-197 (1993).

[12] R.W.P. King, S. Prasad; "**Fundamental electromagnetic theory and applications**," Prentice Hall, Inc., Englewood Cliffs, N.J., p-500 (1986).

[13] D.C. Dube, R. Zurmuhlen, Andrew Bell, N. Setter and W. Wersing; "Dielectric measurements of high-Q ceramics in the microwave region," *J. Am. Ceram. Soc.*, **80**[5] 1095-1100 (1997).

[14] "A designer's guide to microwave dielectric ceramics," Trans. Tech., Inc; U.K. Oct. 1990

[15] G. Wolfram and H.E. Gobel; "Existence range, structural and dielectric properties of $Zr_xTi_ySn_zO_4$ ceramics (x+y+z = 2)," it Mat. Res. Bull., **16**[11] 1455-1463 (1981).

[16] H.Tamura; "Microwave loss quality of $(Zr_{0.8}Sn_{0.2})TiO_4$," *Amer. Ceram. Soc. Bull.*, **73**[10], 92-95 (1994).

[17] J.K. Plourde and D.F. Linn, H.M. O'Bryan, Jr. and John Thomson, Jr., *J. Am. Ceram. Soc.*, **58**[9-10] 418-420 (1995).

[18] S. Kucheiko, Ji-Won Choi, H. Kim and H.Jung; "Microwave dielectric properties of $CaTiO_3$ - $Ca(Al_{1/2}Ta_{1/2})O_3$ ceramics," *J. Am. Ceram. Soc.*, **79**[10] 2739-43 (1996).

[19] H. Kim, S. Kucheiko, S. Yoon and H.Jung; "Microwave dielectrics in the $(La_{1/2}Na_{1/2})TiO_3$ - $Ca(Fe_{1/2}Nb_{1/2})O_3$ system," *J. Am. Ceram. Soc.*, **80**[5] 1316-18 (1997).

[20] R. Piagi, I. Kim, J. Park and Y. Kim; "Preparation of magnesium-calcium titanate powders by alkoxide precursor," *J. Am. Ceram. Soc.*, **81**[5] 1361-64 (1998).

[21] Ferrira, V.M., Azough, F., Baptista, J.L. and Freer, R.; *Proceedings of ECAPD - 2 (London, 1992), Ferroelectrics*, **133** 127-132 (1992) (Si. 26 in Ref. 11).

[22] D.J. Masse, R.A. Purcel, D.W.Ready, E.A. Maguire and C.P. Hartwing; "New low-loss high-K temperature-compensated dielectric for microwave applications," *Proc. IEEE*, **59**[11] 1628-29 (1971).

[23] H.M. O'Bryan and John Thomson; "$Ba_2Ti_9O_{20}$ phase equillibria, " *J. Am. Ceram. Soc.*, **66**[1] 66-68 (1983).

[24] Hsin-Chun Lu, L.E. Burkhart and Glenn L. Shardar; "Sol-gel process for the preparation of $Ba_2Ti_9O_{20}$ and $BaTi_5O_{11}$," *J. Am. Ceram. Soc.*, **74**[5] 968-972 (1991).

[25] R. Kudesia, A.E. Mchale and R.L. Snyder; "Effects of La_2O_3/ZnO additives on microstructure and microwave dielectric properties of $Zr_{0.8}Sc_{0.2}TiO_4$ ceramics," *J. Am. Ceram. Soc.*, **77**[12] 3215-3220 (1994).

[26] K. Wakino, K. Minai and H. Tamura; "Microwave characteristics of $(ZrSn)TiO_4$ dielectric resonators," *J. Am. Ceram. Soc.*, **67**[4] 278-281 (1984).

[27] S. Hirano, T. Hayashi and A. Hattori; "Chemical processing and microwave characteristics of $(ZrSn)TiO_4$ microwave dielectrics," *J. Am. Ceram. Soc.*, **74**[6] 1320-1324 (1991).

[28] T. Takada, S.F. Wang, S. Yoshikawa, S.J. Jang and R.E. Newnham; "Effects of glass additions on (ZrSn)TiO_4 for microwave applications," *J. Am. Ceram. Soc.*, **77**[9] 2485-2488 (1994).

[29] Anna E. Mchale and Robert S. Roth; "Investigation of phase transition in $ZrTiO_4$ and $ZrTiO_4$-SnO_2 solid solutions," *J. Am. Ceram. Soc.*. **66**[2] C18-C20 (1983).

[30] Y.C. Heiao, L. Wu and C.C. Wei; "Microwave dielectric properties of (ZrSn)TiO_4 ceramics," *Mat. Res. Bull.*, **23**[12] 1687-1692 (1988).

[31] S.B. Desu and H.M. O'Bryan; "Mirowave loss quality of $BaZn_{1/3}Ta_{2/3}O_3$ ceramics," *J. Am. Ceram. Soc.*, **68**[10] 546-51 (1985).

[32] S. Kawashima, M. Nishida, I. Ueda and H. Ouchi; "$BaZn_{1/3}Ta_{2/3}O_3$ ceramics with low dielectric loss microwave frequencies," *J. Am. Ceram. Soc.*, **66**[6] 421-423 (1983).

[33] In-Taekim, Yoon-Ho and Sunjin Chung; " order-disorder transition and microwave dielectric properties of $Ba(Ni_{1/3}Nb_{2/3})O_3$ ceramics," *Jpn. J. Appl. Phys.*, **34**[8A] 4096-4103 (1995).

[34] M. Onoda, J. Kumata, K. Kaneta and K. Toyama; "$Ba(Zn_{1/3}Nb_{2/3})O_3$-$Sr(Zn_{1/3}Nb_{2/3})O_3$ solid solution ceramics with temperature stable high dielectric constant and low microwave loss," *Jpn. J. Appl. Phys.*, **21**[12] 1707-1710 (1982).

[35] Hiroshi Tamura, Konoike, Y. Sakabe and K. Wakino; "Improved high-Q dielectric resonator with complex perovskite structure," *J. Am. Ceram. Soc.*, **67**[4] C59-C61 (1984).

[36] K. Kageyama; "Crystal structure and microwave dielectric properties $Ba(Zn_{1/3}Ta_{2/3})O_3$-$(Sr,Ba)(Ga_{1/3}Ta_{2/3})O_3$ ceramics," *J. Am. Ceram. Soc.*, **75**[7] 1767-1771 (1992).

[37] Hi Hyun Yoon, Dong Pil Kim and Eung Soo Kim; "Effect of $BaWO_4$ on the microwave

dielectric properties of $Ba(Mg_{1/3}Ta_{2/3})O_3$ ceramics," *J. Am. Ceram. Soc.*, **77**[4] 1062-1066 (1994).

[38] H. Matsumoto, H. Tamura and K. Wakino; "$Ba(MgTa)O_3$ - $BaSnO_3$ high-Q dielectric resonator," *Jpn. J. Appl. Phys.*, **30**[9B] 2347-2349 (1991).

[39] K. Endo, K. Fujimoto and K. Murakawa; "Dielectric properties of ceramics in $Ba(Co_{1/3}Nb_{2/3})O_3$-$Ba(Zn_{1/3}Nb_{2/3})O_3$ solid solutions," *J. Am. Ceram. Soc.*, **70**[9] C215-C218 (1987).

[40] Kolar, P., Stadler, Z., Gaberscek, S. and Savorov, D.; "Ber. Deut. Keram. Ges., **55** 346-348 (1978) (Si. 42, Ref. 11).

[41] H. Oshato, H. Kato, M. Mizuta, S. Nishigaki and T. Okuda; "Microwave dielectric properties of the $Ba_{6-3x}(Sm_{1-y},R_y)Ti_{18}O_{54}$ (R = Nd and La) solid solutions with zero temperature coefficient of resonant frequency," *Jpn. J. Appl. Phys.*, **34**[9B] 5413-5417 (1995).

[42] H. Oshata, T. Ohhashi, H. Kato, S. Nishigaki and T. Okuda; "Microwave dielectric properties and structure of the $Ba_{6-3x}Sm_{8+2x}Ti_{18}O_{54}$ solid solution," *Jpn. J. Appl. Phys.*, **34**[1] 187-191 (1995).

[43] H. Oshato, S. Nishigaki and T. Okuda; "Superlattice and dielectric properties of BaO-R_2O_3-TiO_2 (R = La, Nd and Sm) microwave dielectric compounds," *Jpn. J. Appl. Phys.*, **31**[9B] 3136-3138 (1992).

[44] F. Fukuda, I. Fujii, R. Kitoh, Y. Cho and I. Awai; "Influence of rare earth ions on BaO-TiO_2-Rare earth oxide ceramics for microwave applications," *Jpn. J. Appl. Phys.*, **32**[4] 1712-15 (1993).

[45] M. Ualant, D. Suvorov and D. Kolar; "X-ray investigation and determination of the

dielectric properties of the compound $Ba_{4.5}Gd_9Ti_{18}O_{54}$," *Jpn. J. Appl. Phys.*, **35**[1A] 144-150 (1996).

[46] R.G. Matveeva, M.V. Varfolomeev and L.S. Il'yuschenko; *Russ. J. Inorg. Chem.*, **29** 278 (1984) (Si. 1, Ref. 43).

[47] E.C. Henry; "**Electronic Ceramics**," Gordan City, New York, Doubleday & Company, Inc., P-93 (1969).

[48] B.D. Cullity; "**Elements of X-ray diffraction**," Addison-Wesley Publishing Company, Inc., P-324-333 (1967).

[49] P. Boden and F.P. Glasser; "Phase relationship in the system MgO-Al_2O_3-TiO_2," *Trans. J. Brit. Ceram. Soc.*, **72**[5] 215-20 (1973).

[50] Ref. 4, p225-226.

Appendix A

Weight calculation for a particular batch

The general formula used for a batch preparation is $((Mg_{0.95}Ca_{0.05})TiO_3)_x$ - $(MgAl_2O_4)_{1-x}$ and abbreviated by $(MT)_x$ - $(MA)_{1-x}$. Here 'x' is in moles. So the starting powders for a particular composition can be expressed in terms of moles i.e.

MgO required = 0.95 x + (1-x)

TiO_2 required = x

$CaCO_3$ required = 0.05 x

Al_2O_3 required = 1-x

Let the weight of desired batch be 'W' gm, the molecular weight of MT is M_1 ($\sim$120.985 gm/mole), the molecular weight of MA ($\sim$ 142.26$gm/mole$) and the molecular weight of whole system is 'w' gm/mole. Then one can write

$$x \times M_1 + (1-x) \times M_2 = w \tag{A.1}$$

$$\Rightarrow x \times (120.985) + (1-x) \times (142.26) = w$$

$$\Rightarrow x[120.985 - 142.26] = w - 142.26$$

$$\Rightarrow w = 142.26 - 21.275 \times x \tag{A.2}$$

But for practical point of view, volume fraction is more easier to find out required amount of starting powders. The conversion of mole fraction to volume fraction has been done by the relation

$$1 - v = \frac{\frac{xM_1}{\rho_1}}{\frac{xM_1}{\rho_1} + \frac{(1-x)M_2}{\rho_2}} \tag{A.3}$$

where v_1 is volume fraction of MT; M_1, ρ_1 and M_2, ρ_2 are molecular weights and densities of MT and MA respectively. The density of MT has been calculated (Appendix B) and takes to be 3.9026 gmcm^{-3}. The density of MA from JCPDS files is 3.578 gmcm^{-3}. The conversion from volume fraction to mole fraction is given in the following Table A.1.

Table A.1: Mole fraction to volume fraction conversion data

$(1\text{-}v)_{MT}$	1	0.8	0.6	0.4	0.2	0.1	0.02	0
x	1	0.836	0.658	0.46	0.243	0.125	0.255	0

The required amounts of individual starting powders taken for a particular batch of total weight follows.

The weight of MgO required= $n[0.95x + (1-x)]M_{MgO}$ gm

The weight of TiO_2 required = $n.x.M_{TiO_2}$ gm

The weight of $CaCO_3$ required = $n.(0.05).x.M_{CaCO_3}$ gm

The weight of Al_2O_3 required = $n(1-x)M_{Al_2O_3}$gm

Where the fractional term 'n' is given by

$n = \frac{W}{w}$

M_{MgO}, M_{TiO_2}, M_{CaCO_3} and $M_{Al_2O_3}$ are the molecular weights of MgO, TiO_2, $CaCO_3$ and Al_2O_3 respectively.

After this calculation, the individual losses were taken into consideration. It can be more clear by the following example.

Example

Let us consider a particular batch 0.4(MT)-0.6(MA).

Here $1 - v = 0.4 \Rightarrow x = 0.46$

According to equation (A.2)

$w = 142.26 - 21.275x = 142.26 - 21.275 \times 0.46 = 132.47$

Let desired batch $W = 20$ gm

Then $n = \frac{W}{w} = \frac{20}{132.47} = 0.151$

Amount of MgO required $= n[0.95x + (1 - x)].M_{MgO}$

$= 0.151[0.95(0.46) + (1 - 0.46)] \times 40.3 = 5.945$ gm

But weight loss in MgO is 25 %. The loss can be considered as follows :

The net amount of MgO required $= \frac{100}{100-0.25} \times 5.945 = 7.926$ gm

By this way, the calculation of required amount of TiO_2, Al_2O_3 and $CaCO_3$ has been done.

Appendix B

Density calculation of a mixed phase system

Theoratical density of $Mg_{0.95}Ca_{0.05}TiO_3$ (MTCT) and MTA(v) system has been calculated by using the standard data.

From standard x-ray data file, the theoretical density of $MgTiO_3$ (MT) and $CaTiO_3$ are given by

$\rho_{MT} = 3.895$ gm/cc, $\rho_{CT} = 4.036$ gm/cc

Molecular weights of MT and CT are

$M_{MT} = 120.2$ gm/mole, $M_{CT} = 135.9$ gm/mole

Mass of MT in 1 mole of MTCT $= 0.95 \times 120.2 = 114.19$ gm

Volume of MT in 1 mole of MTCT $= \frac{M_{MT_{0.95}}}{\rho_{MT}} = \frac{114.9}{3.895} = 29.317cc = v_1$

Mass of CT in 1 mole of MTCT $= 0.5 \times 135.9 = 6.795$ gm

Volume of CT in 1 mole of MTCT $= \frac{M_{CT_{0.05}}}{\rho_{CT}} = \frac{6.795}{4.036} = 1.68cc = v_2$

Now total volume $V = v_1 + v_2 = 30.997$ cc

Volume fraction of MT $= v'_{MT} = \frac{v_1}{V} = 0.9458$

Volume fraction of CT $= v'_{CT} = \frac{v_2}{V} = 0.0542$

$\rho_{MTCT} = v'_{MT} \times \rho_{MT} + v'_{CT} \times \rho_{CT}$

$\rho_{MTCT} = 0.9458 \times 3.895 + 0.0542 \times 4.036 = 3.9026$ gm/cc

Similarly the density of (1-v)(MTCT) - v(MA) system (abbreviated MTA(v)) can be obtained.

Example

Consider a particular system MTA(0.6) We have the theoretical density of MA is 3.578 gm/cc.

$$So, \rho_{MTA(0\,6)} = 0.4 \times \rho_{MTCT} + 0.6 \times \rho_{MA} = 0.4 \times 3.9026 + 0.6 \times 3.578 = 3.7078 gm/cc \quad \text{(B.1)}$$

The theoretical density for various compositions calculated as above are given in the following Table.

Table B.1: Theoretical density of all MTA(v) system.

Compositions	Theoretical densities
MCA(0) (MTCT)	3.9026
MCA(0.2)	3.8377
MCA(0.4)	3.7727
MCA(0.6)	3.7078
MCA(0.8)	3.6429
MCA(0.9)	3.6104
MCA(0.98)	3.5845
MCA(1) ($MgAl_2O_4$)	3.578

Appendix C

Predicted data for optimization of dielectric properties

The reported values of relative permittivities and TCF of $MgTiO_3$, $CaTiO_3$ and $MgAl_2O_4$ [50] are

Table C.1: ϵ_r and TCF data of $MgTiO_3$, $CaTiO_3$ and $MgAl_2O_4$ system.

	$MgTiO_3$	$CaTiO_3$	$MgAl_2O_4$
ϵ_r	13	168	7.5
TCF	-57.5	+916	-71.6

Using the above data, the value of TCF and ϵ_r in the system $(Mg_{0.95}Ca_{0.05})TiO_3$ has been calculated and compare with the reported results as shown below (volume fraction of $MgTiO_3$ and $CaTiO_3$ became 0.9458 and 0.0542).

The presence of small amounts of other phases Mg_2TiO_4, $MgTi_2O_5$, Al_2TiO_5, TiO_2 and Al_2O_3 are also likely to affect the values of TCF and ϵ_r. The amounts of these phases in our samples are small. As the data on their individual TCF values is not available, an effective TCF for $MgAl_2O_4$ was calculated using the experimental values. This effective value was taken to include the contributions to TCF by other phases. Using this effective

Table C.2: ϵ_r and TCF data of $Mg_{0.95}Ca_{0.05}TiO_3$ system

	$Mg_{0.95}Ca_{0.05}TiO_3$	
	calculated	reported
ϵ_r	14.93	21
TCF	-4.7	0

value of TCF for $MgAl_2O_4$, the values of other compositions was predicted to design further experiments. These calculations are illustrated below. The value of TCF for composition 0.4 $((MgCa)TiO_3)$ - 0.6 $(MgAl_2O_4)$ was measured to be -26 ppm/^oC. Now taking the calculated value of TCF (-4.7 ppm/^oC) for (MgCa)TiO_3, the effective TCF for $MgAl_2O_4$ plus other phases in small amounts is given by

$$-26.4 = -4.7 \times 0.4 + TCF_{MA_{eff.}} \times 0.6$$

or $TCF_{MA_{eff}} = \frac{-26.4+0.4\times4.7}{0.6} = -40.8$ ppm/^oC

This value of effective TCF is now used to predict the TCF for other compositions assuming three phases $MgTiO_3$, $CaTiO_3$ and $MgAl_2O_4$. The values of ϵ_r and TCF used for calculation as follows.

Phases	$MgTiO_3$	$CaTiO_3$	$MgAl_2O_4$ (effective)
TCF	- 57.5	+ 916	- 40.8
ϵ_r	13	168	7.5

The following relation were used to calculate the TCF and ϵ_r for different compositions

$$(TCF)_{ceramic} = \sum_i v_i (TCF)_i \tag{C.1}$$

$$\log(\epsilon_r)_{ceramic} = \sum_i v_i \log(\epsilon_r)_i \tag{C.2}$$

Where v_i, $(TCF)_i$ and $(\epsilon_r)_i$ are the volume fraction, TCF and ϵ_r of the three constituent phases.

The predicted values for the compositions 0.35 ($Mg_{1-y}Ca_yTiO_3$) - 0.65 ($MgAl_2O_4$) in the range $0.086 \leq y \leq 0.143$ are given in the following Table C.3.

Table C.3: Predicted values of ϵ_r and TCF in the system 0.35 ($Mg_{1-y}Ca_yTiO_3$) – 0.65 ($MgAl_2O_4$).

MT Volume frac.	MT mole frac.	CT volume frac.	CT mole frac. (y)	ϵ_r	TCF (ppm/^oC)
0.3174	0.914	0.0326	0.086	11.52	- 14.97
o.3122	0.9	0.0378	0.1	11.68	- 9.85
0.3047	0.88	0.0453	0.12	11.9	- 2.52
0.296	0.857	0.054	0.143	12.7	+ 5.83

Appendix D

Software for lattice parameter calculation

```
* LATTICE PARAMETER CALCULATION FOR HEXAGONAL SYSTEM */

#include<stdio.h>
#include<math.h>
#define lambda 1.54056
#define pi 3.1416
#define iteration 5

main()
{
float theta[50],h[50],k[50],l[50],a,c,c_a;
float sum_x,sum_xx,sum_y,sum_yy,sum_z,sum_zz,sum_xy,sum_xz,t,b,g,cs_sq
float m_a,m_c,c_y,c_z,p,q,a1,a2,b1,b2,d1,d2;
int i=0,j=0,n=0;
char ifile[10],ofile[10];
FILE *fpt, *spt;
system("clear");
printf("          LATTICE PARAMETER CALCULATION FOR HEXAGONAL SYSTEM ");
printf("\n\n\n\n\n\n\n\n\n");
printf("                    Enter Data File Name: ");
scanf("%s",&ifile);
fpt = fopen(ifile,"r");
 if(fpt == 0){
ifprintf("The File %s Does Not Exist In The Current Directory\n\n\n",ifile);
  exit();
  }
sprintf(ofile,"%s.hex",ifile);
spt = fopen(ofile,"w");
while(fscanf(fpt,"%f %f %f %f",&theta[n],&h[n],&k[n],&l[n])!=EOF)
 {
  n++;
 }
```

```
printf("\n      No  of Data=%d\n\n\n",n);
/*Initial c/a calculation*/
p=sin(pi/180*theta[0]/2);
q=sin(pi/180*theta[1]/2);
a1=p*p/(lambda*lambda);
a2=q*q/(lambda*lambda);
d1=l[0]*l[0]/4;
d2=l[1]*l[1]/4;
b1=(h[0]*h[0]+h[0]*k[0]+k[0]*k[0])/3;
b2=(h[1]*h[1]+h[1]*k[1]+k[1]*k[1])/3;
c_a=sqrt((a1*d2-a2*d1)/(a2*b1-a1*b2));

fprintf(spt,"LATTICE PARAMETER CALCULATION OF HEXAGONAL SYSTEM FOR THE INPUT FILE
\"%s\"\n\n",ifile);
printf("Initial value of c/a = %f\n\n",c_a);
fprintf(spt,"Initial value of c/a = %f\n\n",c_a);

for(j=0;j<iteration;j++)
 {
  sum_x=0;
  sum_xx=0;
  sum_y=0;
  sum_yy=0;
  sum_z=0;
  sum_zz=0;
  sum_xz=0;
  sum_xy=0;
  fprintf(spt,"Iteration No:%d\n\n",(j+1));
  printf("Iteration No.%d\n",(j+1));
  fprintf(spt,"2(theta)      Cos^2(theta)      a          c\n");

 for(i=0;i<=n-1;i++)
   {
     t=(pi/180)*(theta[i]/2);
     b=lambda/sin(t);
     g=(h[i]*h[i]+h[i]*k[i]+k[i]*k[i])/3;
     a=b*sqrt(g+(l[i]*l[i])/(4*c_a*c_a));
     c=b*sqrt(g*(c_a*c_a)+(l[i]*l[i]/4));
     cs_sq=cos(t)*cos(t);
sum_x=sum_x+cs_sq;
     sum_xx=sum_xx+cs_sq*cs_sq;
     sum_y=sum_y+a;
     sum_yy=sum_yy+a*a;
     sum_z=sum_z+c;
     sum_zz=sum_zz+c*c;
     sum_xy=sum_xy+cs_sq*a;
     sum_xz=sum_xz+cs_sq*c;
     fprintf(spt,"\n%5.5f %15.5f %15.5f %15.5f",theta[i],cs_sq,a,c);
   }
  printf("\n a = %f*(c = %f(ac/a = %f\n\n\n",c_y,c_z,c_a);",c_y,c_z,c_a);
}
fclose(fpt);
fclose(spt);
printf("\n        Results Available In %s \n\n\n",ofile);
printf("                Thank You\n\n\n\n\n");

}
```

```
/* LATTICE PARAMETER CALCULATION FOR CUBIC SYSTEM */

#include<stdio.h>
#include<math.h>
#define lambda 1.54056
#define pi 3.1416

main()
{
float theta[50],h[50],k[50],l[50],a,t,d,b,g,cs_sq,
float sum_x,sum_xx,sum_y,sum_yy,sum_xy;
float m_a,c_y,
int i=0,n=0,
char ifile[10],ofile[10],
FILE *fpt, *spt,
system("clear");
printf("          LATTICE PARAMETER CALCULATION FOR CUBIC SYSTEM ");
printf("\n\n\n\n\n\n\n\n\n");
printf("                    Enter Data File Name: ");
scanf("%s",&ifile);
fpt = fopen(ifile,"r");
 if(fpt == 0){
  printf("The File %s Does Not Exist In The Current Directory\n\n\n",ifile);
  exit();
  }
sprintf(ofile,"%s.cbc",ifile);
spt = fopen(ofile,"w");
while(fscanf(fpt,"%f %f %f %f",&theta[n],&h[n],&k[n],&l[n])!=EOF)
 {
  n++;

  }
 printf("\n                    No. of Data = %d\n\n",n);
 fprintf(spt," RESULTS OF CUBIC SYSTEM FOR THE INPUT FILE \"%s\"\n \n",ifile);
 fprintf(spt,"2(theta)     Cos^2(theta)     a  \n");
  sum_x=0;
  sum_xx=0;
  sum_y=0;
  sum_yy=0;
  sum_xy=0;


  for(i=0;i<=n-1;i++)
     {
       t=(pi/180)*(theta[i]/2);
       b=lambda/(sin(t)*2);
       g=(h[i]*h[i]+k[i]*k[i]+l[i]*l[i]);
       a=b*sqrt(g);
       if(d=a;0)
```

```
        cs_sq=cos(t)*cos(t);
        sum_x=sum_x+cs_sq;
sum_xx=sum_xx+cs_sq*cs_sq;
        sum_y=sum_y+a;
       sum_yy=sum_yy+a*a;
    sum_xy=sum_xy+cs_sq*a;

        fprintf(spt,"\n%5.5f %15.5f %15.5f ",theta[i],cs_sq,a);
       }
      m_a=(sum_xc_y=(sum_y/n)-m_a*(sum_x/(float)n),sum_x*sum_x/(float)n));
   fprintf(spt,"\n\n After Extrapolation (cos sq  theta = 0) a = %f  \n",c_y);
fclose(fpt);
fclose(spt);                    ResultsThank You\n\n\n\n\n");n\n",ofile);
printf("\n
}
```

Date Slip

This book is to be returned on the date last stamped.